INTERNATIONAL IBERIAN NANOTECHNOLOGY LABORATORY

Assessing nanoscale (opto-)electronic properties through advanced scanning probe microscopy

Sascha Sadewasser

International Iberian Nanotechnology Laboratory (INL),

Braga, Portugal

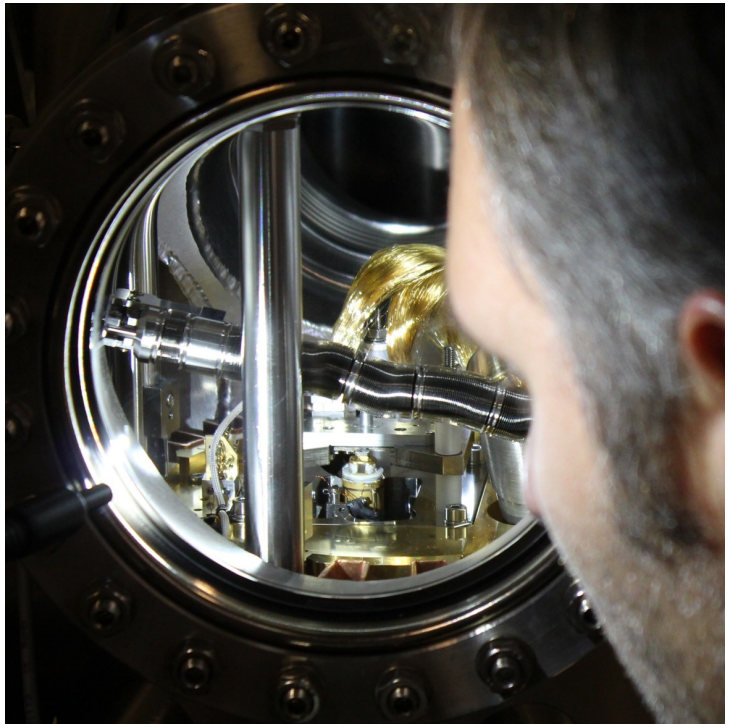

Outline:

- Brief intro to scanning probe microscopy
- Grain boundaries in chalcopyrites
- Alkali-fluoride post-deposition treatments for chalcopyrites
- Time-resolved Kelvin probe force microscopy
- Conclusion

Part I:
Introduction to scanning probe microscopy - SPM

Scanning probe microscopy - SPM

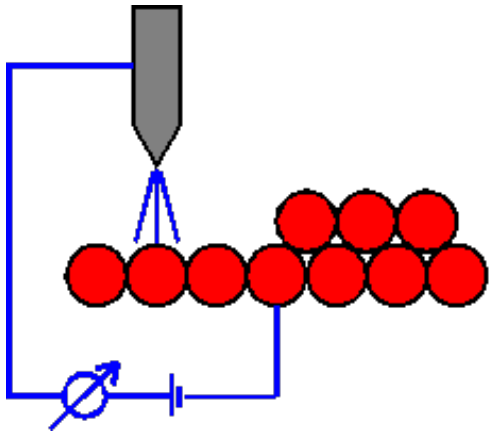

Scanning tunneling microscope:

Developed by

G. Binnig and H. Rohrer

IBM Research Laboratory, 1982

Nobel Prize in 1986

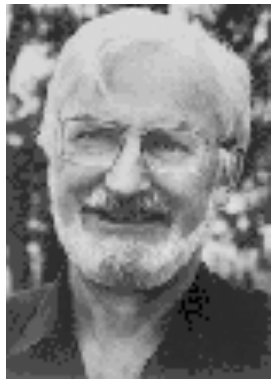

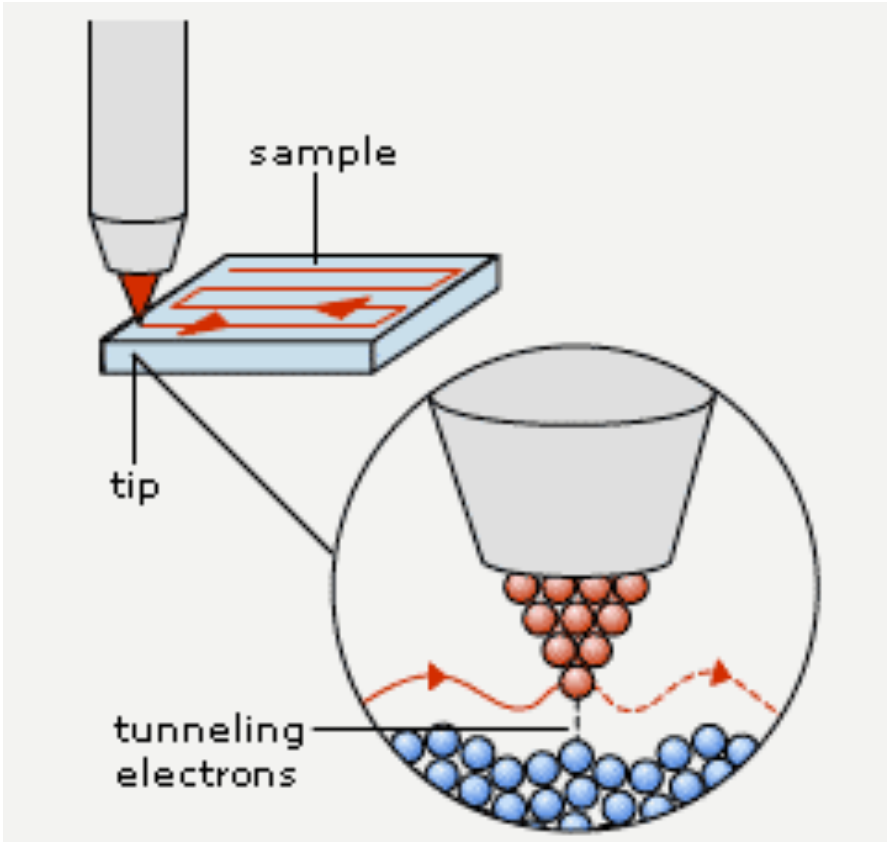

images from: http://www.fkp.uni-erlangen.de

Scanning probe microscopy - SPM

The microscope is very sensitive to vibrations,

Therefore, a system for vibration insulation is required

Sources of vibration: building vibrations: 15 – 20 Hz

walking people: 2 - 4 Hz

vacuum pumps

sound

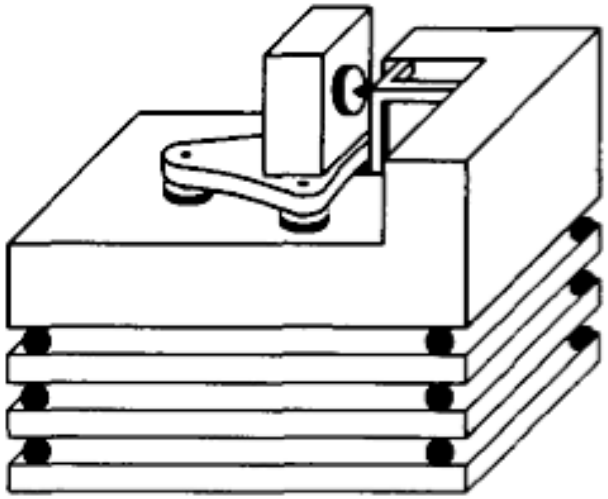

viton

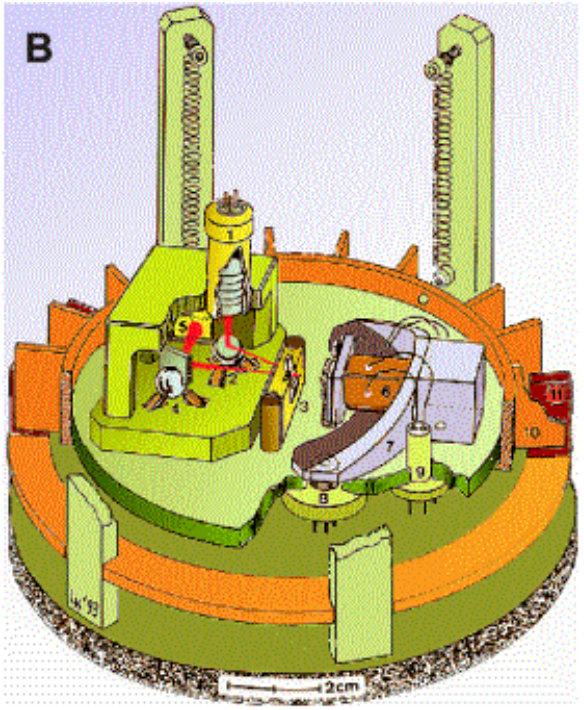

springs

Block diagram of an STM

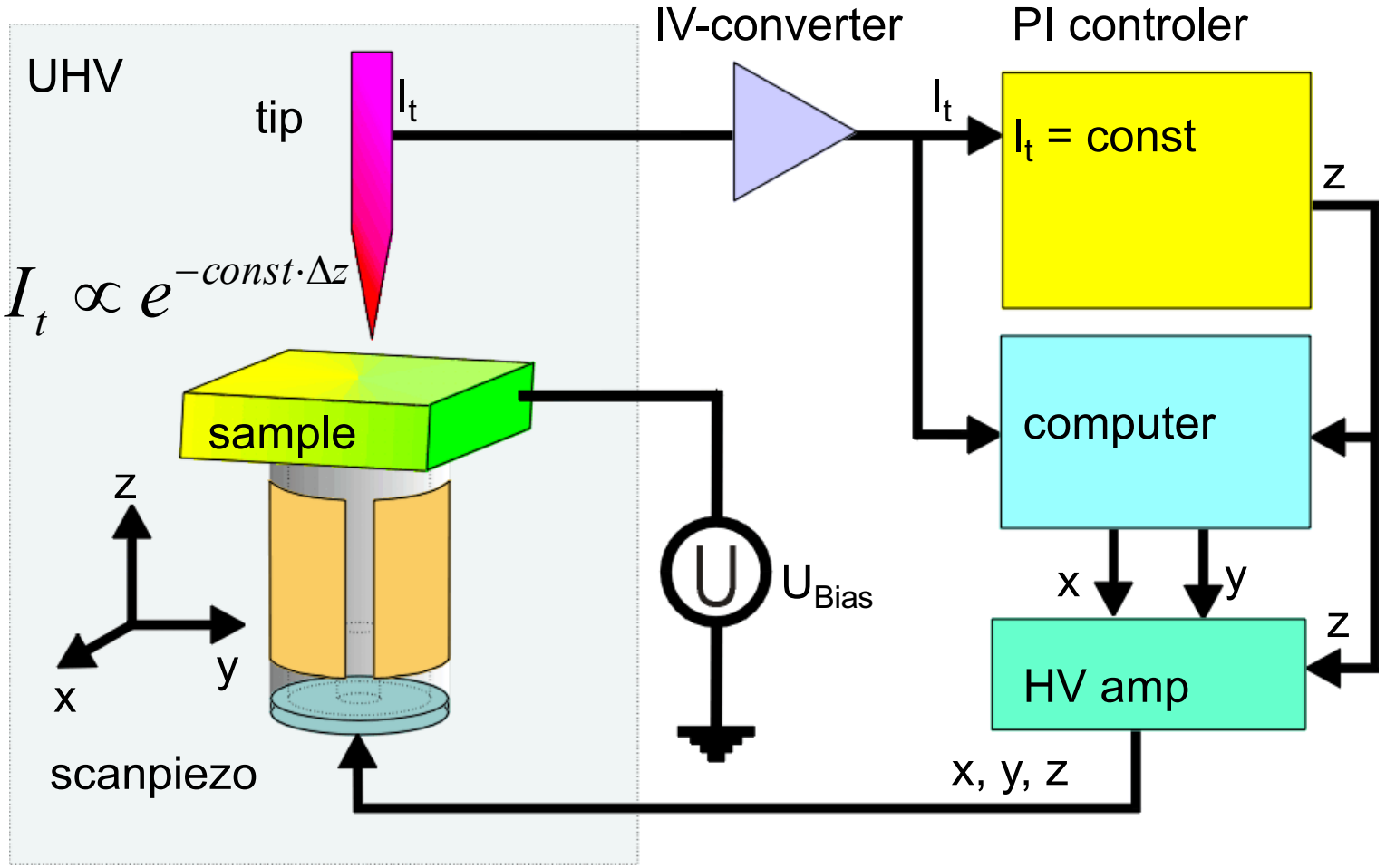

Scanning probe microscopy - SPM

Scanning is realized through piezoelectric elements

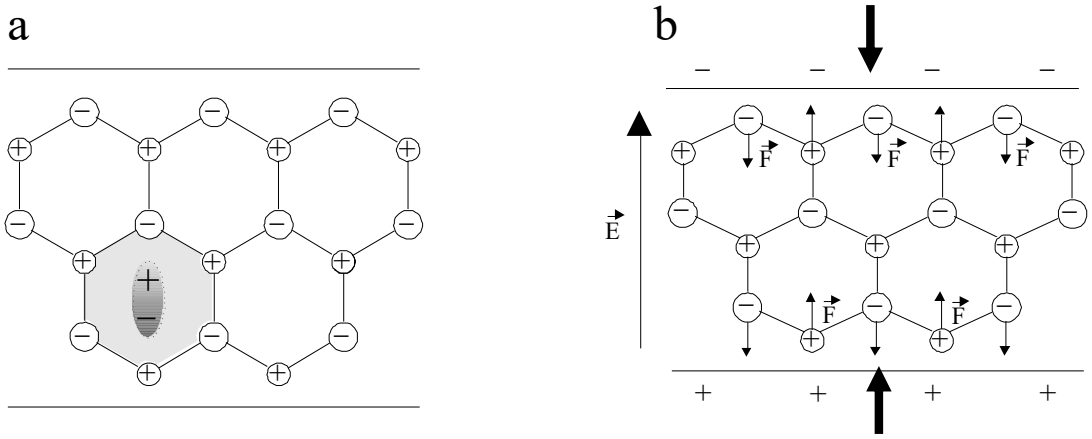

Center of positive and negative charge do not coincide

Deformation as a result of application of an electric voltage

Typical piezoelectric materials:

- quarz
- bariumtitanate
- lead zirconium titanate (PZT)
- etc.

Scanning probe microscopy - SPM

Scanning is realized through piezoelectric elements

bimorph

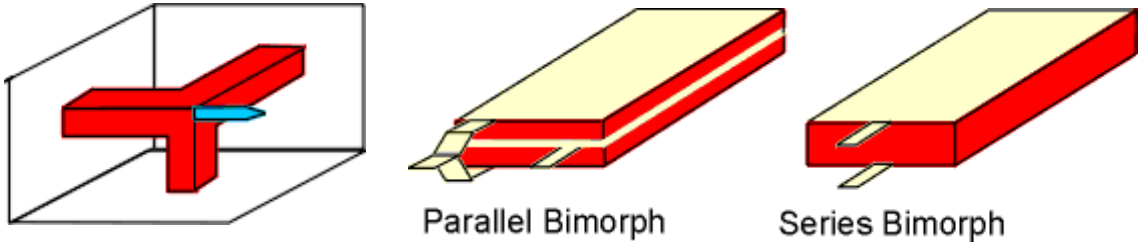

tripod

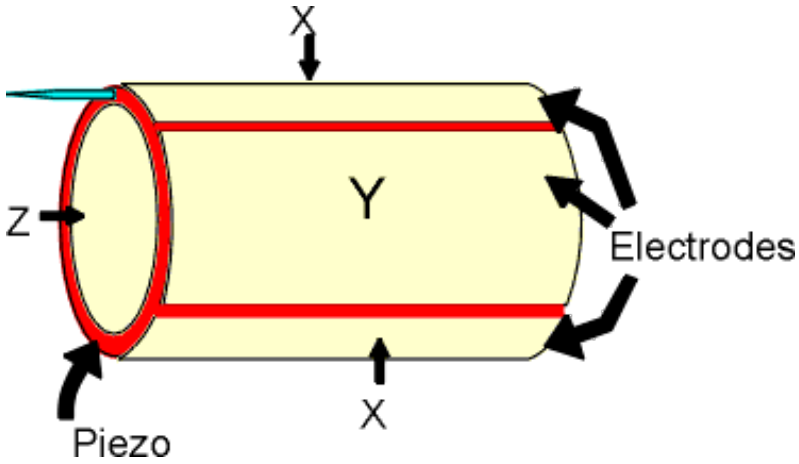

tube scanner

beetle

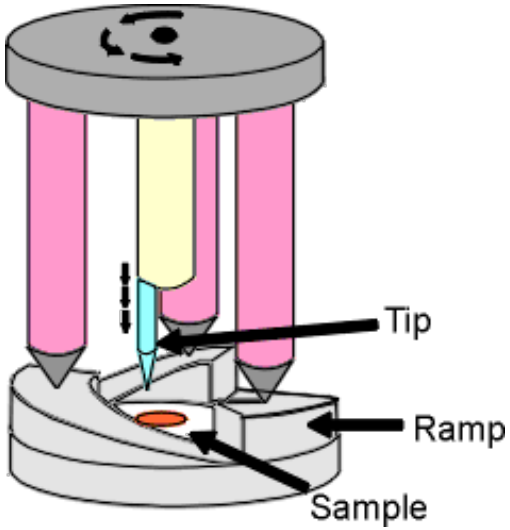

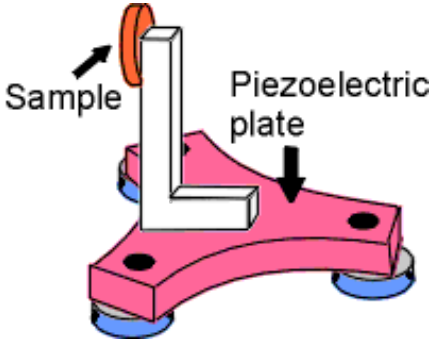

louse

images from: http://www.fkp.uni-erlangen.de

Block diagram of an STM

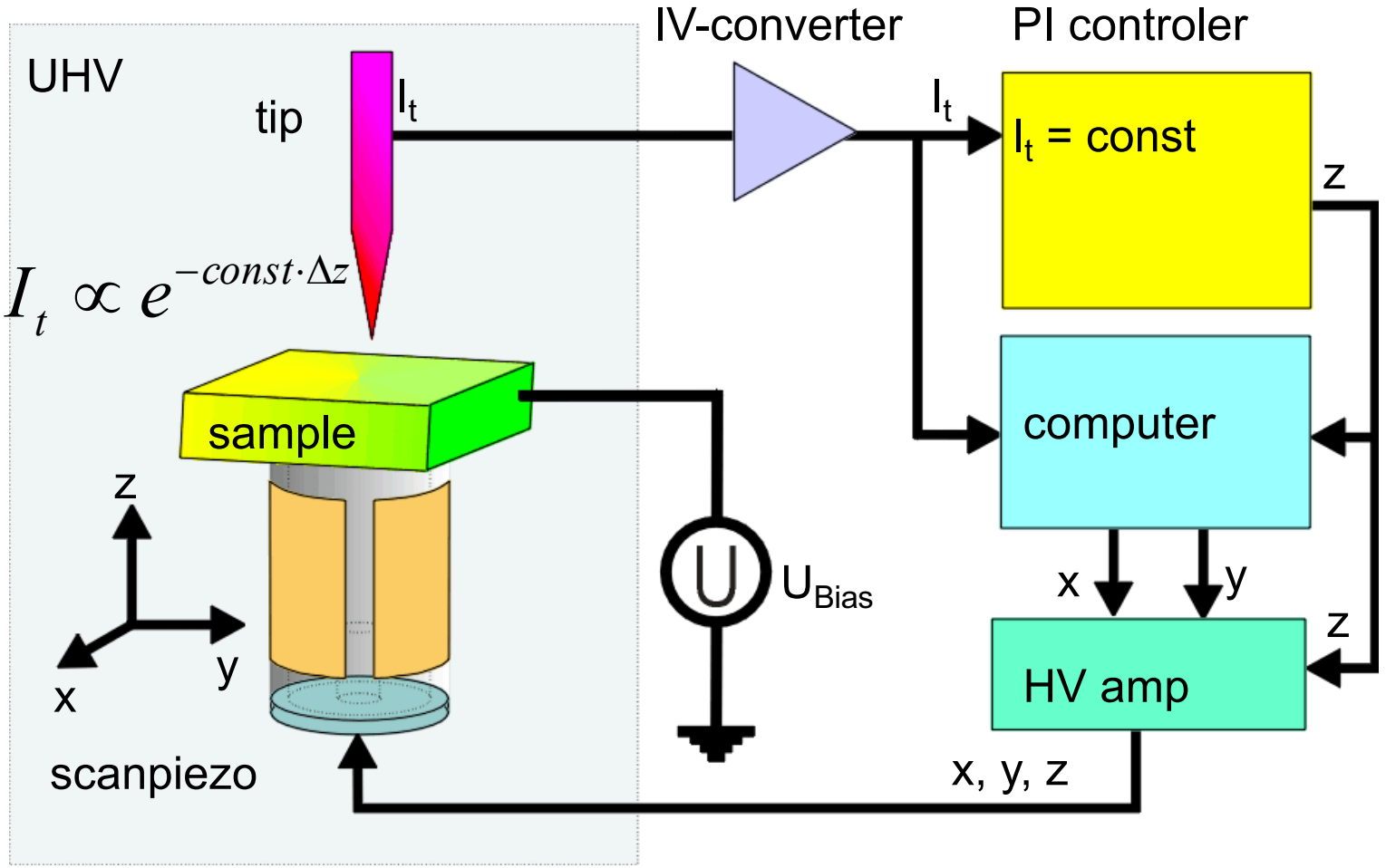

Atomic Force Microscope

VOLUME 56, NUMBER 9 PHYSICAL REVIEW LETTERS 3 MARCH 1986

Atomic Force Microscope

G. Binnig[a] and C. F. Quate[b]
Edward L. Ginzton Laboratory, Stanford University, Stanford, California 94305
and
Ch. Gerber[c]
IBM San Jose Research Laboratory, San Jose, California 95193
(Received 5 December 1985)

The scanning tunneling microscope is proposed as a method to measure forces as small as 10^{-18} N. As one application for this concept, we introduce a new type of microscope capable of investigating surfaces of insulators on an atomic scale. The atomic force microscope is a combination of the principles of the scanning tunneling microscope and the stylus profilometer. It incorporates a probe that does not damage the surface. Our preliminary results *in air* demonstrate a lateral resolution of 30 Å and a vertical resolution less than 1 Å.

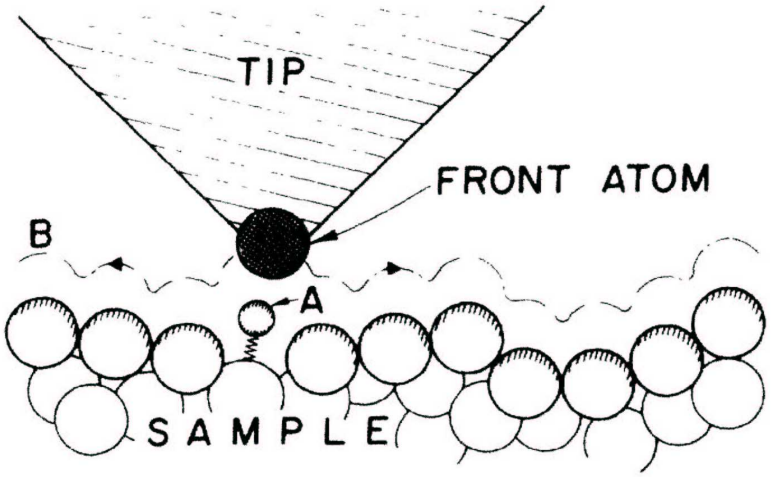

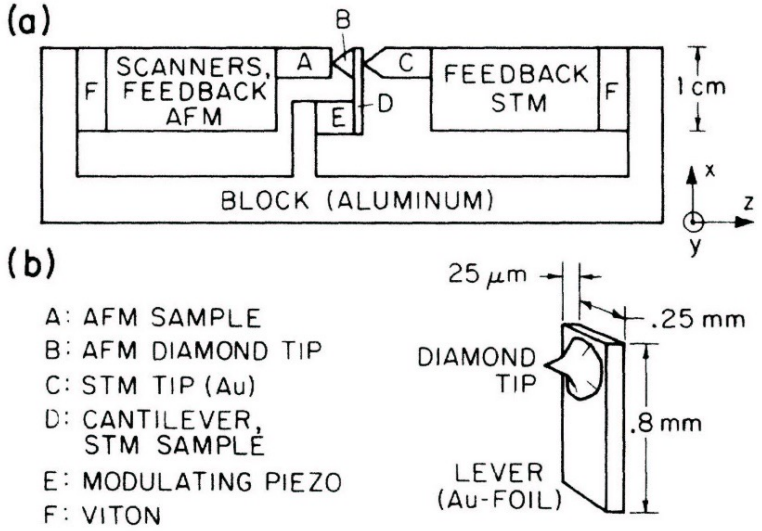

> 11000 citations

Scanning probe microscopy - SPM

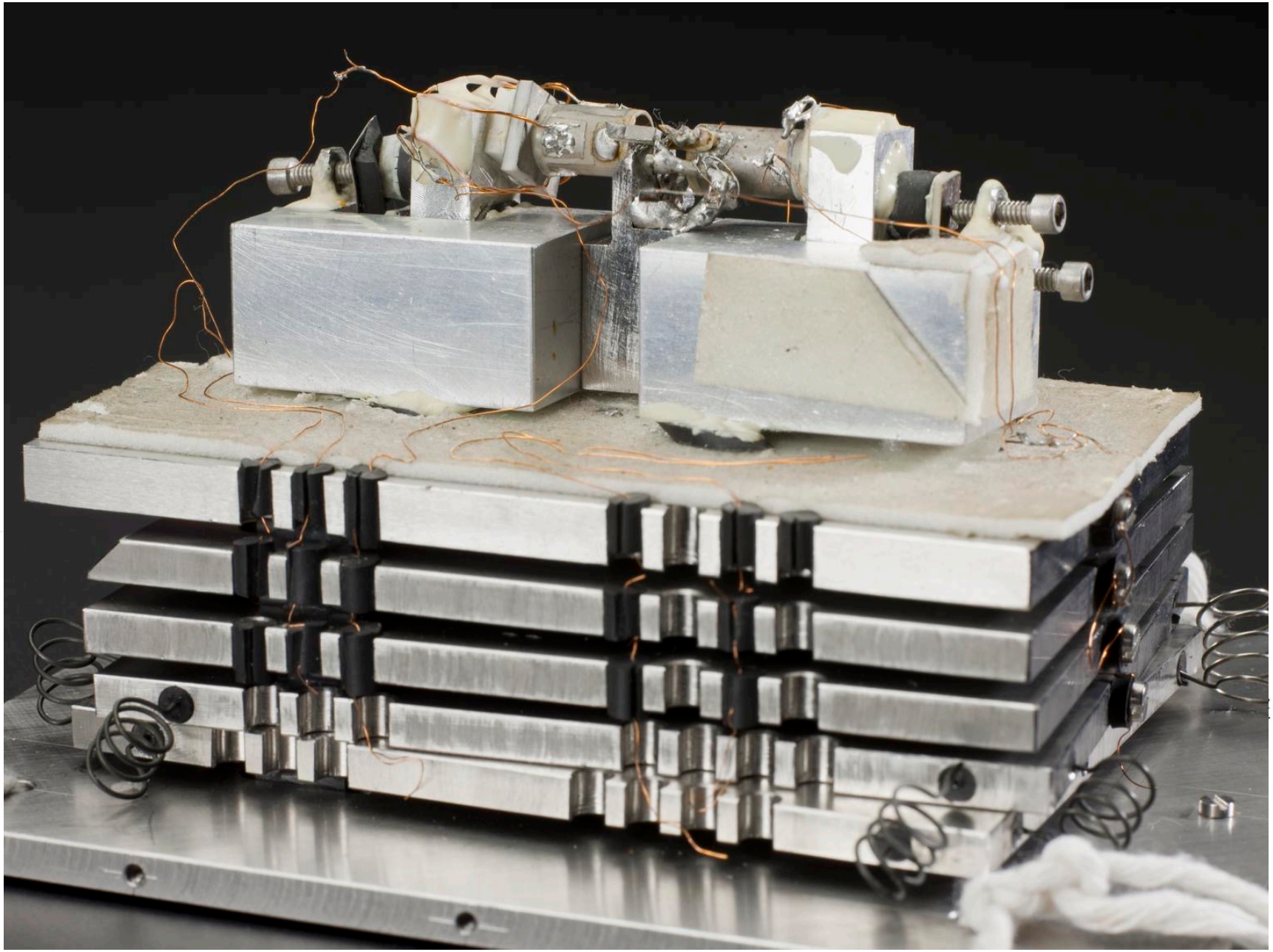

Scanning probe microscopy - SPM

Force between two atoms:

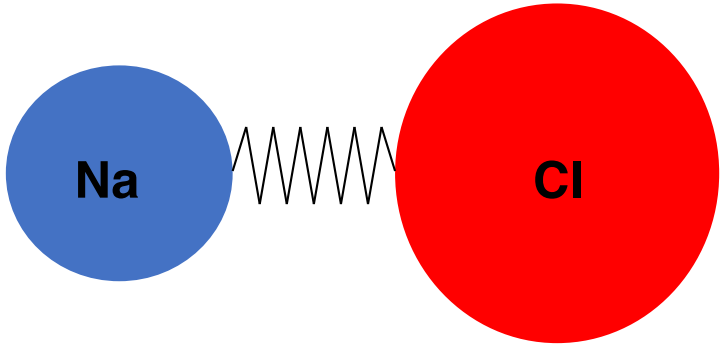

chemical bond

F_{chem} = 1eV/ 0.1 nm

1.6 nN

Sensing forces:

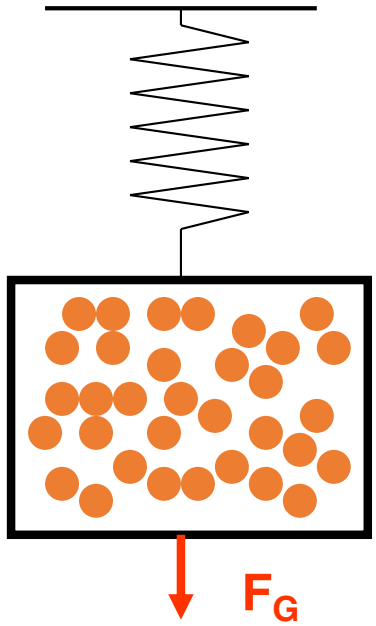

1 nm^3 water (33 molecules)

$F_G=10^{-23}$ N = 10^{-14} nN

0.01 g

F= 0.1 mN = 10^5 nN

Atomic Force Microscope

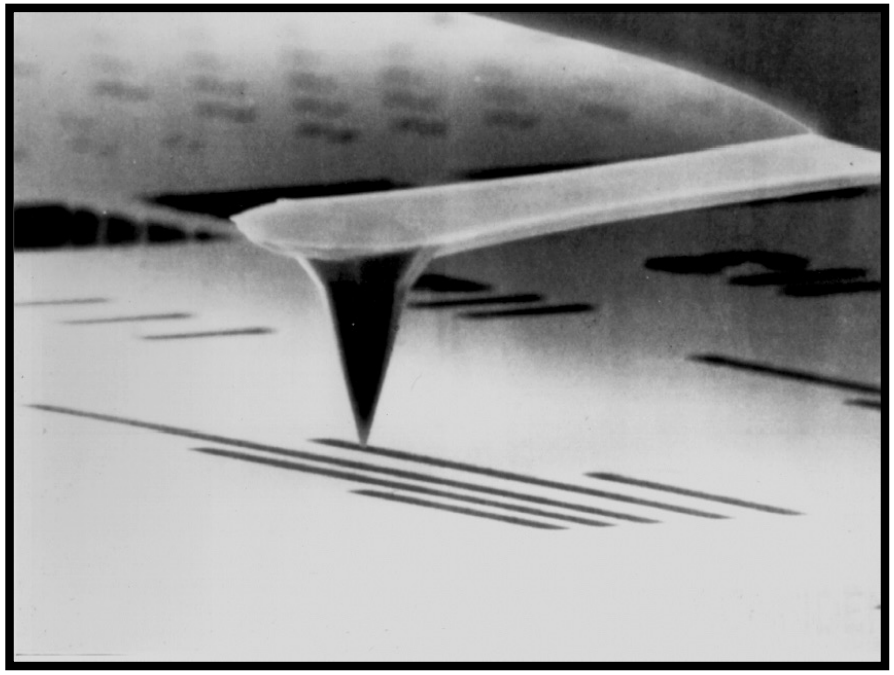

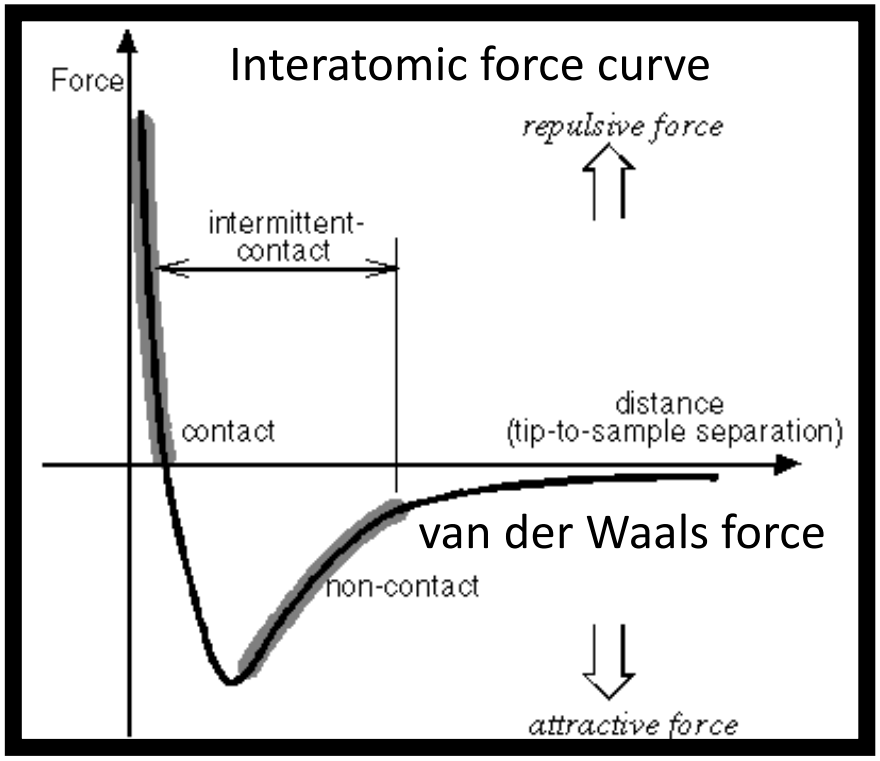

Lennard-Jones potential:

$$U_{LJ} = 4\epsilon \left[\left(\frac{\sigma_0}{r} \right)^{12} - \left(\frac{\sigma_0}{r} \right)^{6} \right]$$

Atomic Force Microscope

Cantilever and tip

Usually fabricated by silicon microfabrication techniques

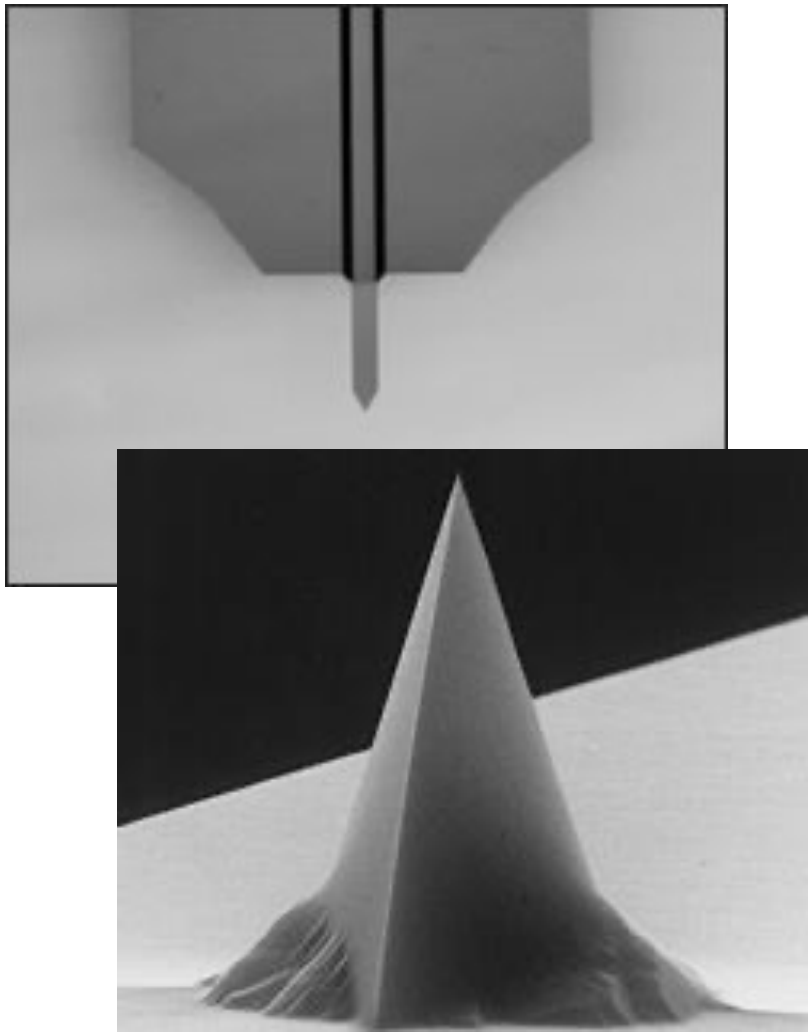

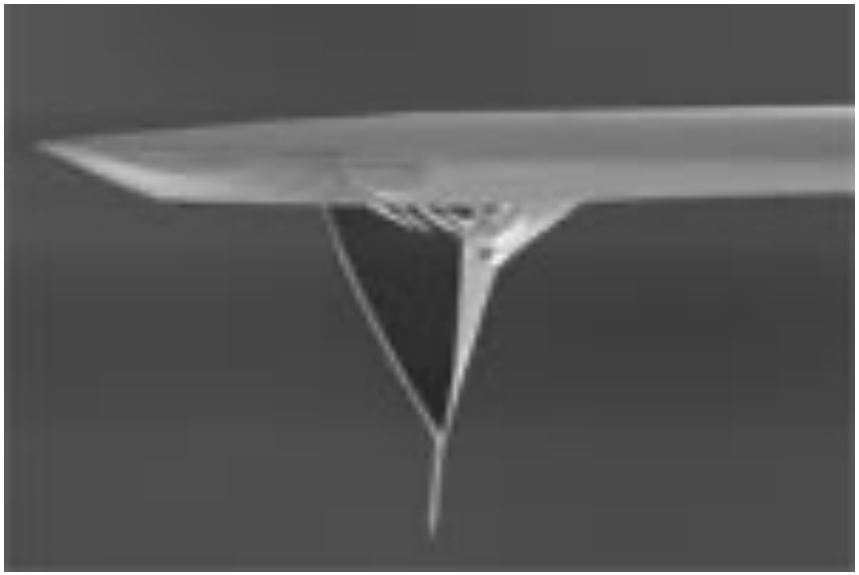

http://store.nanoscience.com/

Carbon nanotube tip

http://www.nanoworld.com

Atomic Force Microscope

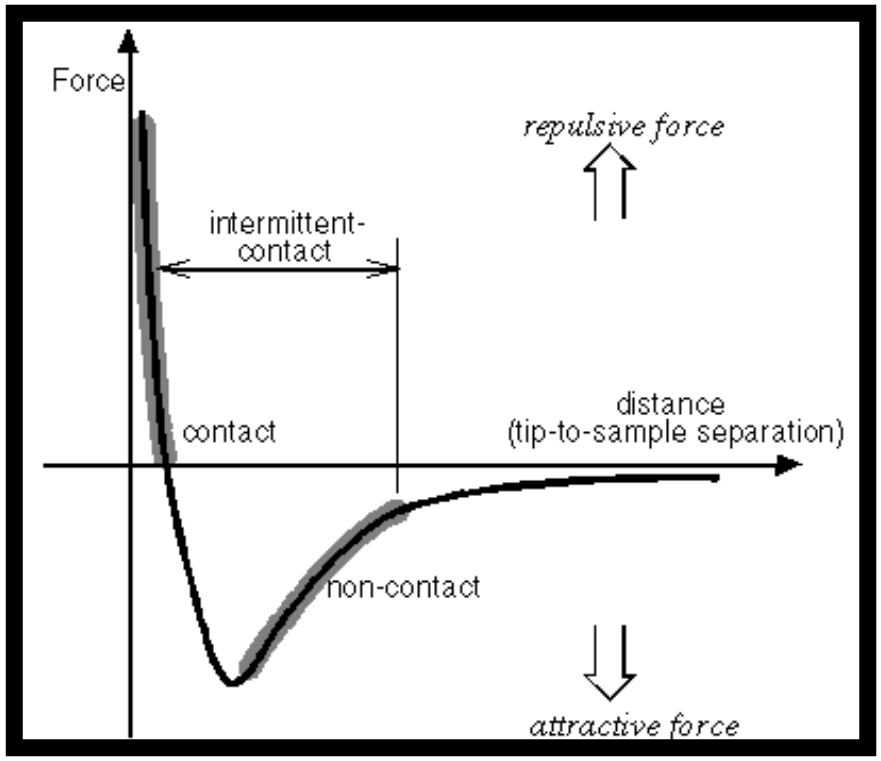

Contact mode

- Operates in the repulsive part of the force-distance curve
- Cantilever with a small force constant (~0.2 N/m)
- There is also a capillary force due to the water layer on the surface in ambient conditions

Atomic Force Microscope

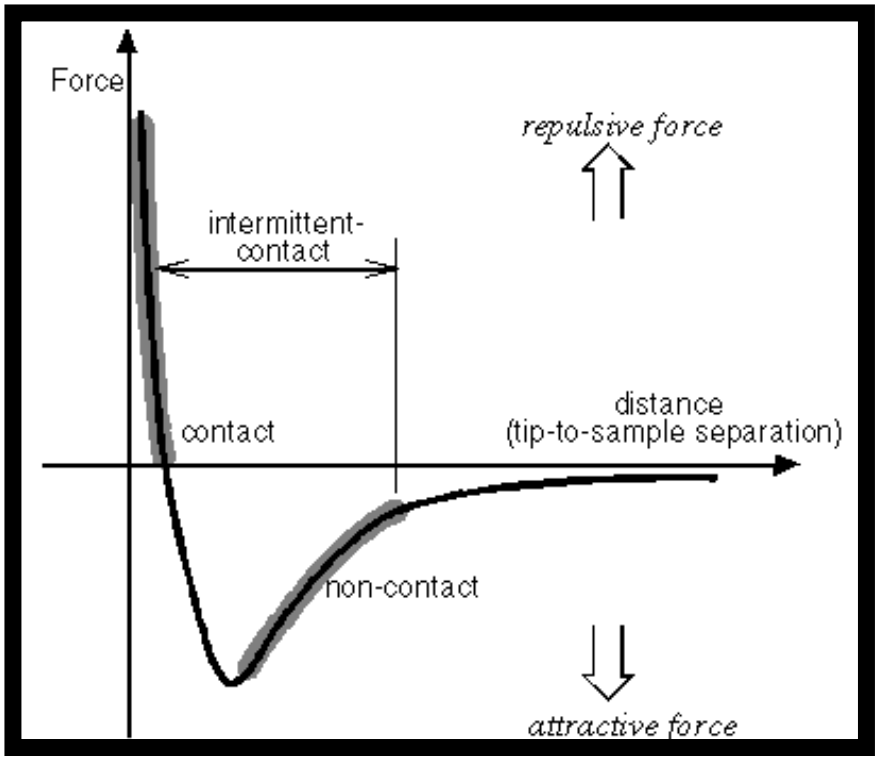

Non-contact mode

- Operates in the attractive force regime
- The cantilever oscillates near its resonance frequency (~ 70-350 kHz, force constant 3-40 N/m)
- Advantages over the contact mode:
  - smaller force interaction with the sample
  - no lateral forces
  - no contamination of the tip

Atomic Force Microscope

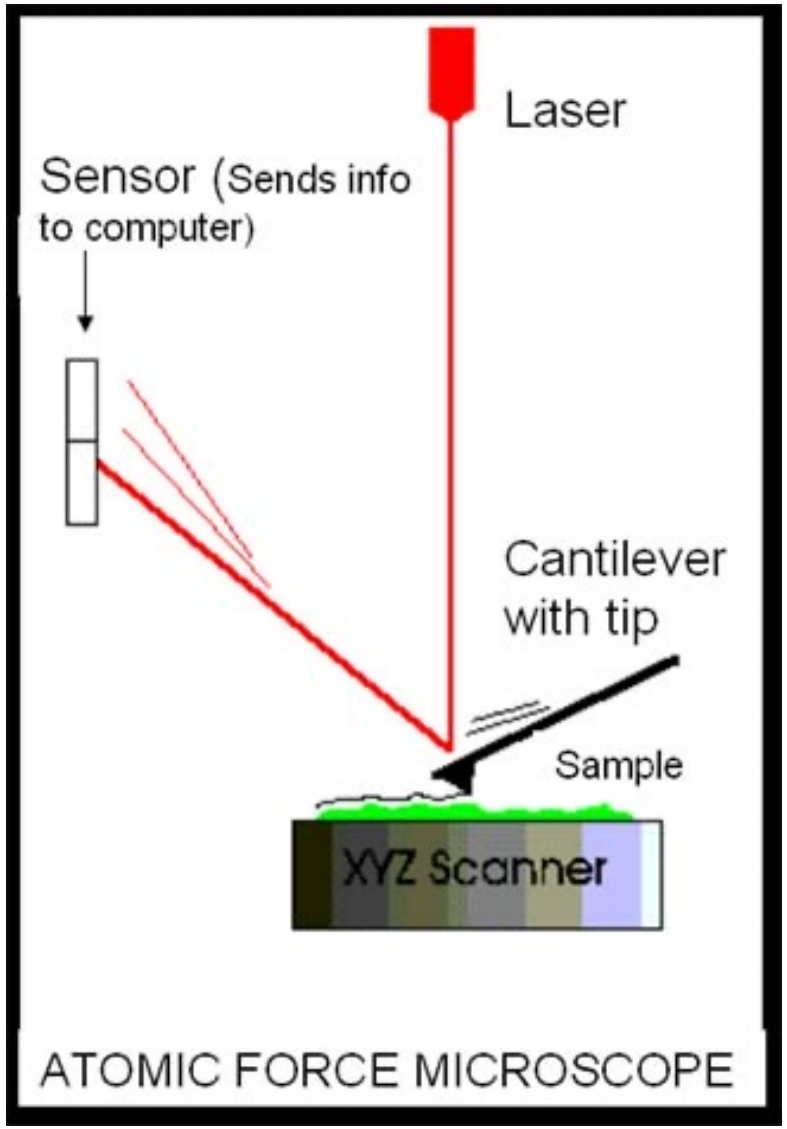

Detection of the cantilever position:

- optical:

  a laser beam is reflected from the back-side of the cantilever onto a four quadrant photodiode

Atomic Force Microscope

Other deflection sensors

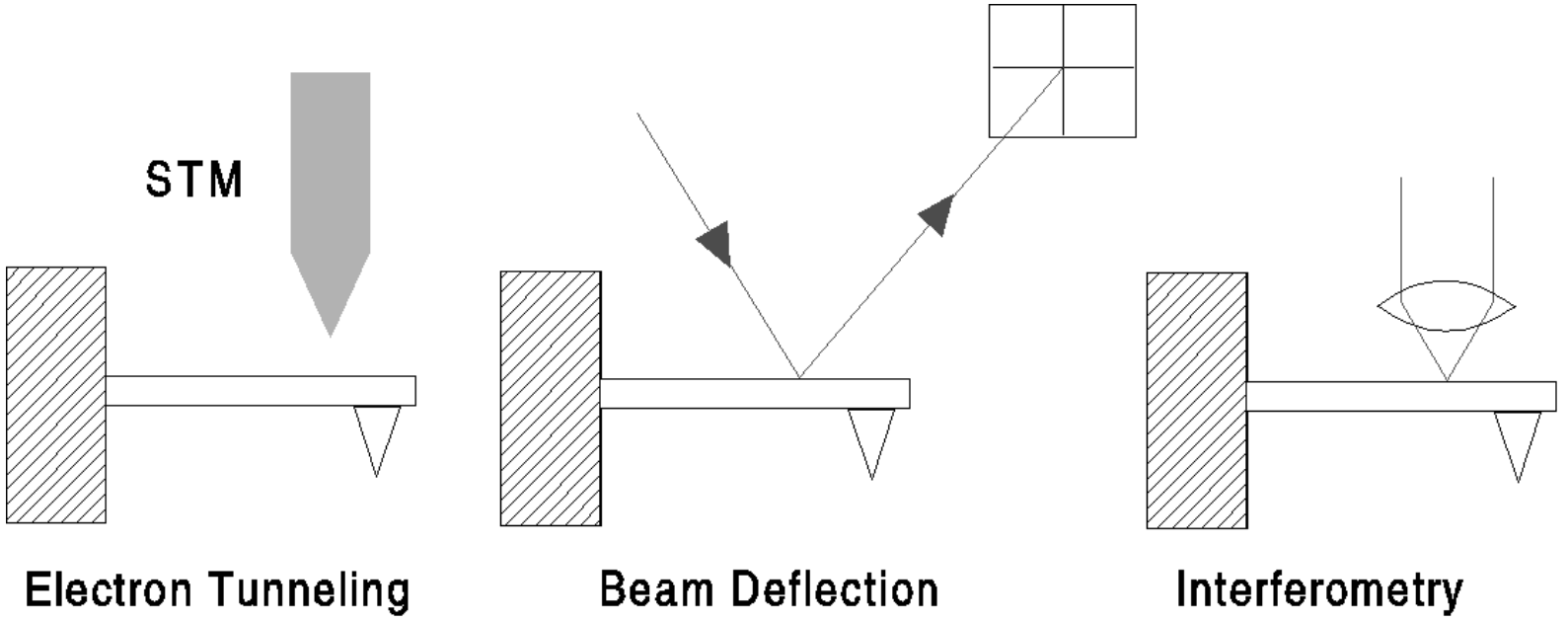

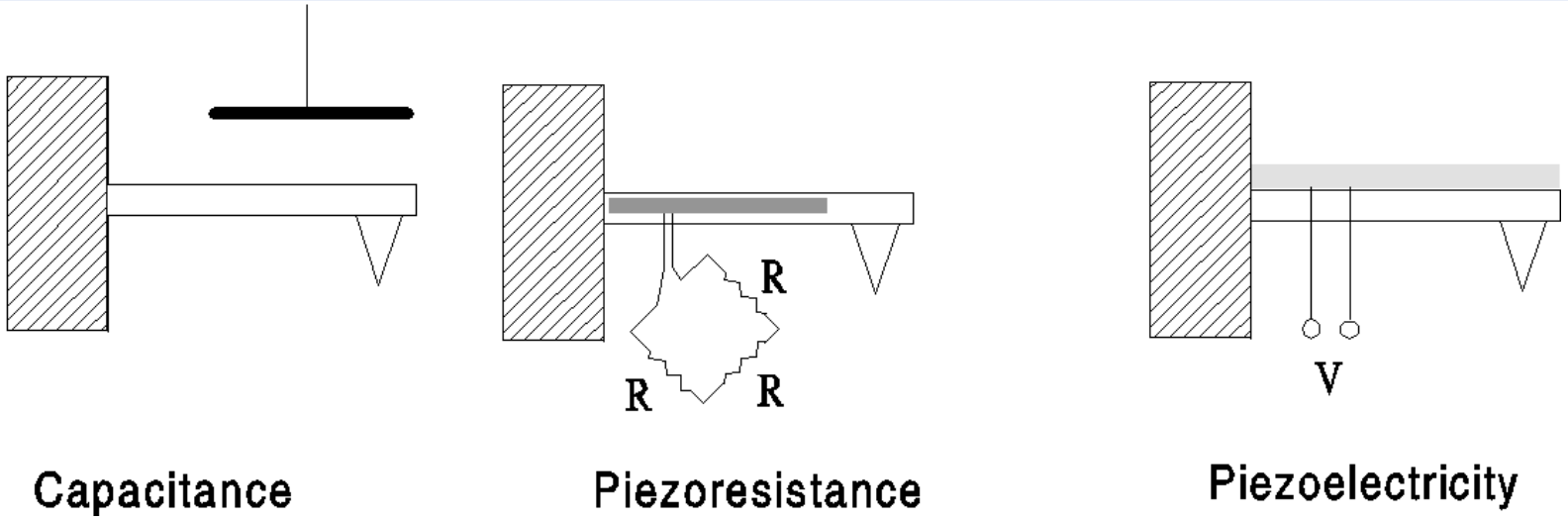

Scanning probe microscopy - SPM

Atomic Force Microscope

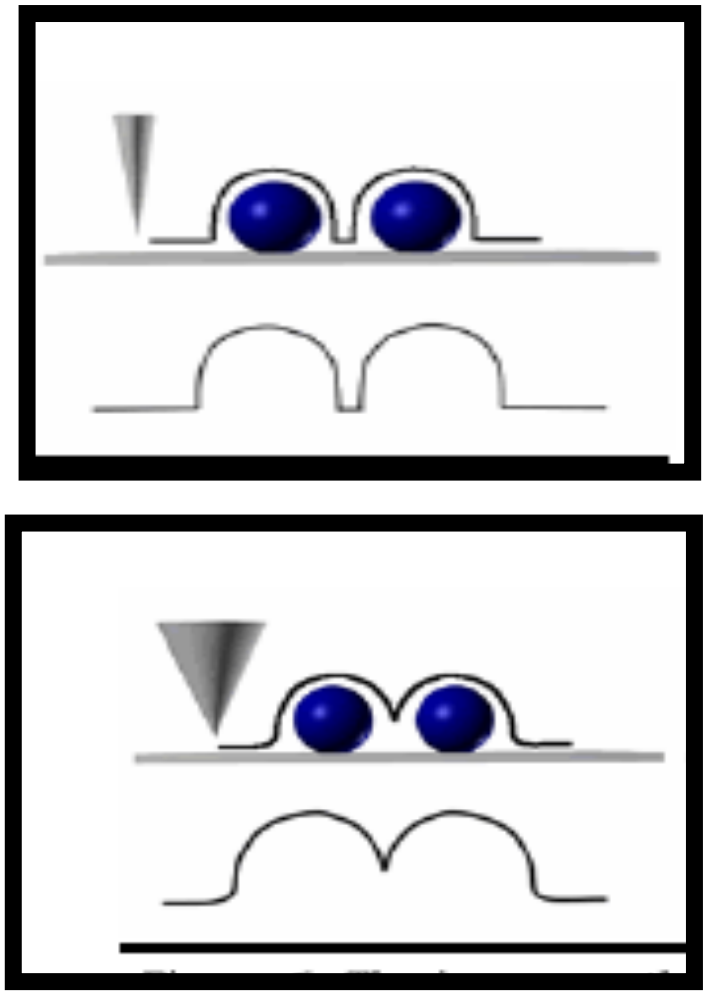

The tip radius determines the resolution of the image

!!! Careful with tip artifacts in the imaging !!!

Atomic Force Microscope

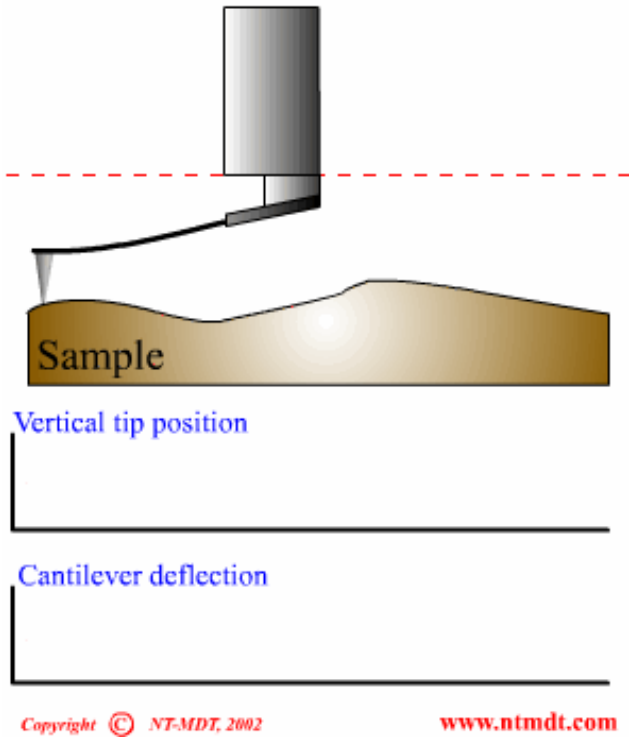

Contact mode

Cantilever in repulsive force regime

Constant height mode

The cantilever bending corresponds directly to the topography

pelicula de: http://www.ntmdt.ru/SPM-Techniques/Principles/

Atomic Force Microscope

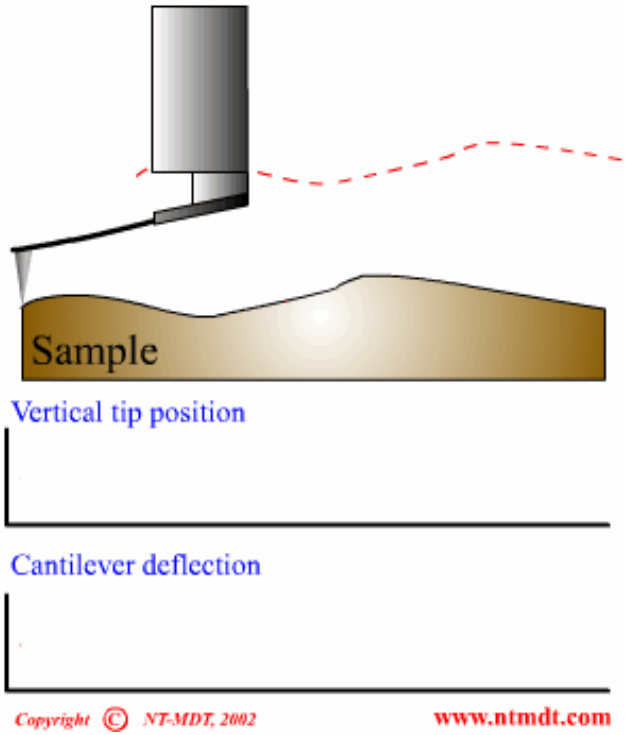

Contact mode

Cantilever in repulsive force regime

Constant force mode

A feedback circuit adjusts the height of the cantilever to maintain the bending of the cantilever.

pelicula de: http://www.ntmdt.ru/SPM-Techniques/Principles/

Atomic Force Microscope

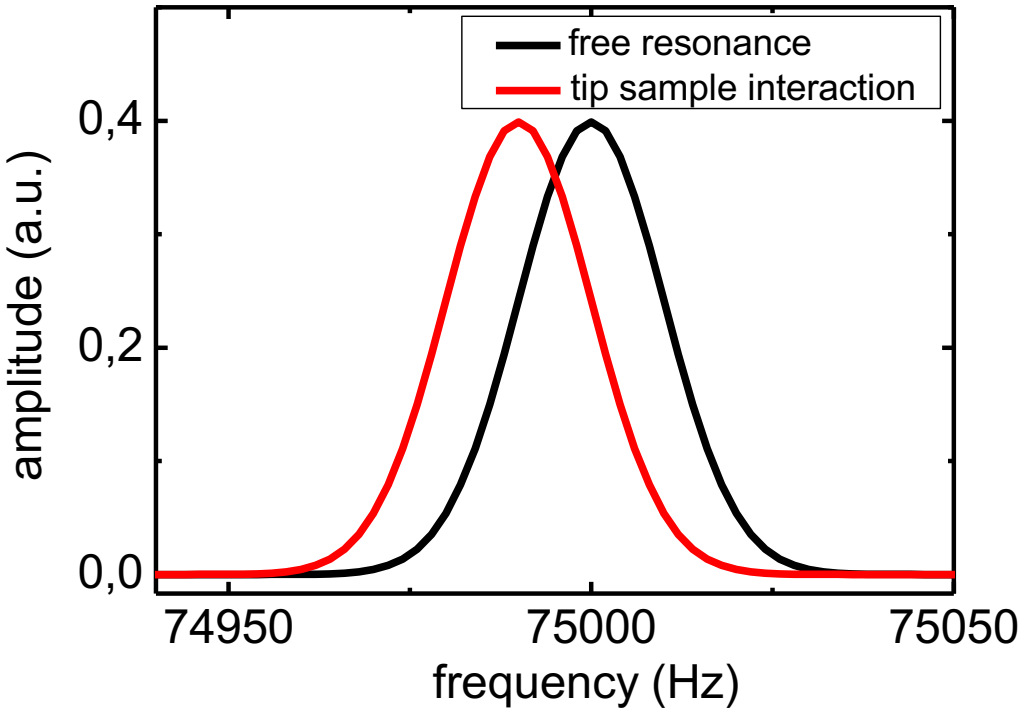

Non-contact mode

The cantilever oscillates close to its resonance frequency:

$$f_0 = \frac{1}{2\pi}\sqrt{\frac{k}{m^*}}$$

Force between tip and sample

$$\Rightarrow \quad \Delta f_0 = -\frac{f_0}{2k}\frac{\partial F}{\partial z}$$

In air: amplitude modulation technique

In vacuum: frequency modulation technique

Atomic Force Microscope

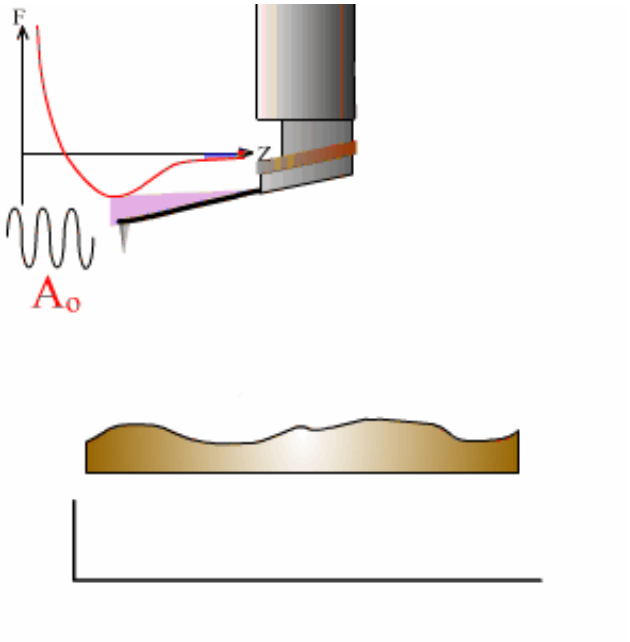

Non-contact mode

The cantilever oscillates close to its resonance frequency

Amplitude modulation technique

The tip-sample forces change the amplitude of the oscillation.

A feedback controls the vertical position of the cantilever to maintain the amplitude.

pelicula de: http://www.ntmdt.ru/SPM-Techniques/Principles/

Atomic Force Microscope

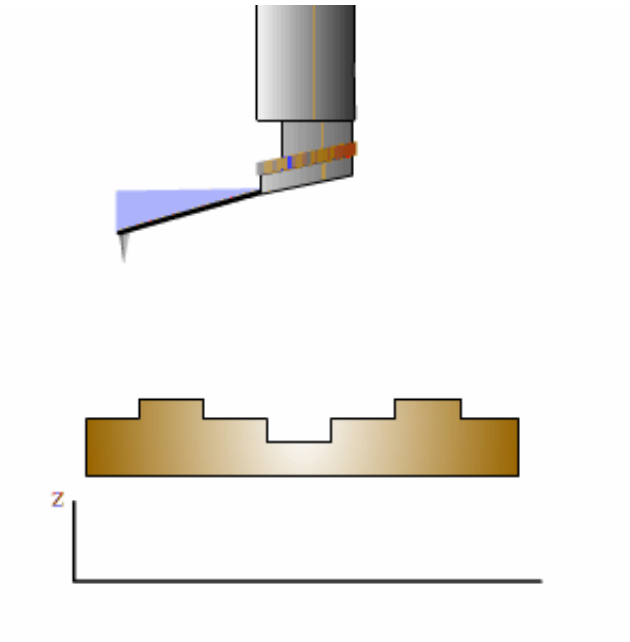

Non-contact mode

The cantilever oscillates close to its resonance frequency

Frequency modulation technique

The tip-sample forces change the resonance frequency of the cantilever.

A feedback controls the vertical position of the cantilever to maintain the resonance frequency.

pelicula de: http://www.ntmdt.ru/SPM-Techniques/Principles/

Scanning probe microscopy - SPM

Atomic Force Microscopy

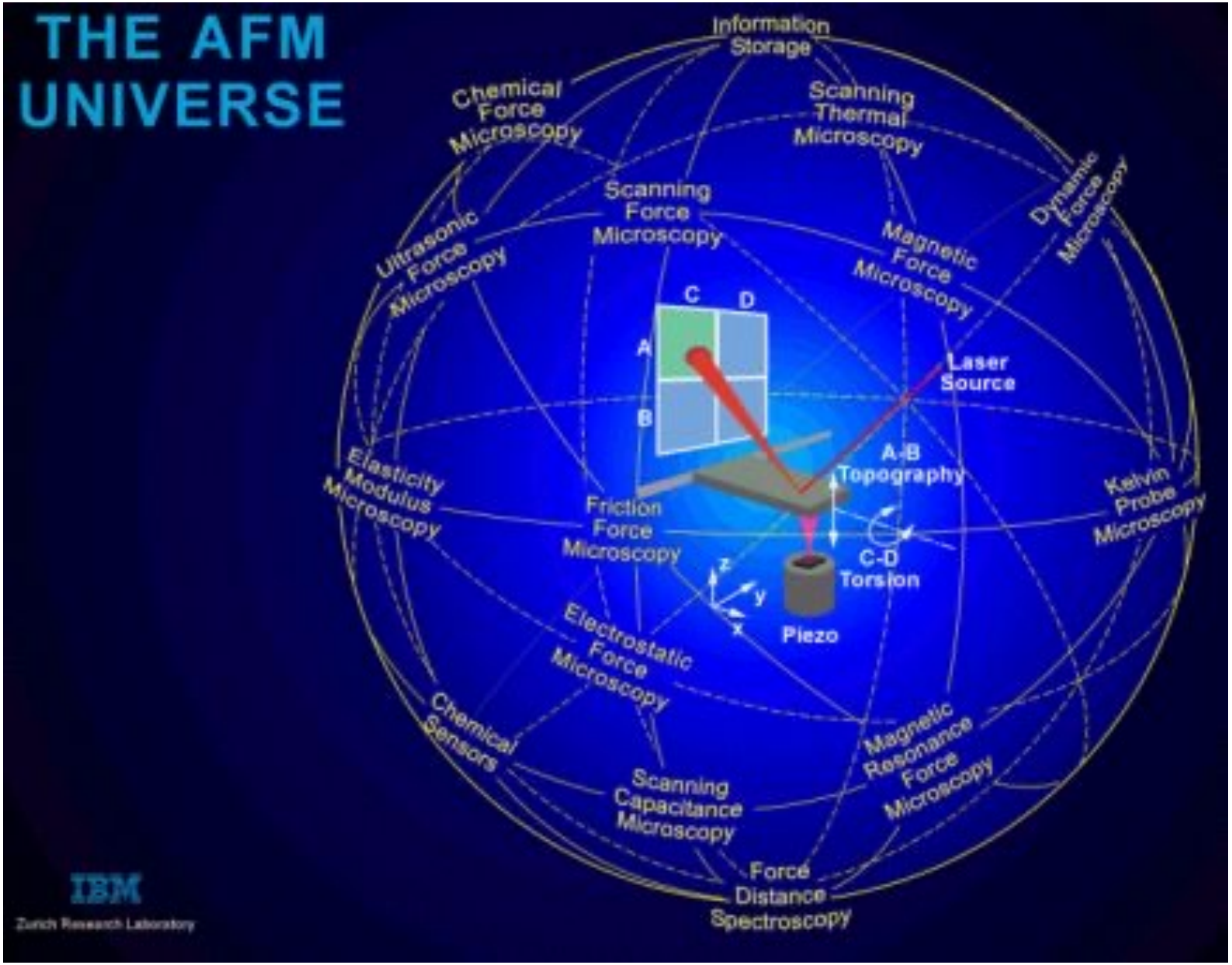

Kelvin probe force microscopy - KPFM

Contact potential difference

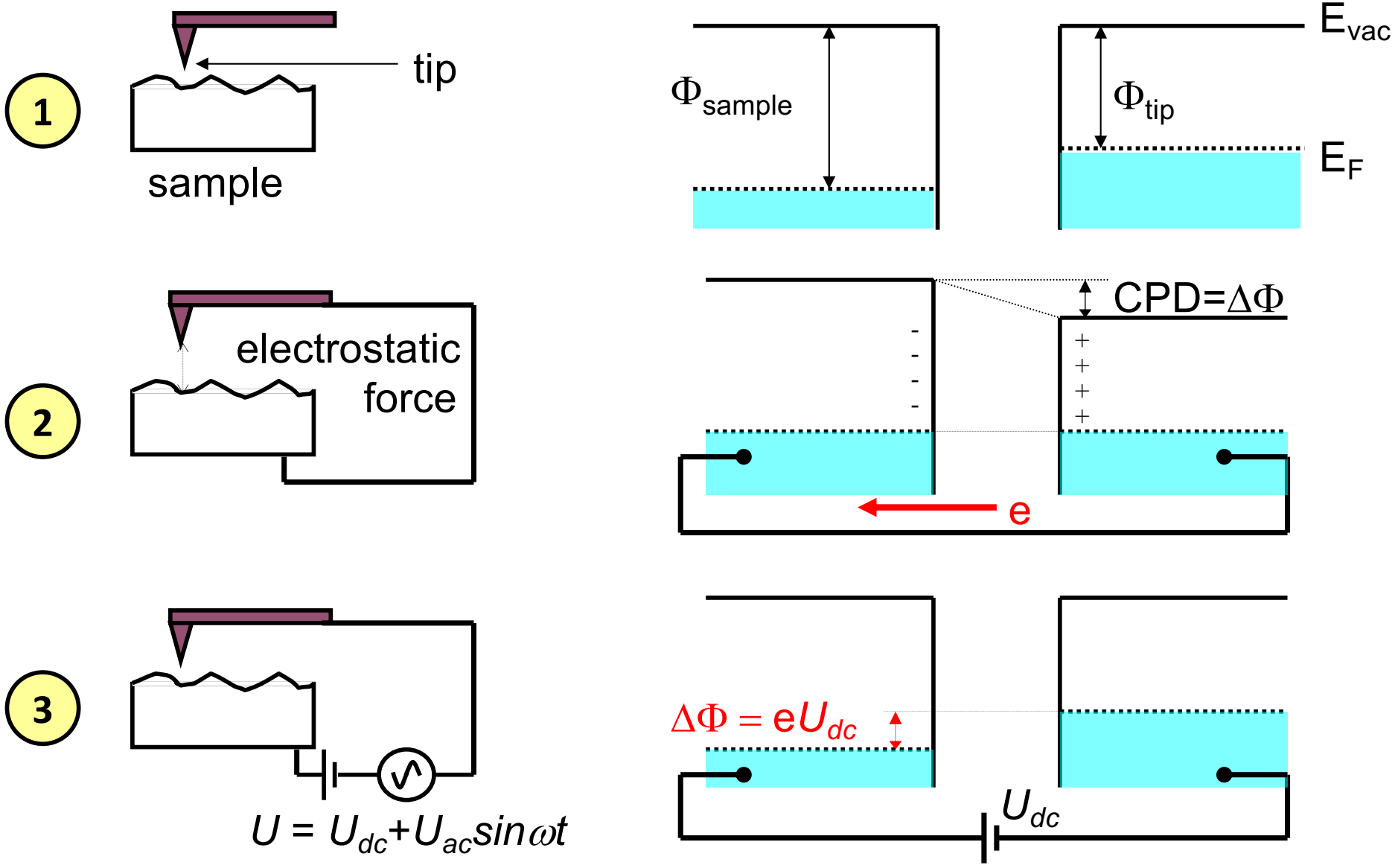

Kelvin probe force microscopy - KPFM

in UHV ($p < 10^{-10}$ mbar)

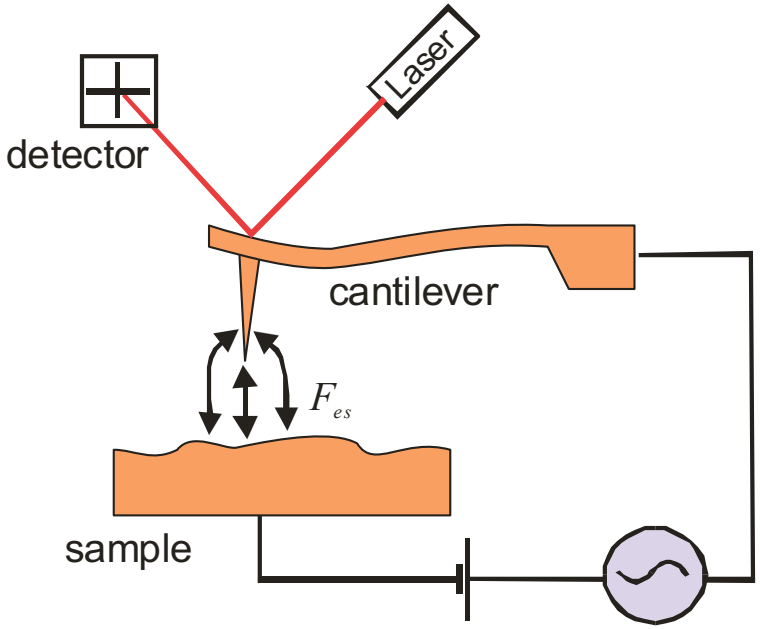

$$V(t) = (V_{dc} - \Delta\Phi / e) + V_{ac} \sin(\omega t)$$

$$\Phi_{sample} = \Phi_{tip} + e \cdot V_{dc}$$

tip calibration on HOPG

electrostatic force:

$$F_{es} = -\frac{1}{2}\frac{\partial C}{\partial z}U(t)^2 = F_{dc} + F_{\omega} + F_{2\omega}$$

$$F_{dc} = -\frac{\partial C}{\partial z}\left[\frac{1}{2}\left(U_{dc} - \Delta\Phi / e\right)^2 + \frac{U_{ac}^2}{4}\right]$$

⟶ crosstalk to topography

$$F_{\omega} = -\frac{\partial C}{\partial z}\left[\left(U_{dc} - \Delta\Phi / e\right)U_{ac}\sin(\omega t)\right]$$

⟶ contact potential difference

$$F_{2\omega} = +\frac{\partial C}{\partial z}\frac{U_{ac}^2}{4}\cos(2\omega t)$$

⟶ capacitance spectroscopy

Kelvin probe force microscopy - KPFM

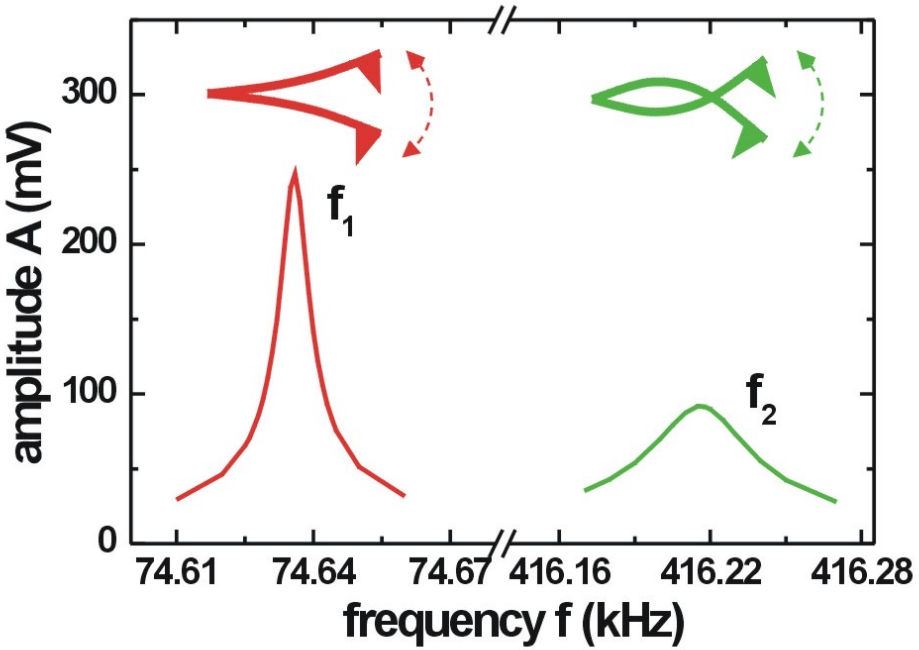

- ac-frequency ω at the **second resonance** (f_2) of the cantilever
- detection of the oscillation amplitude A_ω with a Lock-In
- **A_ω is proportional to F_ω**
- limiting factor: bandwidth of the photodiode

$$F_\omega = -\frac{\partial C}{\partial z}\left[\left(U_{dc} - \Delta\Phi / e\right)U_{ac}\sin(\omega t)\right]$$

Kelvin probe force microscopy - KPFM

KPFM detection is sensitive on electrostatic forces

→ long range interaction

→ lateral averaging affects spatial resolution

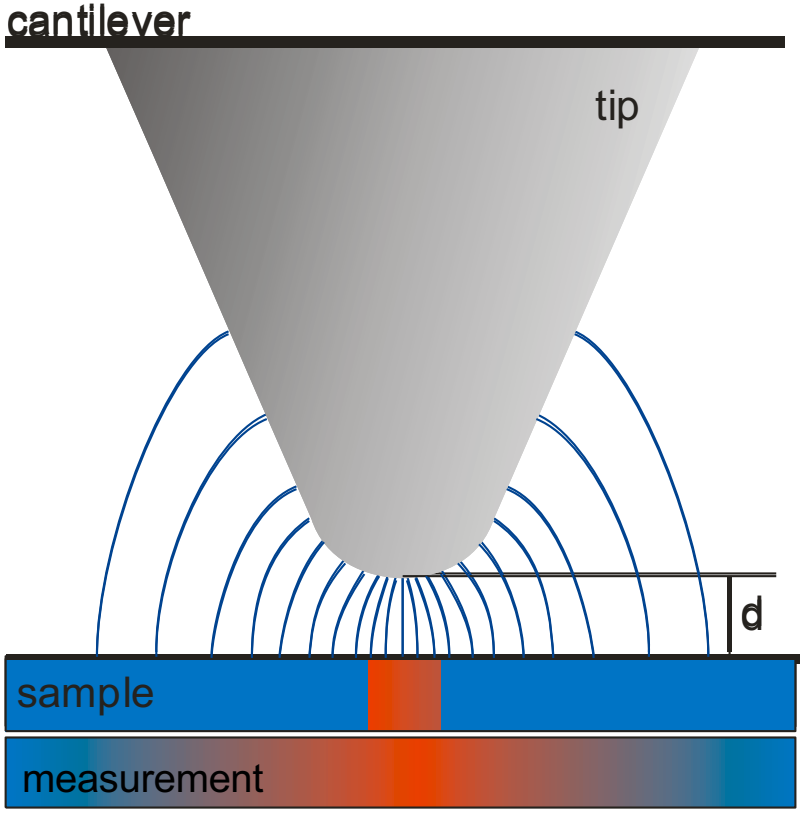

Simulation:

- Finite element methods to describe field distribution
- summation over hole tip area
- metallic surfaces

Sadewasser *et al.*, Appl. Surf. Sci. **210**, 32 (2003).

Leendertz *et al.*, Appl. Phys. Lett. 89, 113120 (2006).

Kelvin probe force microscopy - KPFM

Three examples:

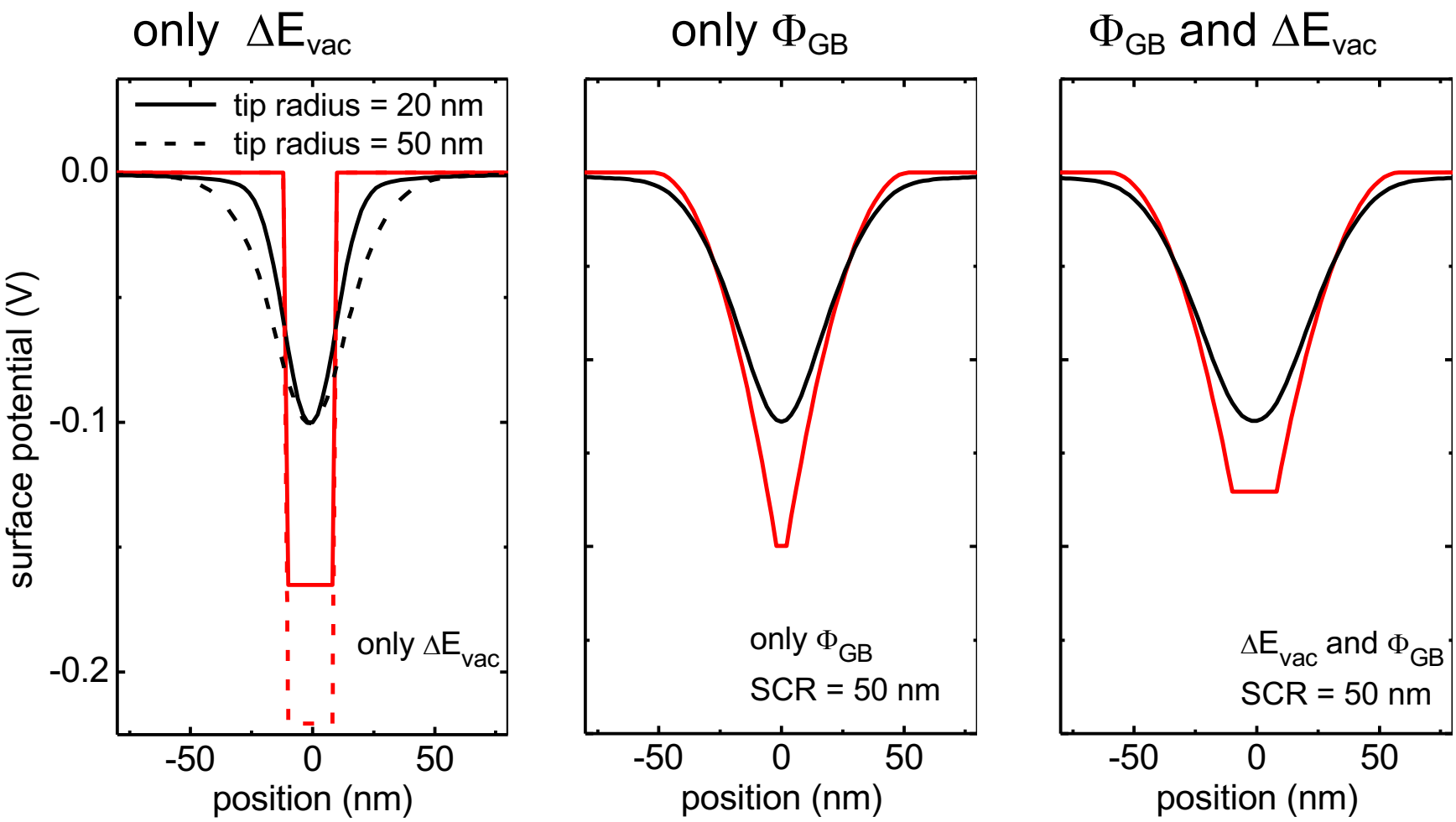

peak height

~ 45% – 61%

~ 67%

~ 78%

→ simulated KPFM peak shape very similar for all 3 cases

Band bending at semiconductor surfaces and interfaces

- **Surface**

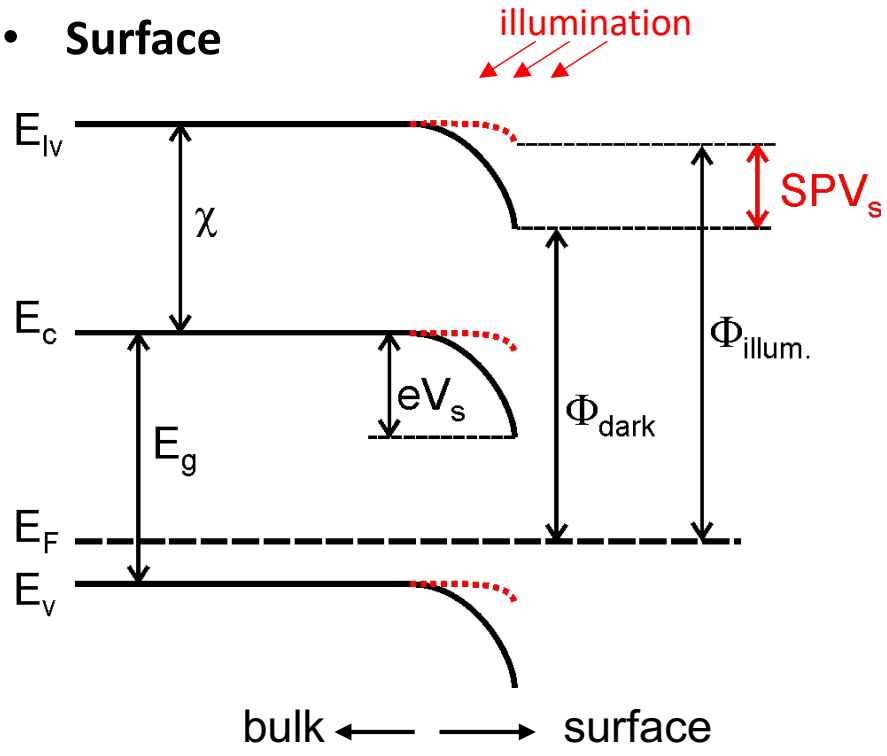

- **Interface**

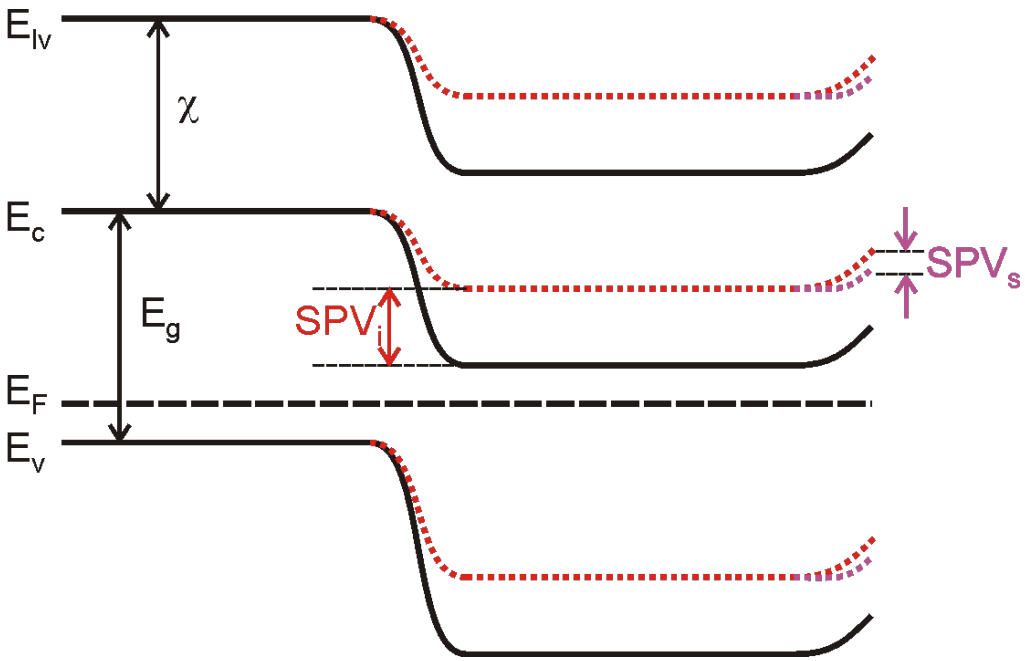

- SPV gives information about surface band bending

- Interface band bending contributes to SPV
- $SPV_{total} = SPV_{interface} + SPV_{surface}$

Kronik & Shapira, *Surf. Sci. Rep. 37, 1 (1999).*

Part II:
Grain boundaries in chalcopyrites photovoltaic materials

Motivation

Solar cells based on chalcopyrite materials $Cu(In,Ga)(Se,S)_2$

- efficiency up to 23.35% [1]
- Band gap in visible spectrum (1.04 – 2.43 eV)
- Short absorption length: (α^{-1} ~ 100 nm)
- Stack of 5 different polycrystalline materials with layer thicknesses from 5 - 2000 nm

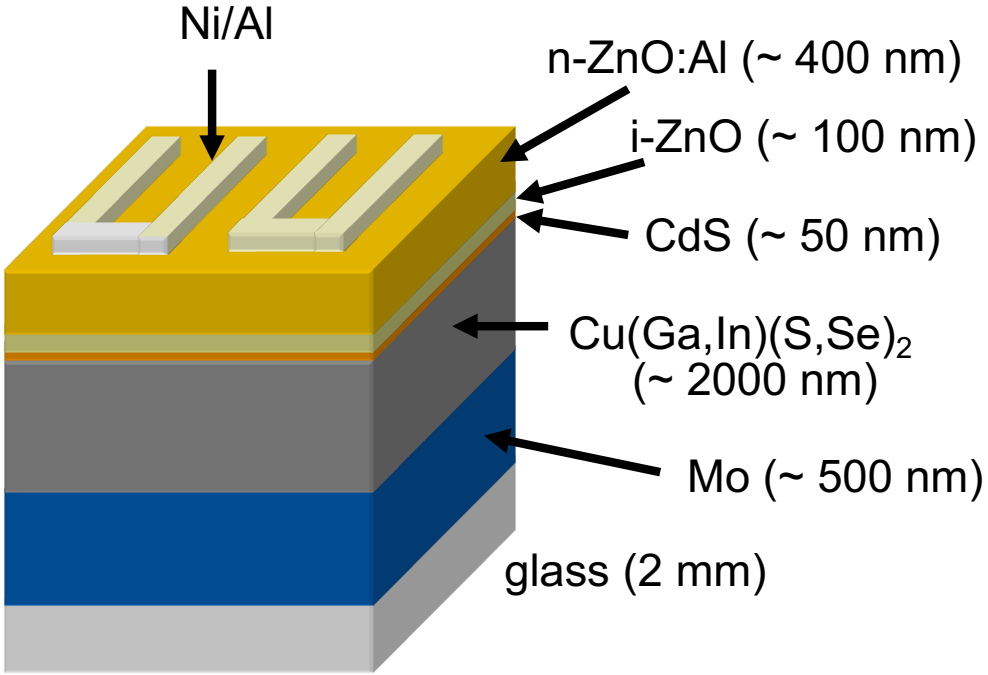

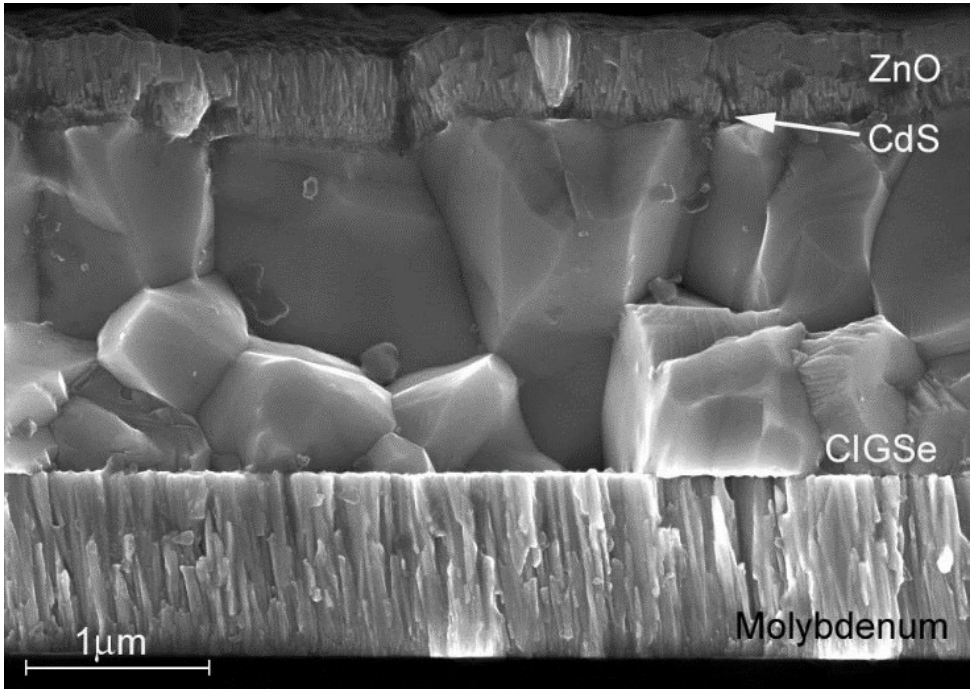

From: R. Klenk, M.Ch. Lux-Steiner in Thin film solar cells - fabrication, characterization (2006).

[1] http://www.solar-frontier.com/eng/news/2019/0117_press.html

Motivation – KPFM on chalcopyrite materials

- high efficiency for polycrystalline chalcopyrite solar cells: $Cu(In,Ga)(Se,S)_2$ despite the presence of grain boundaries
- pn-junction at hetero contact chalcopyrite/CdS

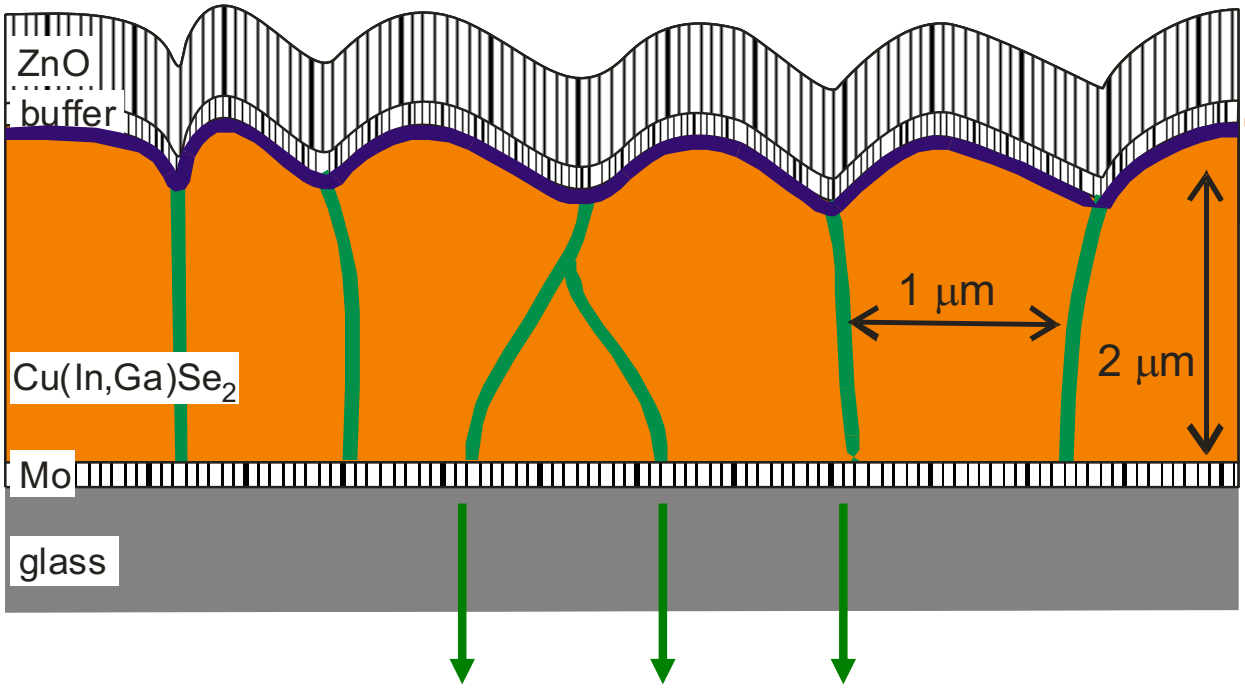

effects at the absorber surface ?

effects at the grain boundaries ?

Previous Results – Polycrystalline Samples

$CuGaSe_2$: CVD growth and peel-off in UHV, rear-side images

topography

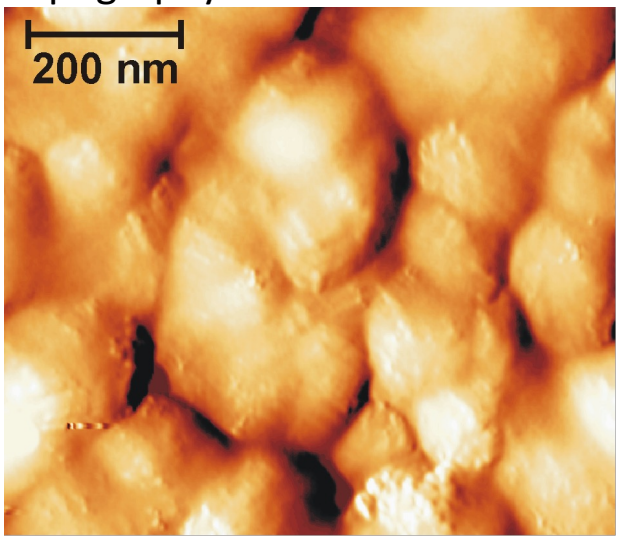

work function, dark

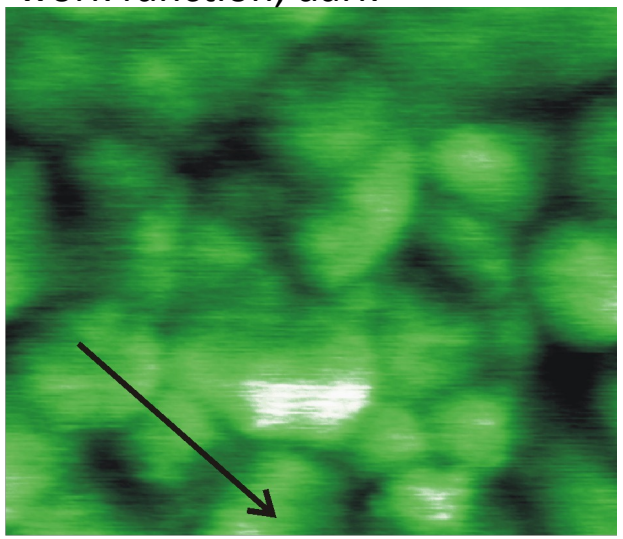

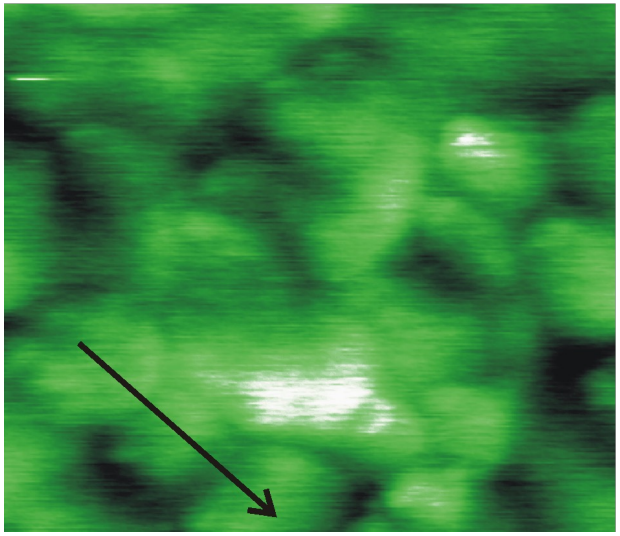

work function, illuminated

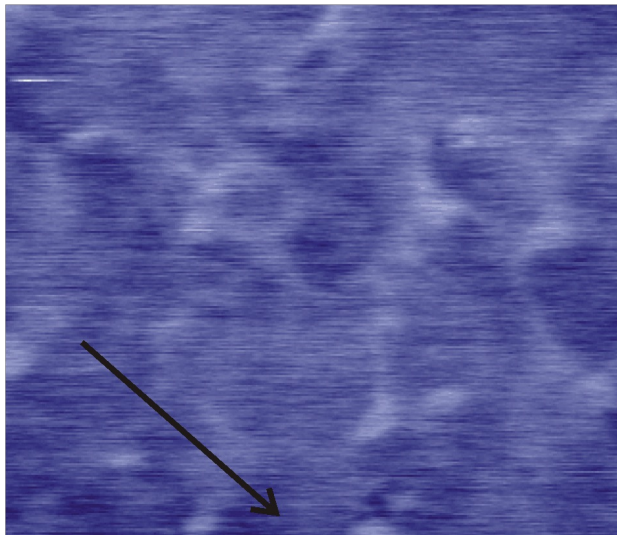

SPV image

Fuertes Marrón *et al.*, Phys. Rev. B **71**, 033306 (2005).

Previous Results – Polycrystalline Samples

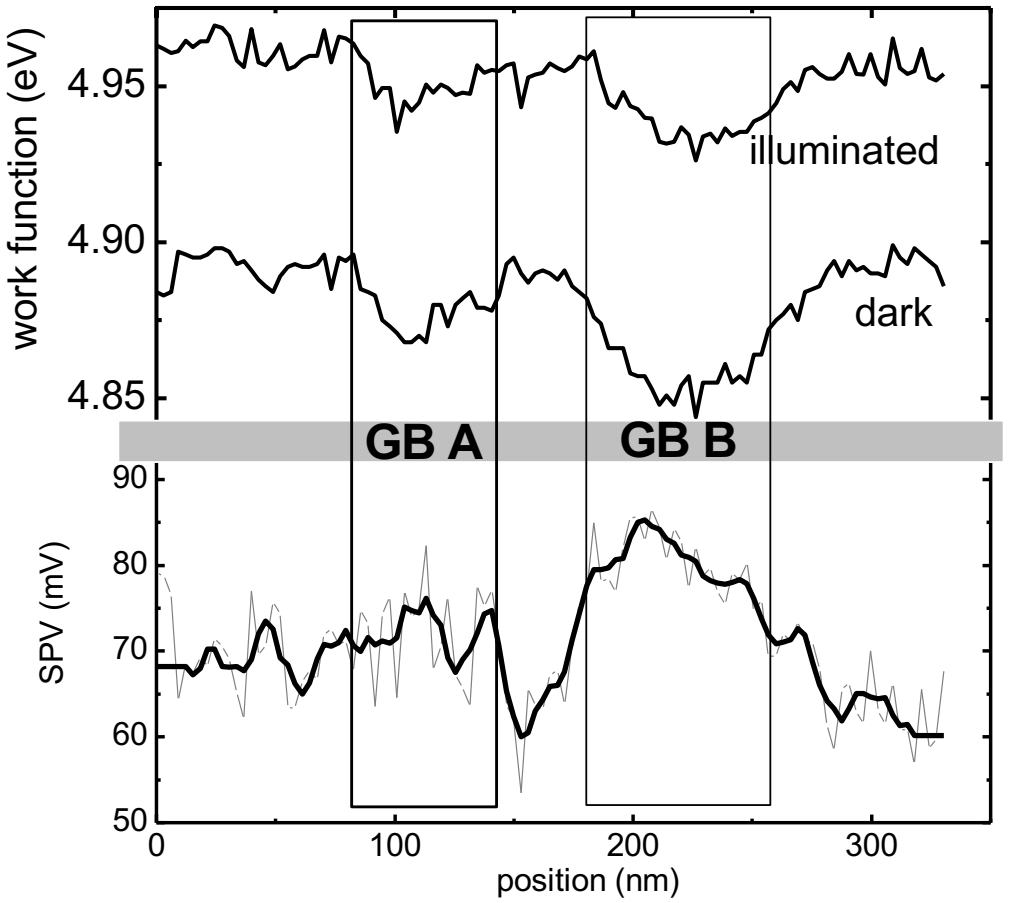

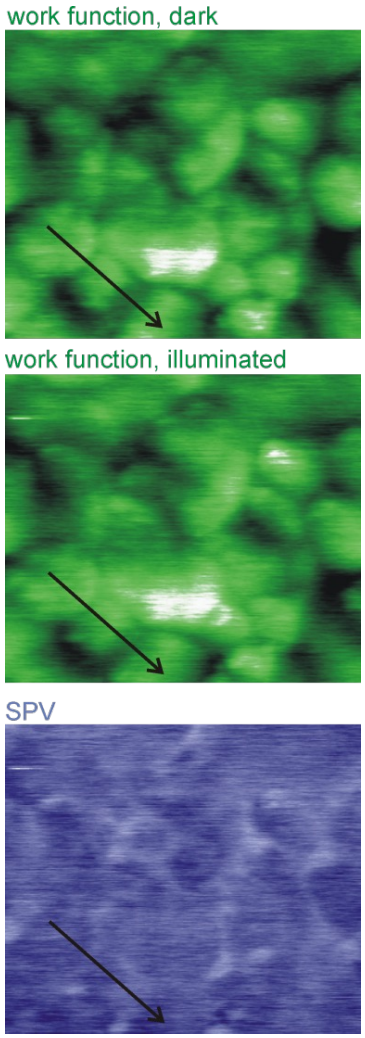

- Grain boundaries show potential drop
- Different potential drop for different grain boundaries
- Different electronic activity for different grain boundaries

Fuertes Marrón *et al.*, Phys. Rev. B **71**, 033306 (2005).

How can we learn more about the GB properties ?

→ Combine macroscopic and microscopic methods

Electron back scatter diffraction: local structural information

Resistance + Hall-effect: carrier type, concentration and mobility

KPFM: local surface potential

Problem:

→ how to provide electrical contact

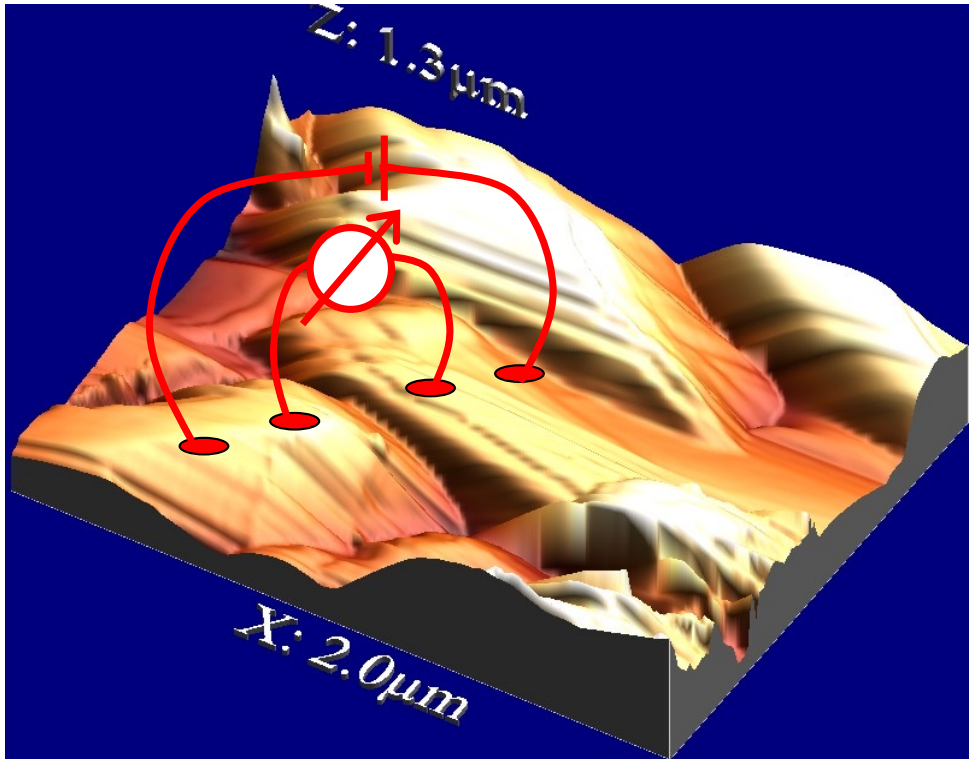

Bicrystal model structures

Approach: $CuGaSe_2$ growth on a GaAs wafer with a single grain boundary

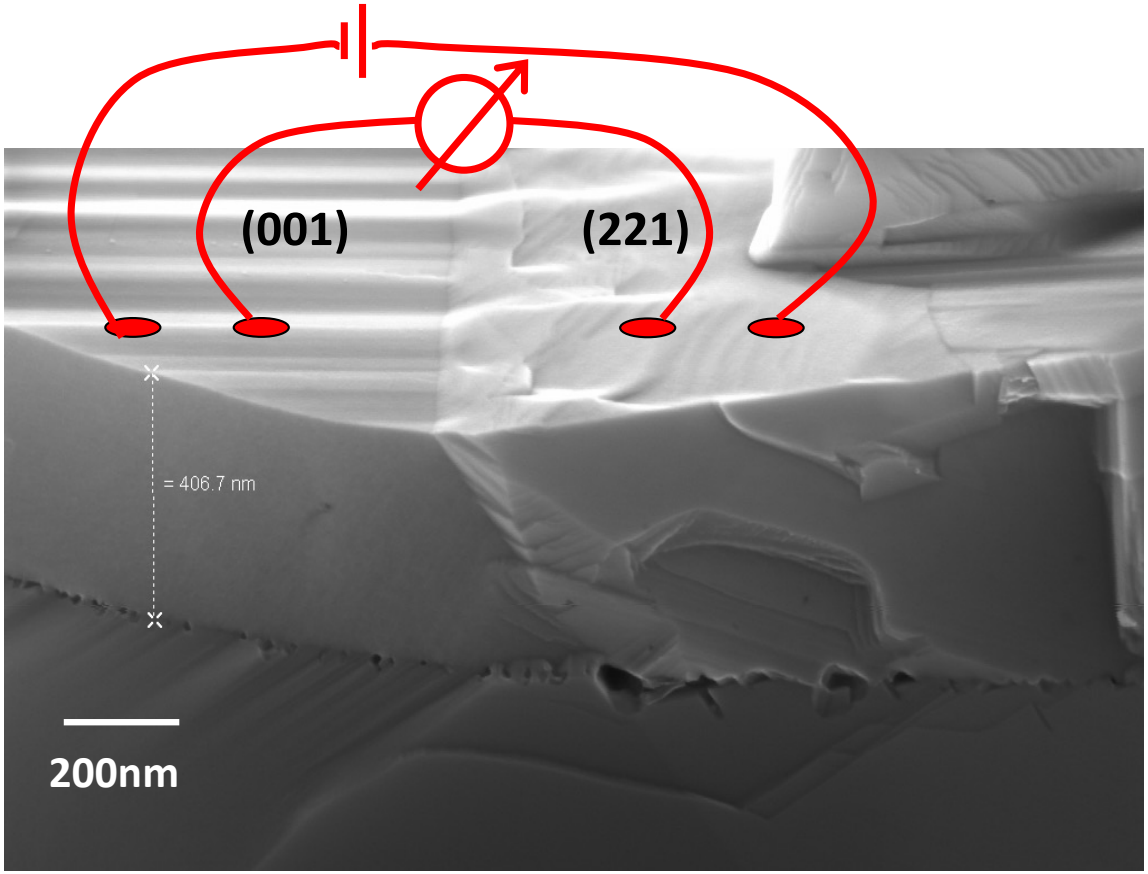

→ mm-size grains !

twin grain boundary, Σ3

grain boundary

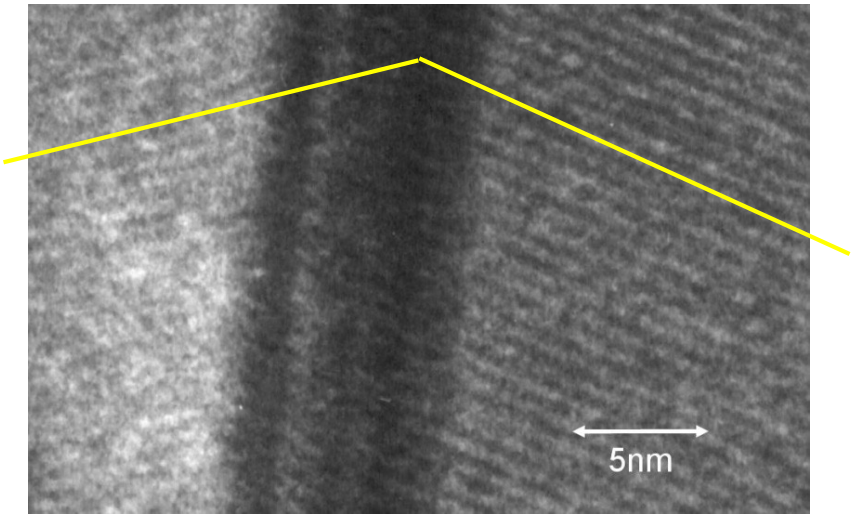

HR-TEM

→ Successful growth of

Σ3 and Σ9 grain boundaries

Siebentritt, Sadewasser *et al.*, Phys. Rev. Lett. **97**, 146601 (2006).

Σ3 grain boundary - KPFM

Siebentritt, Sadewasser *et al.*, Phys. Rev. Lett. **97**, 146601 (2006).

Topography:

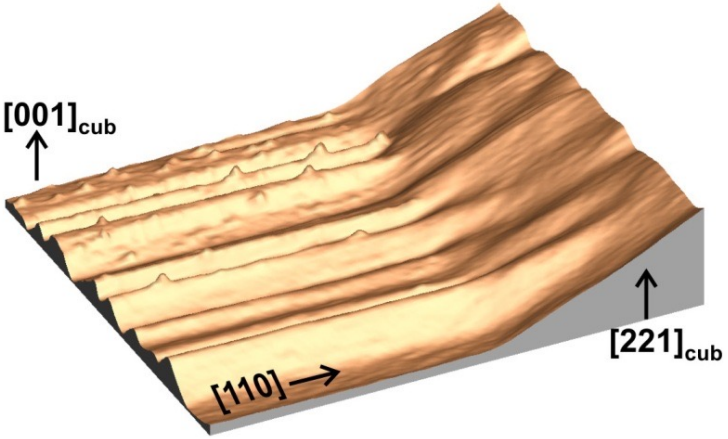

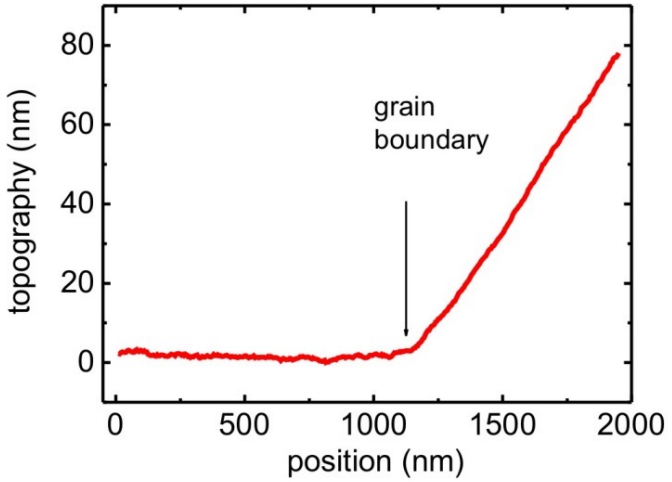

Work function:

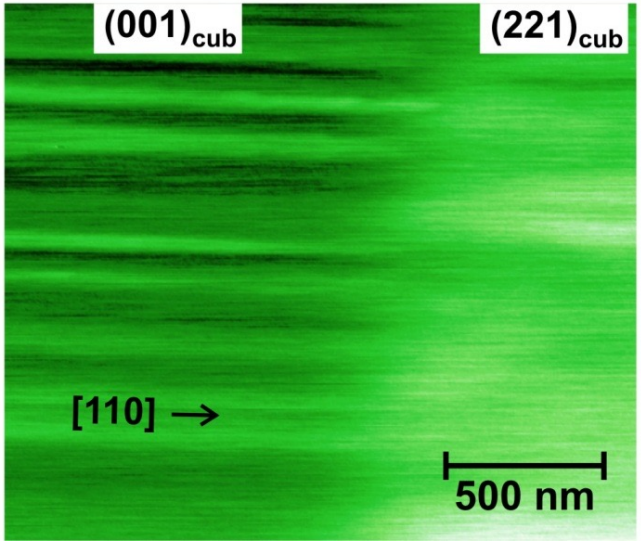

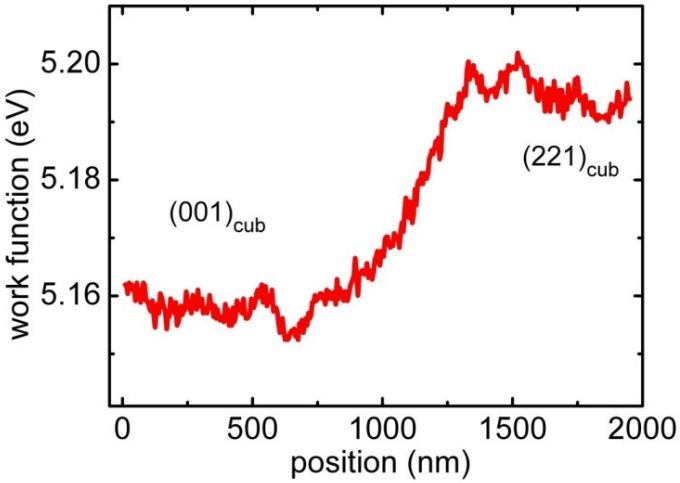

No band bending at grain boundary → charge neutral grain boundary

Σ9 grain boundary - KPFM

Hafemeister *et al.*, Phys. Rev. Lett. **104**, 196602 (2010).

Topography:

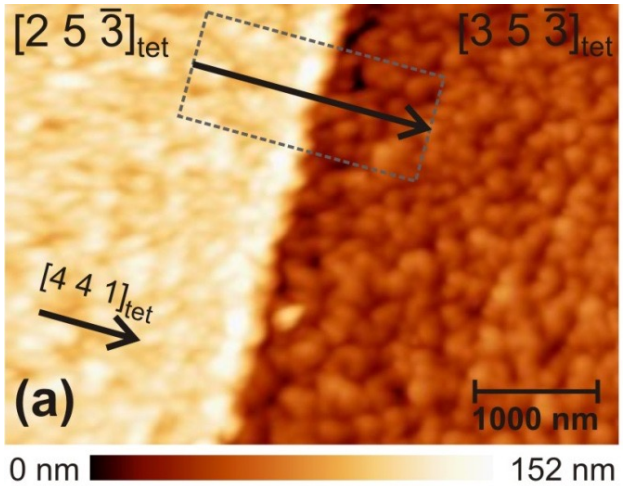

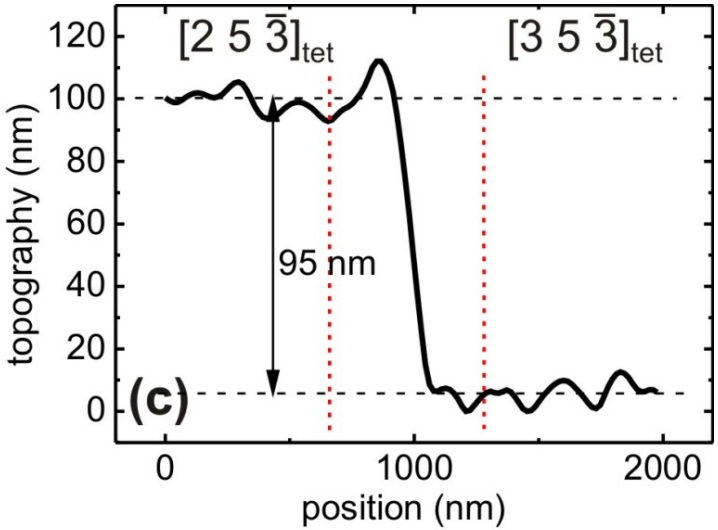

Work function:

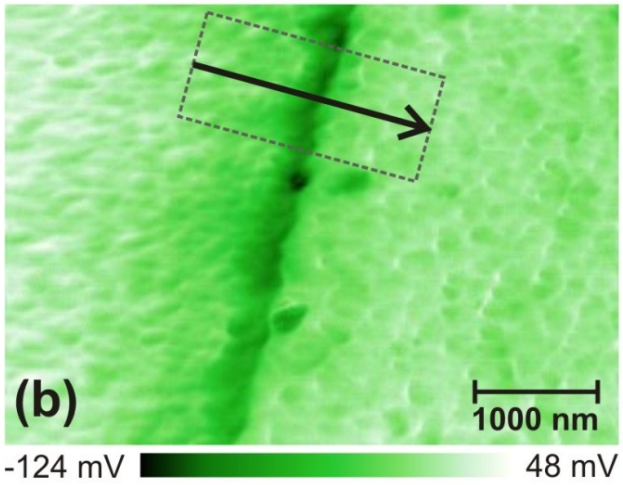

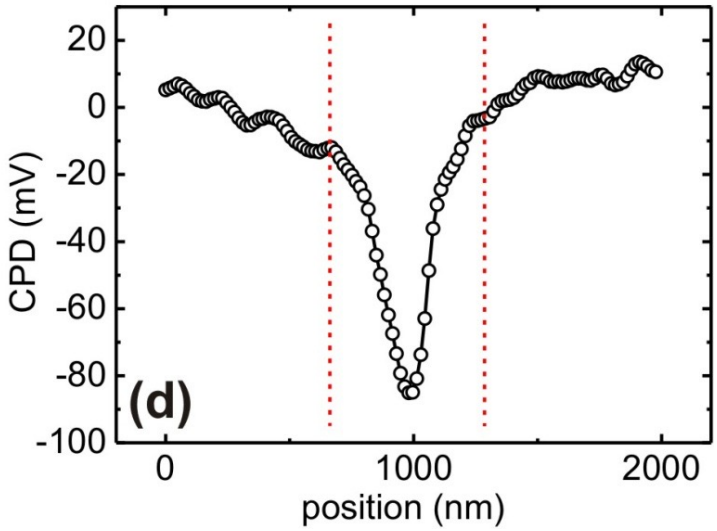

Band bending ~ 90 meV at grain boundary → Presence of charged defect states

Σ3 grain boundary – electrical characterization

Hall-effect

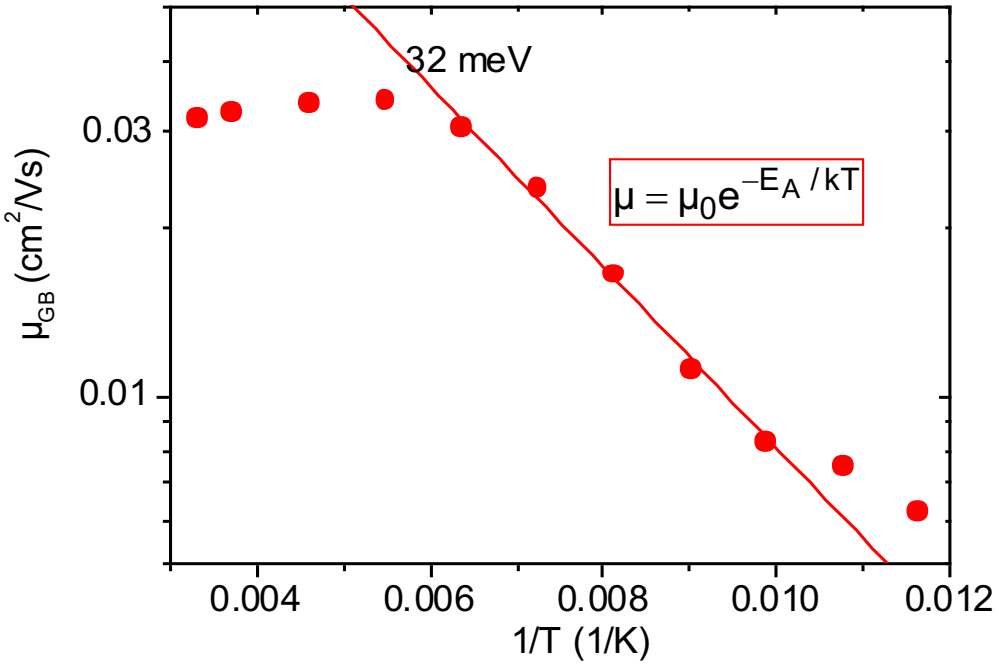

Resistance (T)

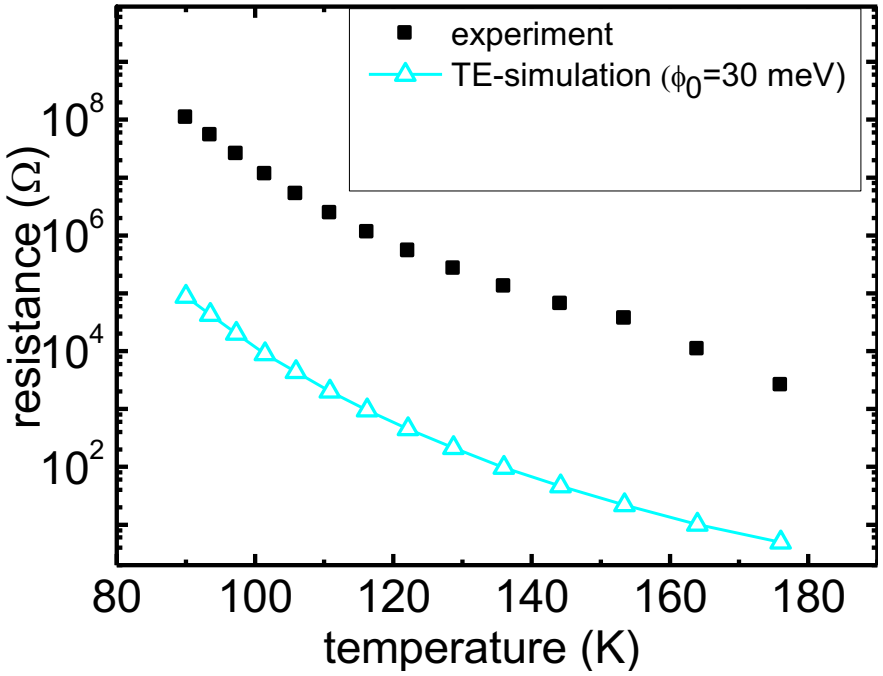

- Hall-effect shows transport barrier of ~30 meV
- Simulation of transport across 30 meV barrier by thermionic emmission:

→ Similar shape, BUT: absolute value too low

Thermionic emission: $$J_{TE} = e^2 pV \left(\frac{1}{2\pi m^* k_B T} \right)^{1/2} \exp\left(\frac{\phi_0}{k_B T} \right)$$

Siebentritt, *et al.*, PRL **97**, 146601 (2006).

Σ9 grain boundary – electrical characterization

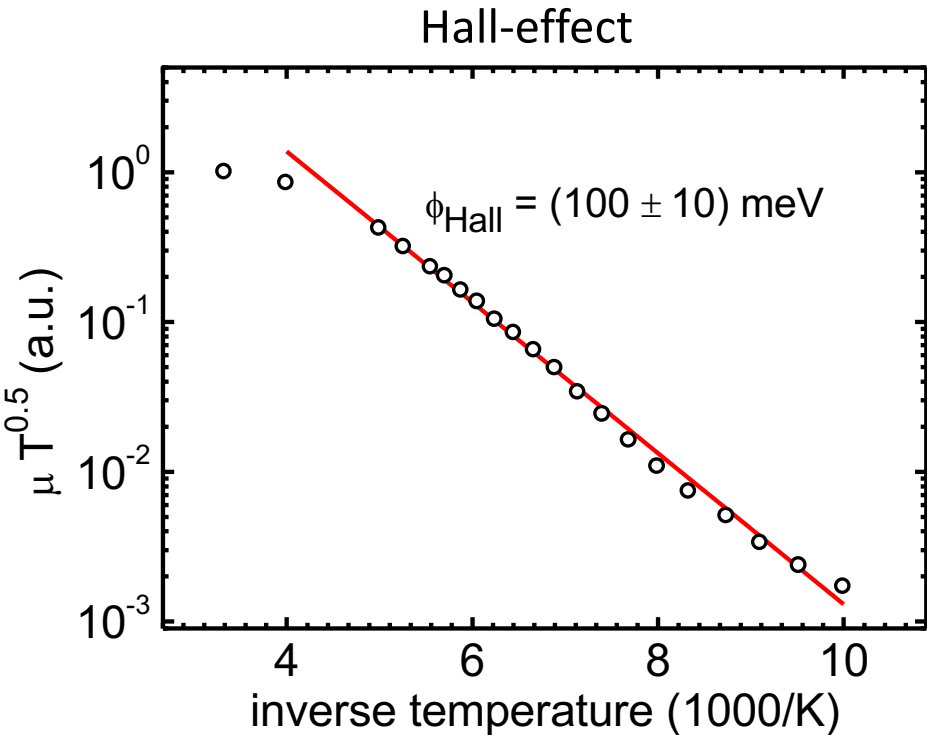

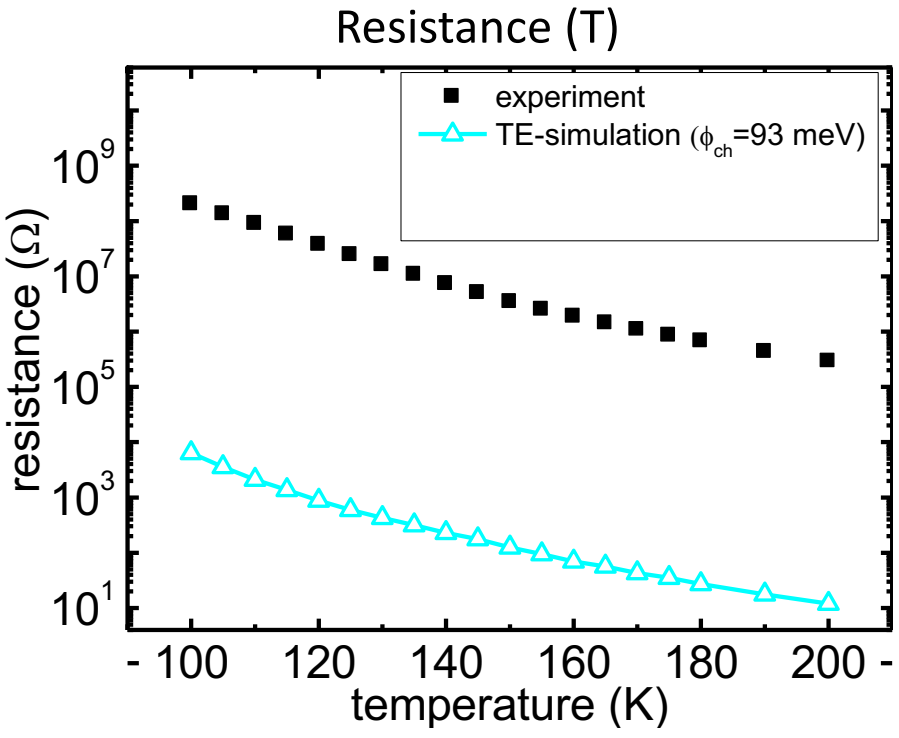

- Hall-effect shows transport barrier of ~100 meV, similar to KPFM
- Simulation of transport across 93 meV barrier by thermionic emmission:

  → Similar shape, BUT: absolute value too low

Hafemeister *et al.*, Phys. Rev. Lett. **104**, 196602 (2010).

Σ9 grain boundary – new model for electronic structure

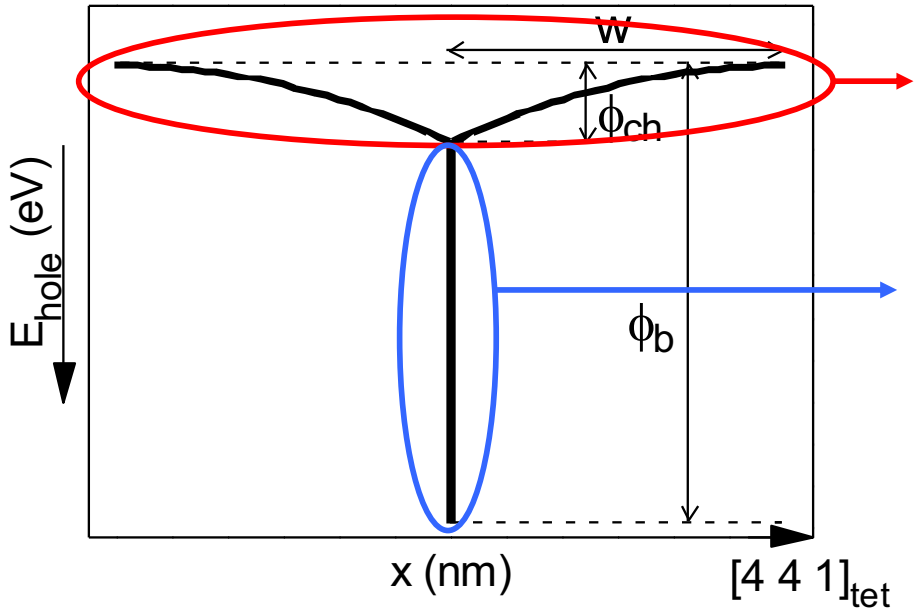

Size and shape from KPFM measurement in agreement with Hall-mobility

New:
Thin and high barrier at grain boundary

Transport across this barrier by thermionic emission and tunneling:

$$J_{total} = J_{TE} + J_T = e^2 p \beta V \left(\frac{\beta}{2\pi m^*} \right)^{1/2} \left[\int_0^{\phi_{ch}} e^{-\beta E} \tau_{SCR}(E) \tau_b(E) dE + \int_{\phi_{ch}}^{\phi_b} e^{-\beta E} \tau_b(E) dE + \int_{\phi_b}^{\infty} e^{-\beta E} dE \right]$$

with: $\beta = (k_B T)^{-1}$

$\tau_{SCR}(E)$: transmission probability for space charge barrier

$\tau_b(E)$: transmission probability for thin barrier

Hafemeister *et al.*, Phys. Rev. Lett. **104**, 196602 (2010).

Results – Barrier Model

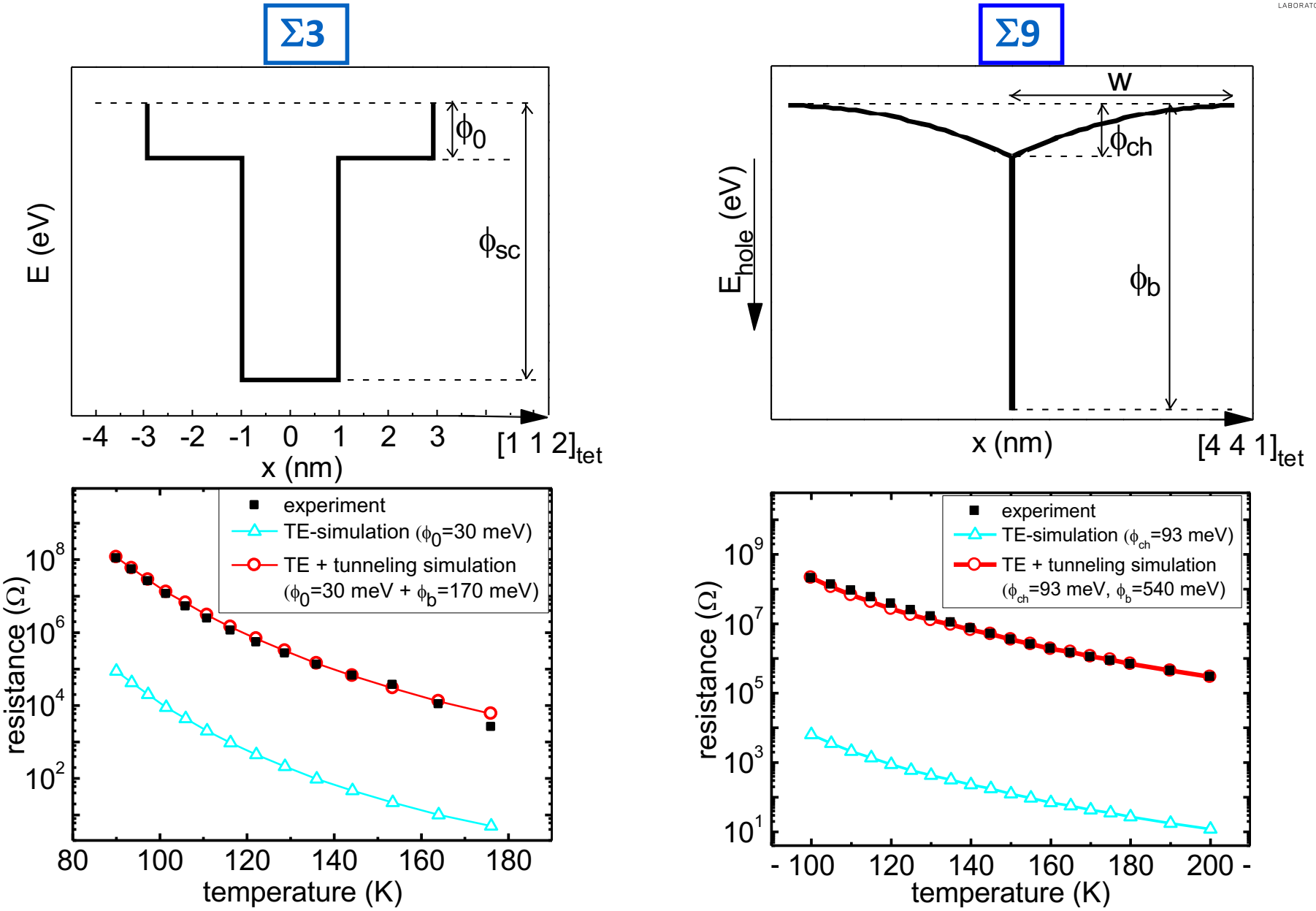

Excellent fit to resistance(T) for electronic structure including thin and high barrier

Results – Grain Boundary Atomic Structure

- Atomic structure different for different orientations
- High hole barrier caused by Cu-depletion, as proposed by Persson & Zunger, PRL **91**, 266401 (2003): barrier ~ 200 – 500 meV
- Space charge region caused by charged defect states

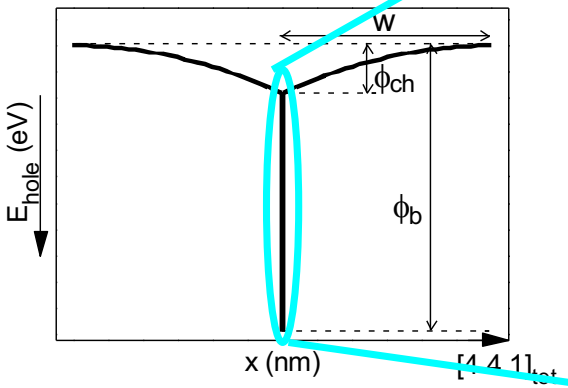

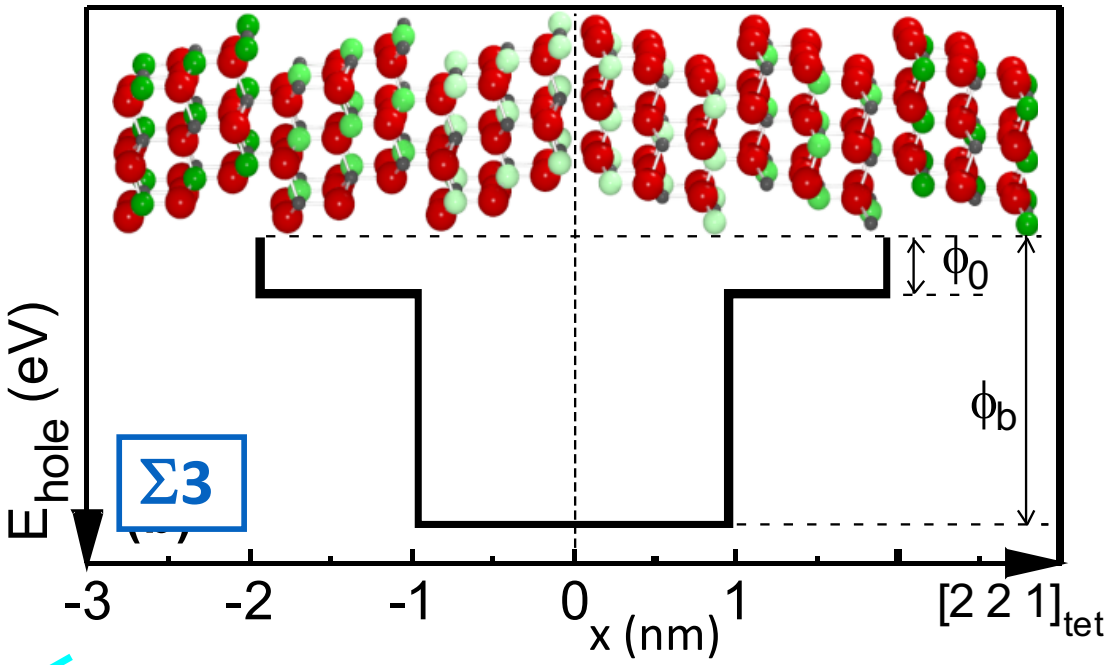

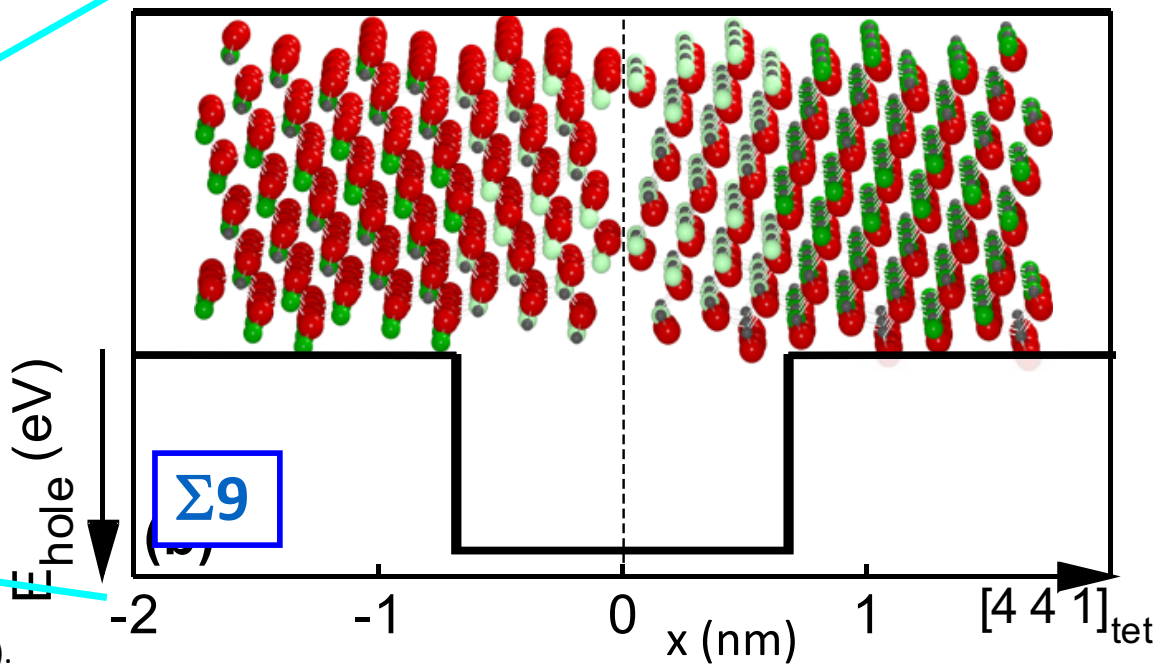

Hafemeister *et al.*, Phys. Rev. Lett. **104**, 196602 (2010).

In-line holography in transmission electron microscopy

→ Determines the mean inner potential

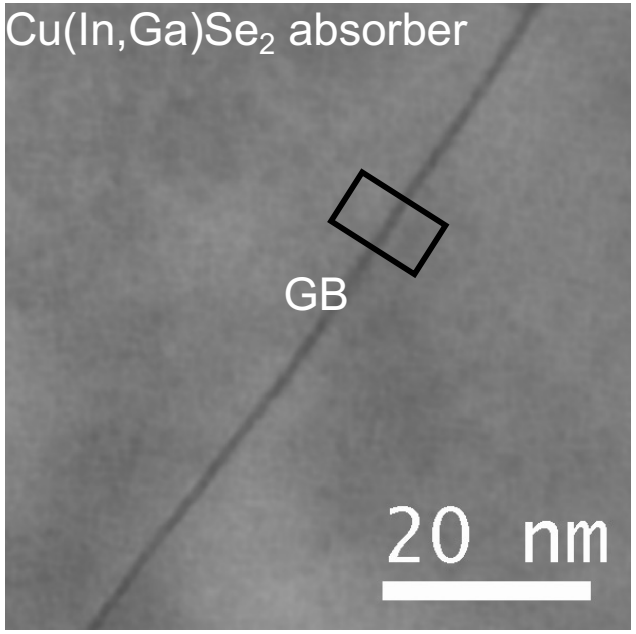

Relative phase Δφ of the electron wave function

profile $\Delta V_{MIP} \approx \Delta\varphi/\sigma t$

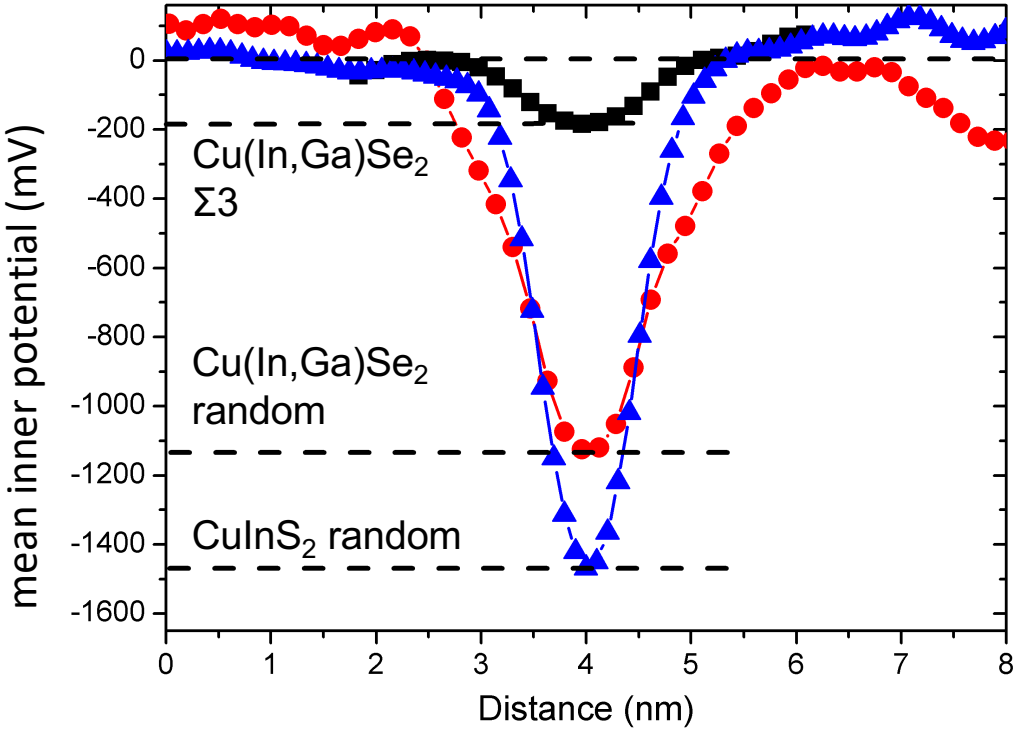

S.S. Schmidt et al., Phys. Rev. Lett. 109, 095506 (2012).

Results – Combining electronic and structure measurement

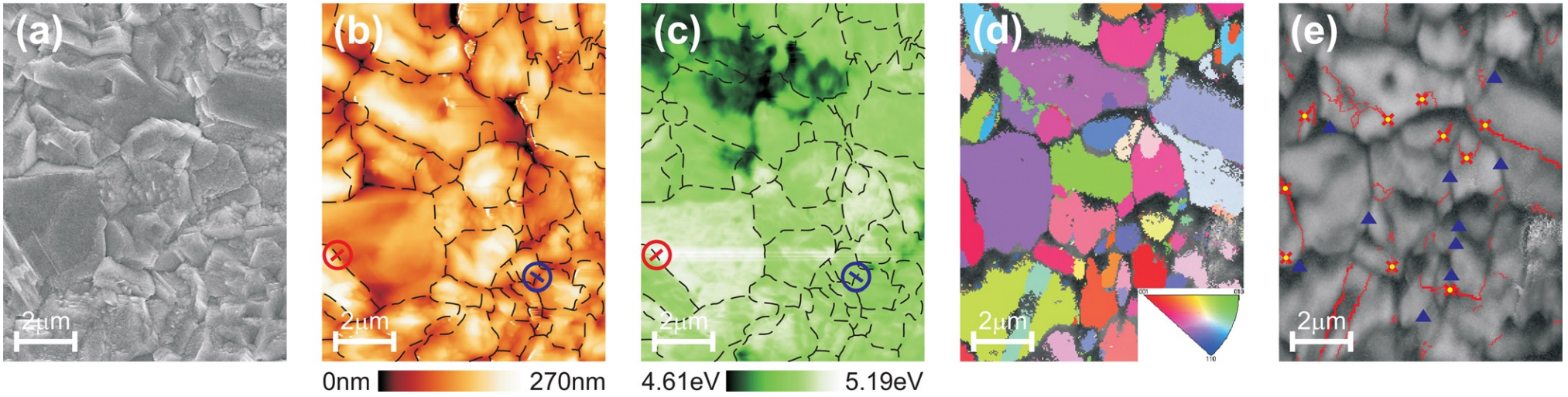

Experimental procedure:

- measure surface in KPFM
- find position in SEM
- EBSD measurement for orientation map
- correlate GB symmetry with electronic information

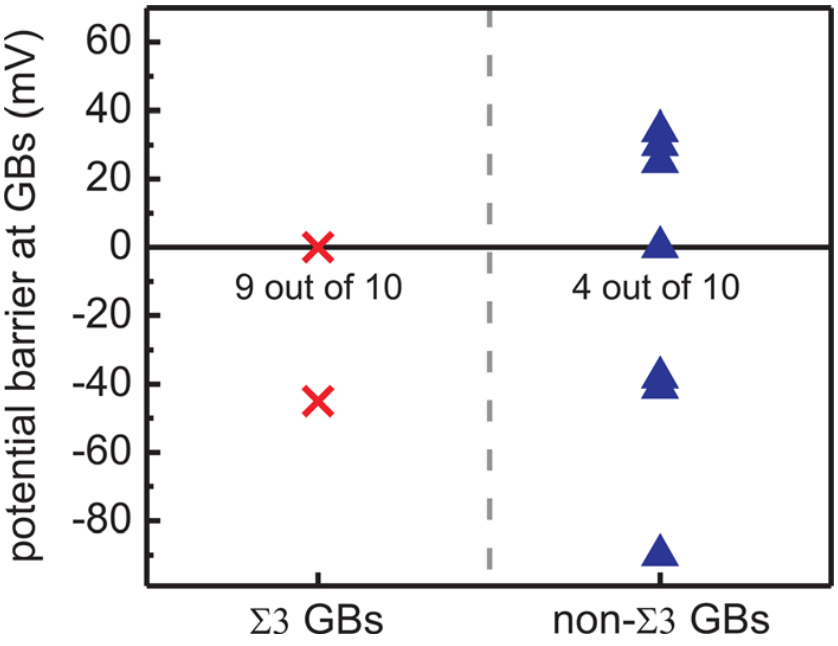

Baier *et al.*, Appl. Phys. Lett. **99**, 172102 (2011).

Part III:

Different alkali-fluoride post-deposition treatments of $Cu(In,Ga)Se_2$ investigated by Kelvin probe force microscopy

Nicoleta Nicoara[1], Roby Manaligod[1], Philip Jackson[2], Dimitrios Hariskos[2], Giovanna Sozzi[3], Roberto Menozzi[3], Wolfram Witte[2], Sascha Sadewasser[1]

[1] International Iberian Nanotechnology Laboratory (INL), Braga, Portugal
[2] Zentrum für Sonnenenergie- und Wasserstoff-Forschung Baden-Württemberg (ZSW), Stuttgart, Germany
[3] Department of Engineering and Architecture, University of Parma, 43124 Parma

Motivation

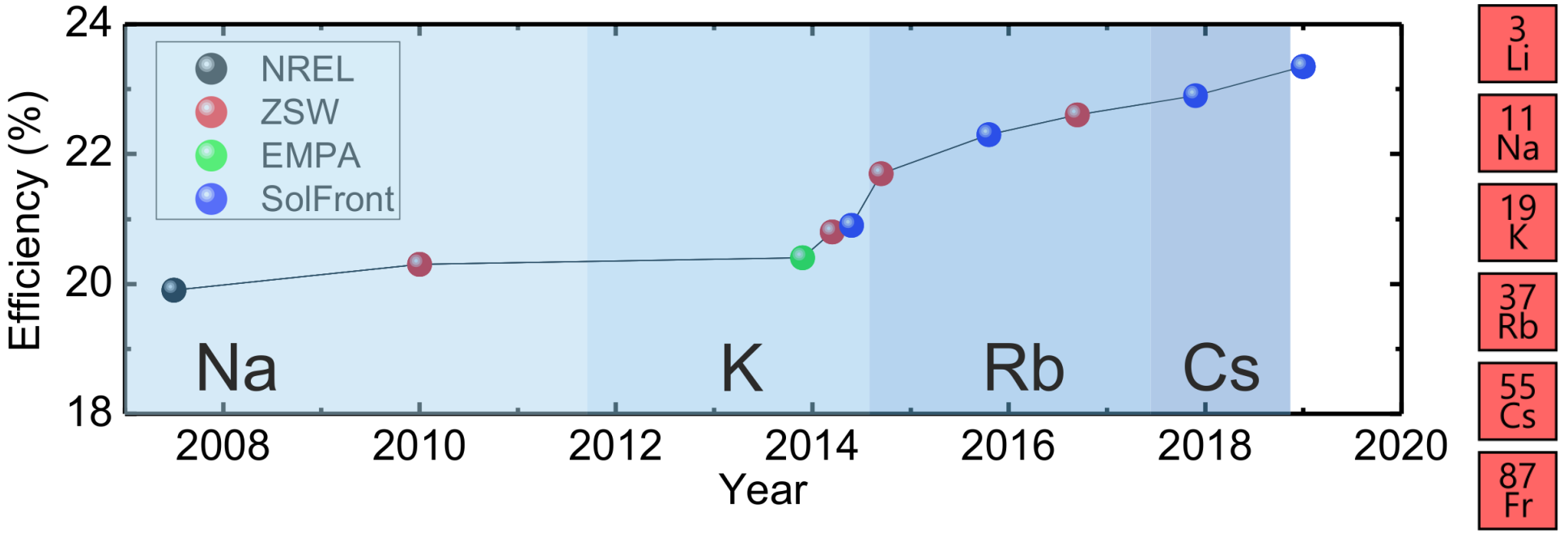

- Efficiency improvements since 2011 through alkali-fluoride post deposition treatments (AlkF-PDT)
- PDT process successfully applied in many labs
- PDT enabled efficiency > 20 %
- PDT effective for CIGSe by co-evaporation (NREL, EMPA, ZSW) and sequential deposition (Solar Frontier)
- Employing PDTs with heavier alkalis apparently leads to increased efficiencies
  - **Are heavier AlkF-PDTs better ?**
  - **Are and how are grain boundaries relevant for this?**

Samples

$Cu(In,Ga)Se_2$ with different alkali – PDT prepared at ZSW:

- Standard procedure for high-efficiency CIGSe solar cell manufacturing
- Reference solar cells reach efficiencies around 20% (w/ ARC).

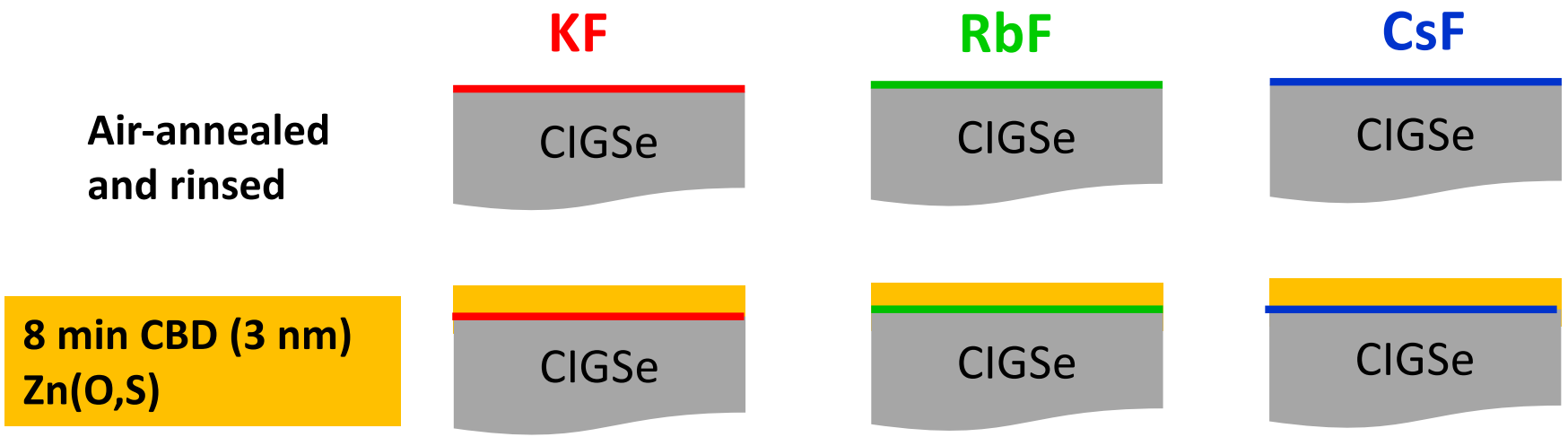

- Growth of CIGSe identical between the different AlkF-PDTs
- Growth optimized for CIGSe with RbF-PDT

KPFM of grain boundaries: analysis procedure

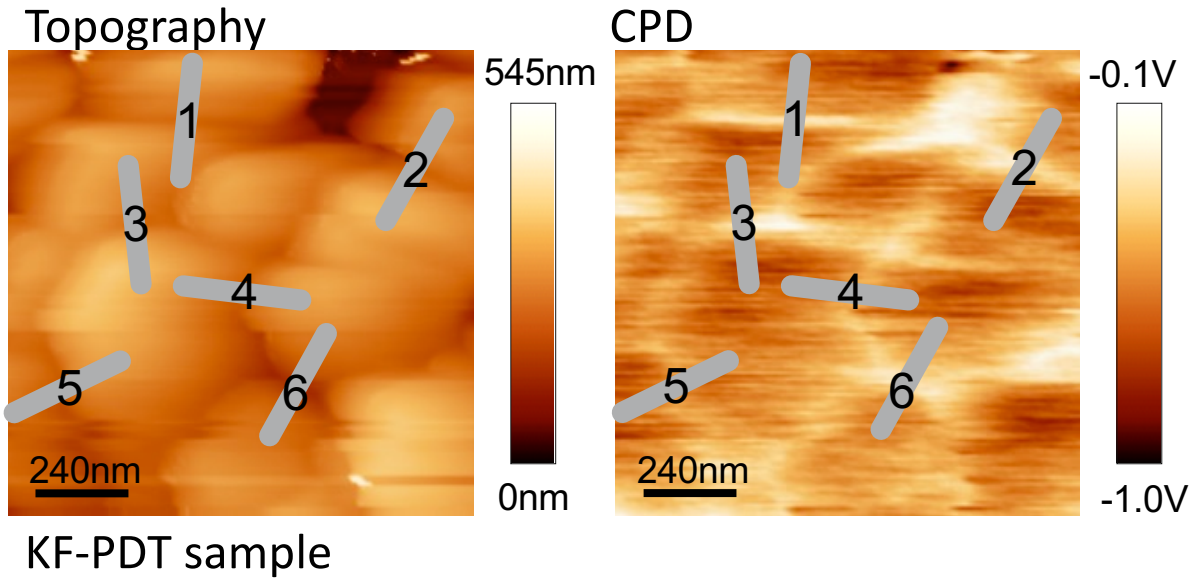

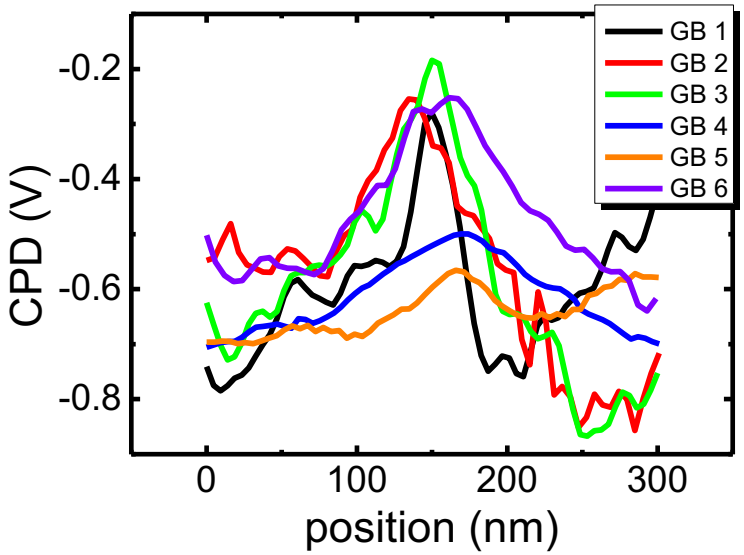

- Locate GB position in topography image
- Extract line profiles from topography and CPD images
- Determine variation of CPD at GB
  - Average of CPD on left and right grain
  - CPD at GB position
- Extract 20-60 GBs per sample
- Plot the CPD difference at the GBs for each sample.

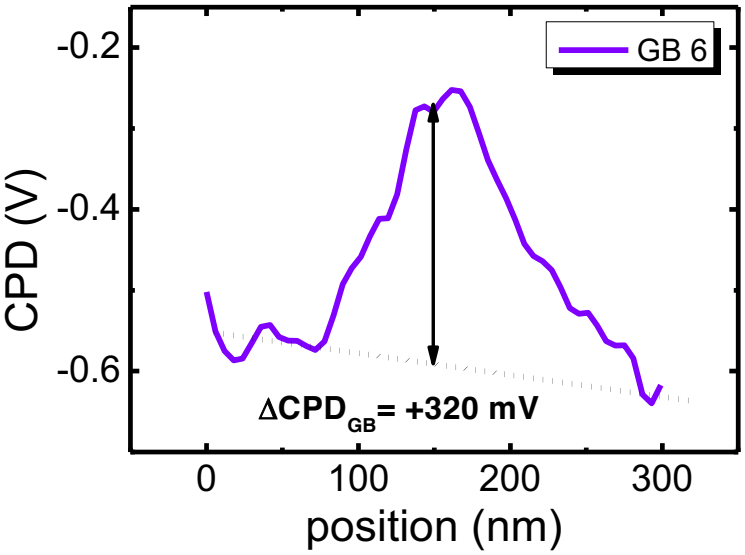

Baier *et al.,* Sol. Energy Mater. Sol. Cells 103, 86 (2012)

Alkali-dependent electronic properties of grain boundaries

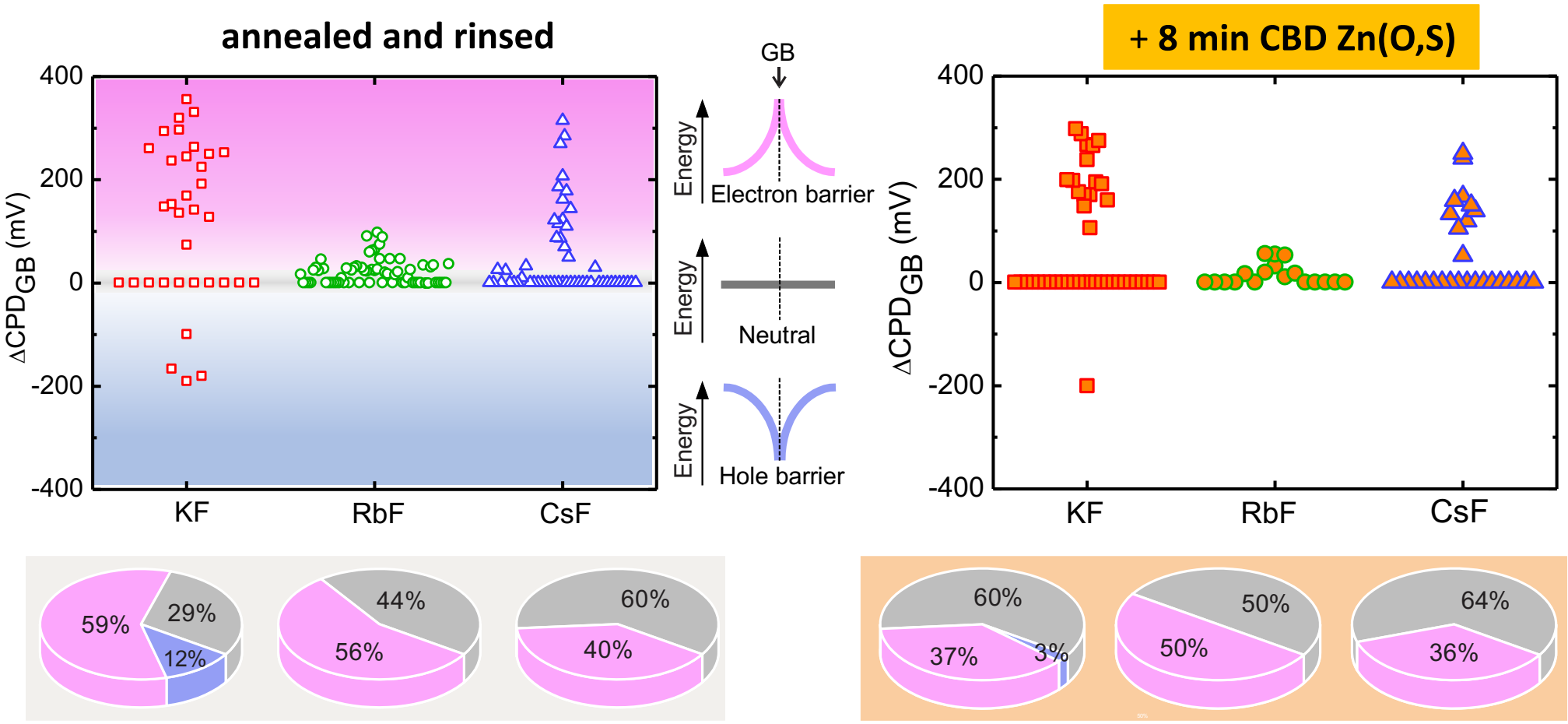

(i) For all samples, about half of the GBs show no potential barrier (except for annealed-rinsed KF-PDT)

(ii) All samples show GBs with electron barriers

(iii) Only the KF-PDT samples shows a non-negligible fraction of GBs with hole barriers

(iv) The magnitude of potential barriers for RbF-PDT is significantly smaller than for KF- and CsF-PDT.

Simulations to understand impact of grain boundaries

- 3D numerical simulations with Synopsys Sentaurus TCAD suite
- Poisson, electron and hole continuity, and drift-diffusion equations
- Shockley-Read-Hall for non-radiative recombination
- Light propagation by transfer matrix method under AM1.5G
- CIGS absorber with the double-graded [Ga]/([Ga]+[In]) (GGI) composition of the 21.7% efficiency cell

Base line result without grain boundary:

- V_{oc} = 0.742 V
- J_{sc} = 36.8 mA/cm^2
- FF = 80.6 %
- η = 22 %

For grain boundaries:

- cylindrical CIGSe grain with a 1 μm diameter surrounded by a 1-nm-thick grain boundary
- fixed charges of different density and polarity to simulate band bending

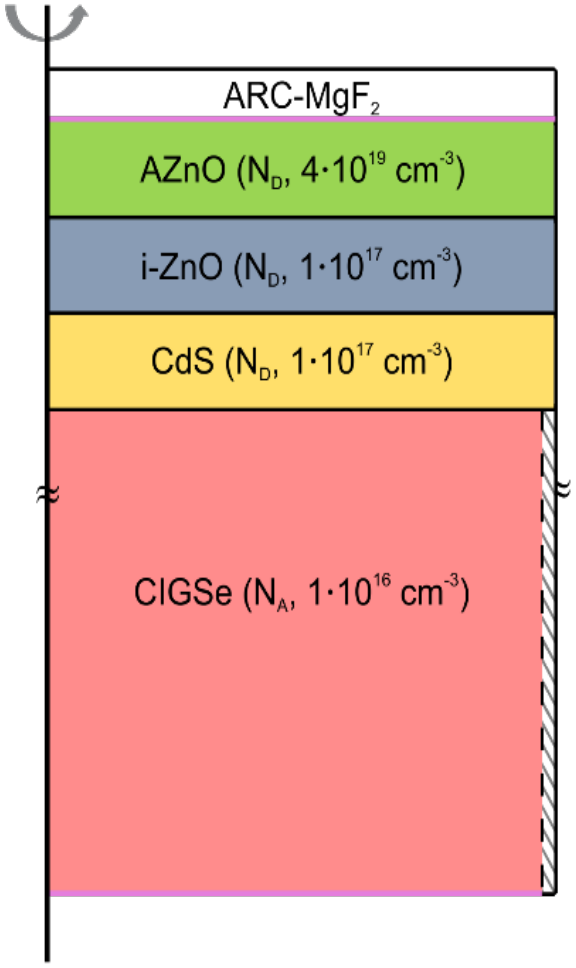

Simulations to understand impact of grain boundaries

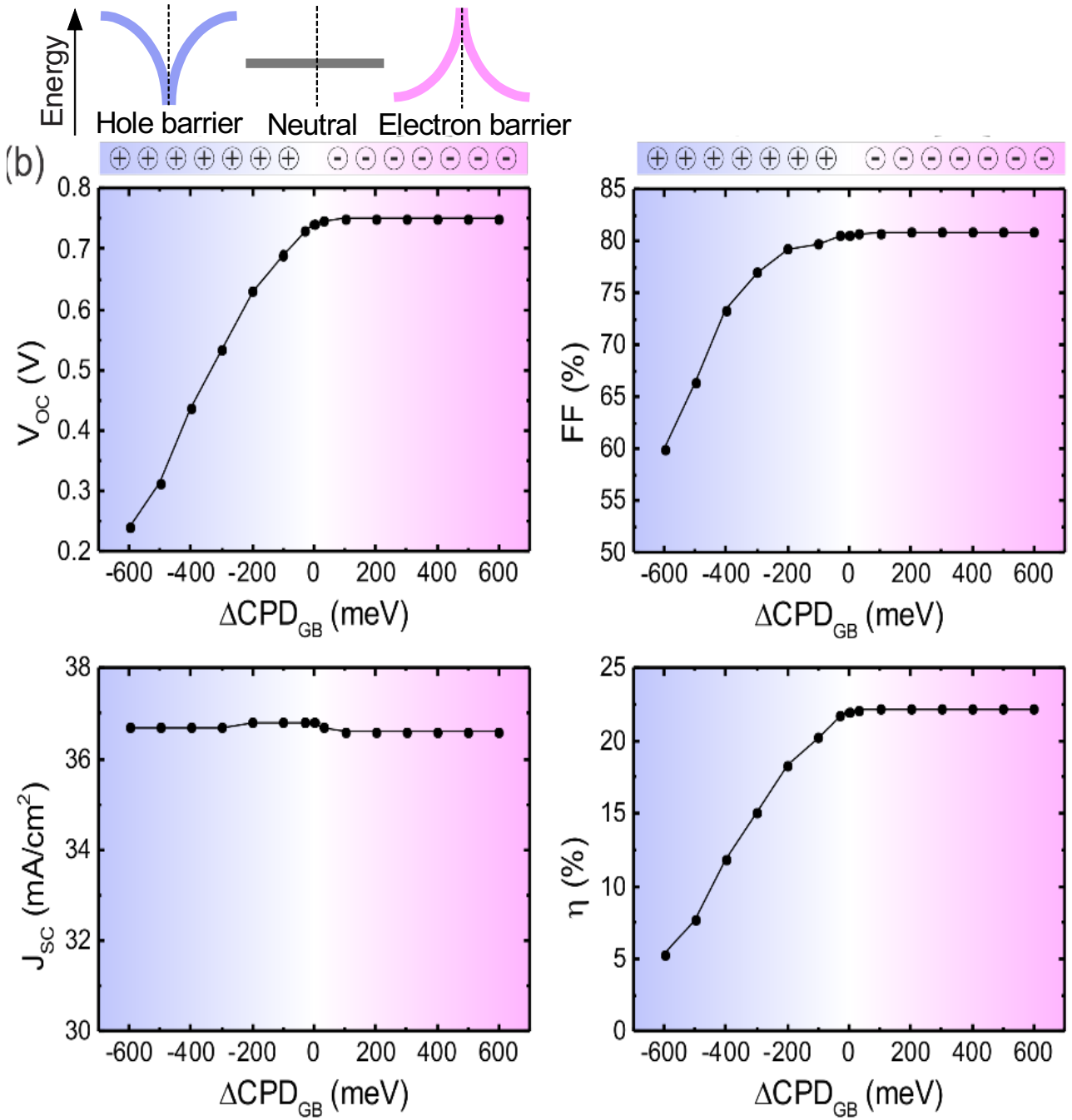

- Hole barrier is detrimental for V_{oc} and FF
- Electron barrier has nearly no impact on device performance

Experimental device characteristics

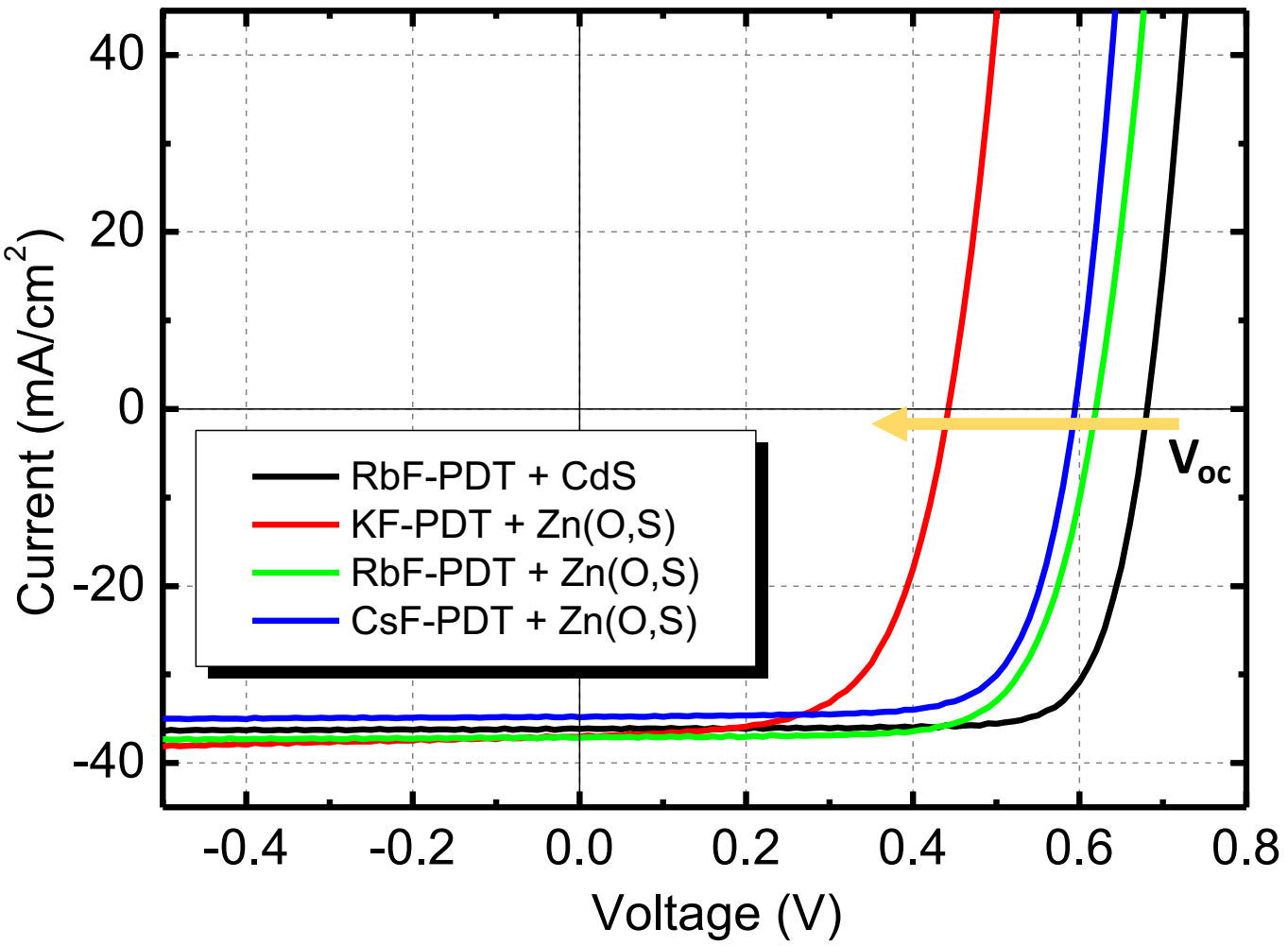

- No ARC
- No post-annealing
- No light soaking

Quantitative comparison of experiments and simulation

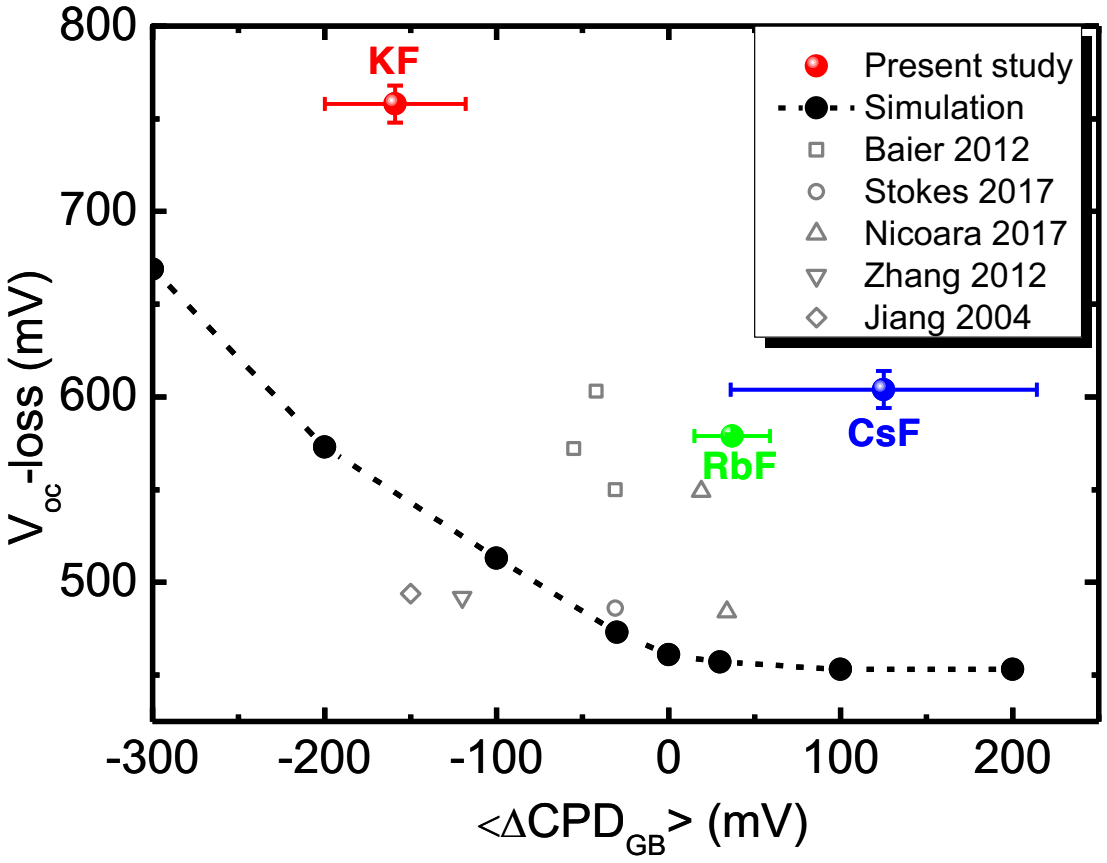

- Decent agreement of experiments with simulations
- Most data points above the simulated curve

  → grain boundaries are not the only loss mechanism
- KF-PDT sample below optimum performance

→ Optimization of CIGSe growth process in conjunction with AlkF-PDT process required

Analysis of optoelectronic properties of grain boundaries

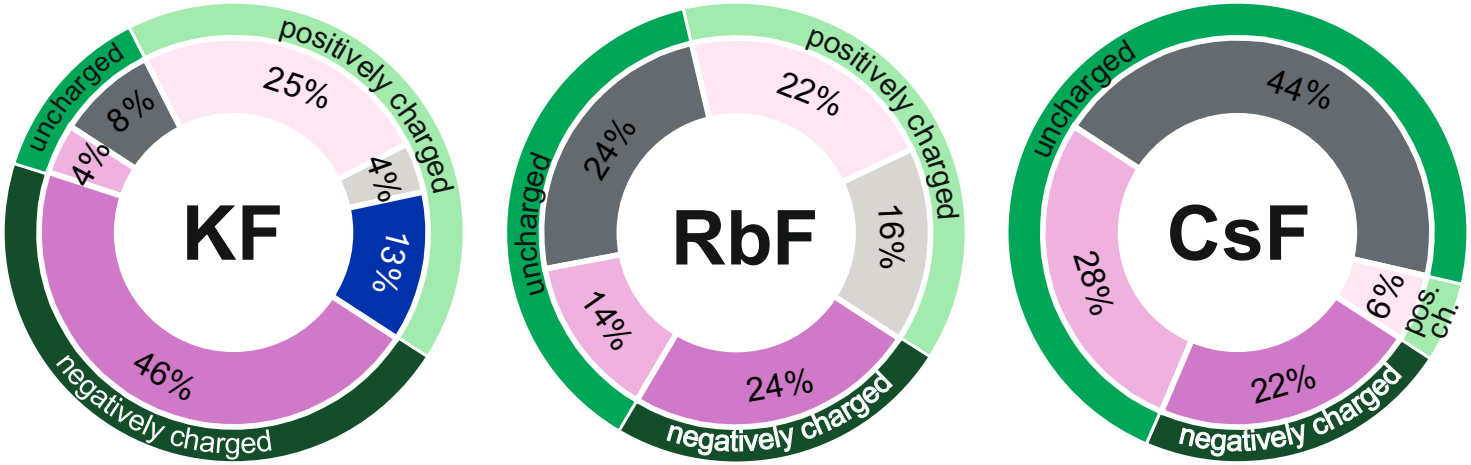

CPD+ SPV-	CPD 0 SPV-	CPD- SPV-	neg. charged
CPD+ SPV 0	CPD 0 SPV0	CPD- SPV 0	uncharged
CPD+ SPV+	CPD 0 SPV+	CPD- SPV+	pos. charged

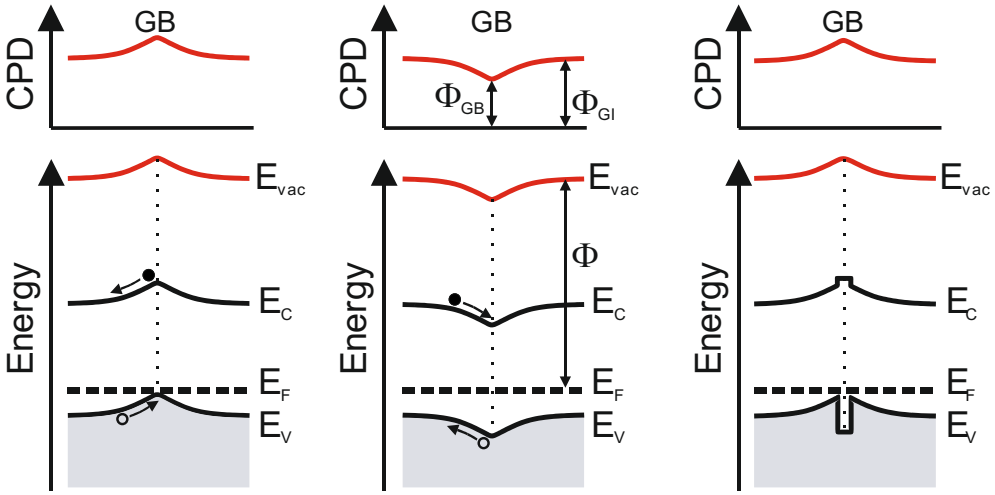

(-) trapped charge
Electron barrier

(+) trapped charge
Hole barrier

(+) trapped charge
and band offset

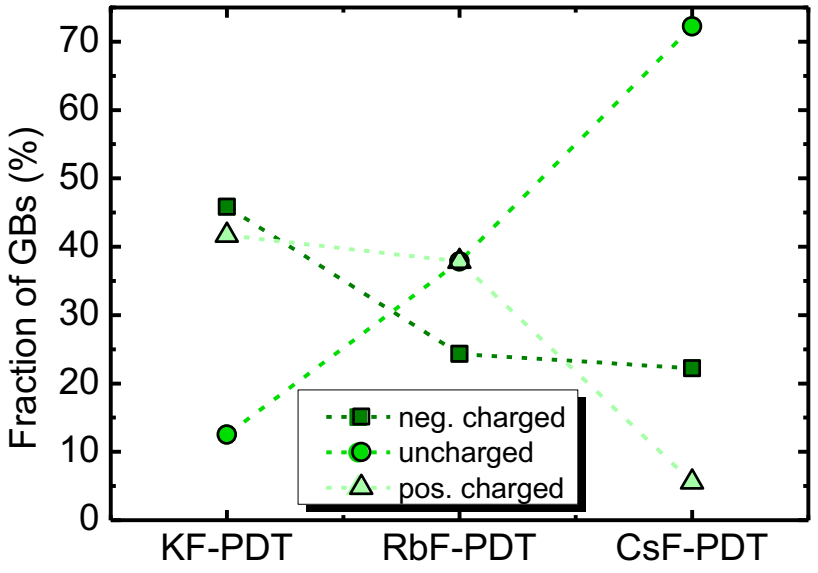

Model of alkali-compound passivation at grain boundaries

11 Na
19 K
37 Rb
55 Cs
87 Fr

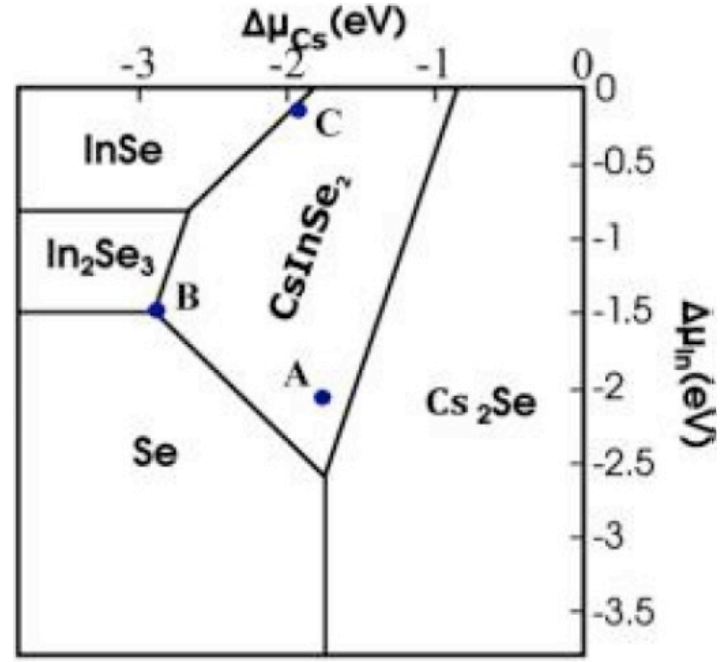

M. Malitckaya, J. Phys. Chem. C 121, 15516 (2017)

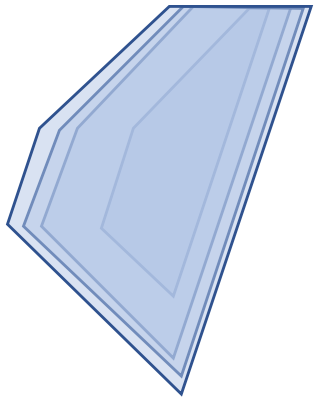

- Increasing size of the stability range of the $AlkInSe_2$ phase
- $AlkInSe_2$ phase has larger band gap than $CuInSe_2$

→ Passivation effect due to conduction and valence band offset

Schematic process for the effect of AlkF-PDT on grain boundaries

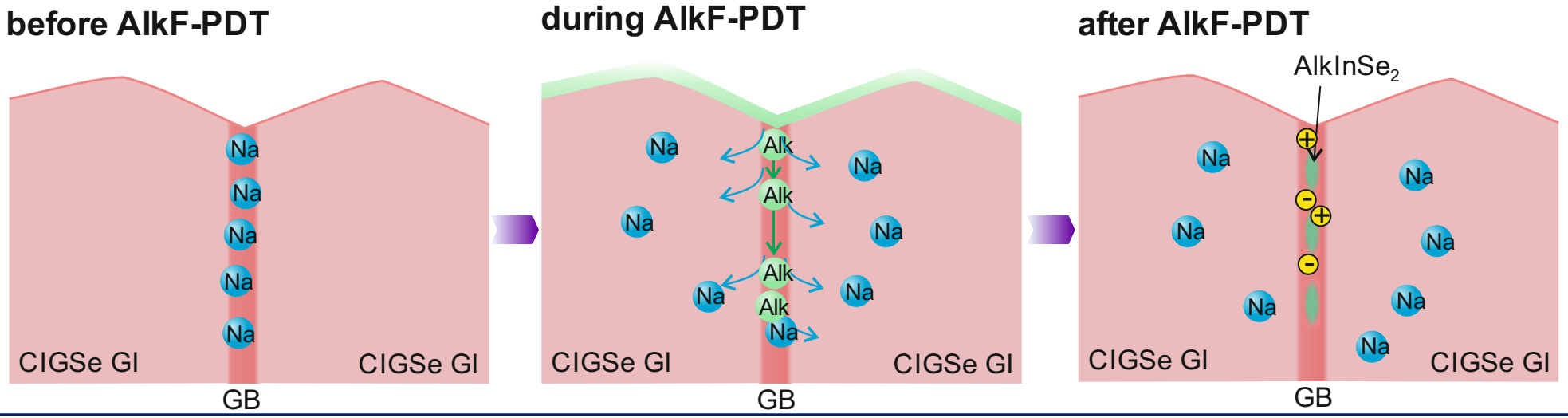

Interface evolution during buffer deposition

- 3-stage CIGSe by ZSW on Mo/glass at the high efficiency line → η > 20% (w/ ARC)
- Alkali post deposition treatment (PDT): **RbF PDT** [2]
- Buffers: Chemical bath deposition (CBD) of CdS (T=65°C) and Zn(O,S) (T=80°C)
- Sealed in N_2 before shipping (exposed to air 5-10 min before loading in the UHV – base pressure < 10^{-10} mbar)

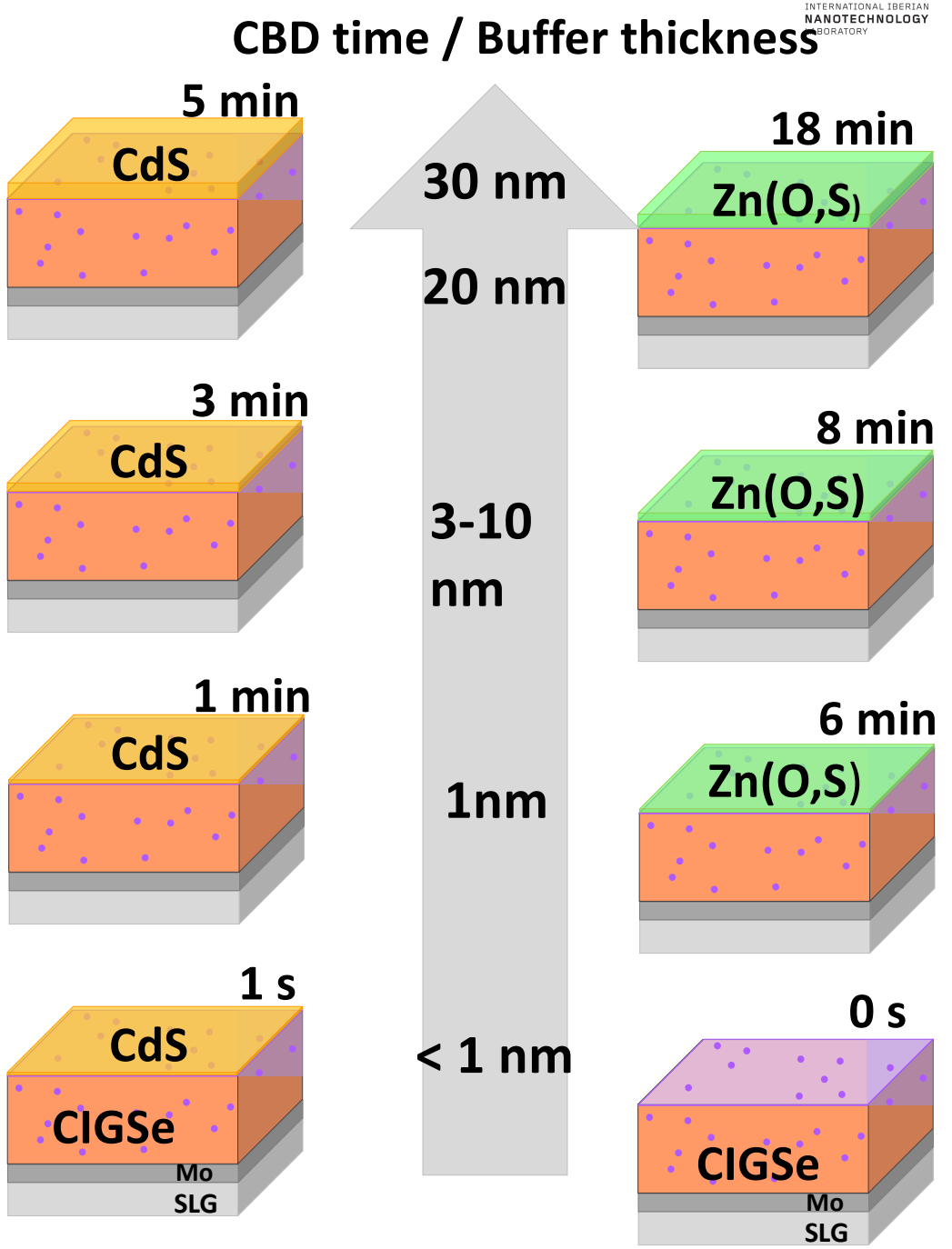

[2] P. Jackson *et al.*, Phys. Status Solidi RRL 10, 583 (2016).

KPFM data analysis procedure

RbF-CIGSe/CdS (1 s CBD)

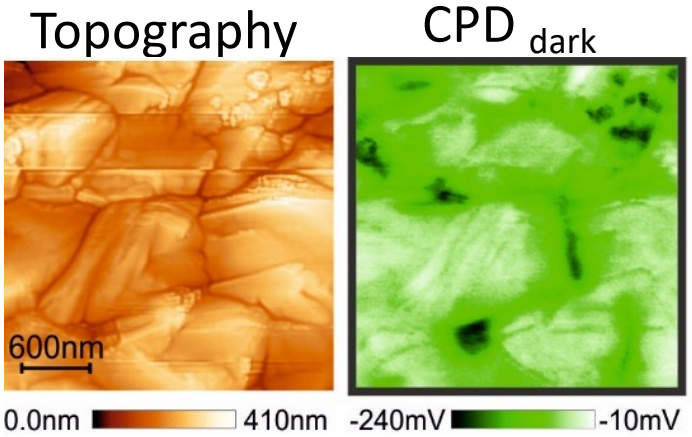

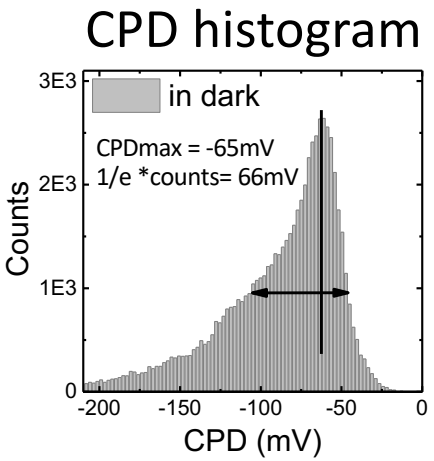

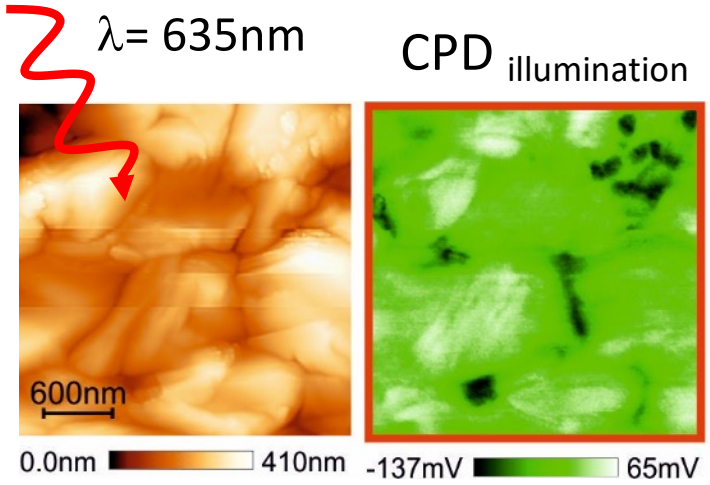

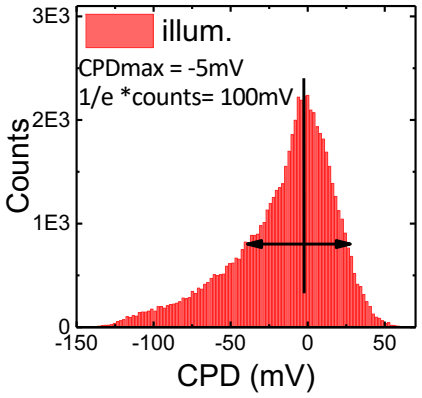

$SPV = CPD_{illum.} - CPD_{dark}$

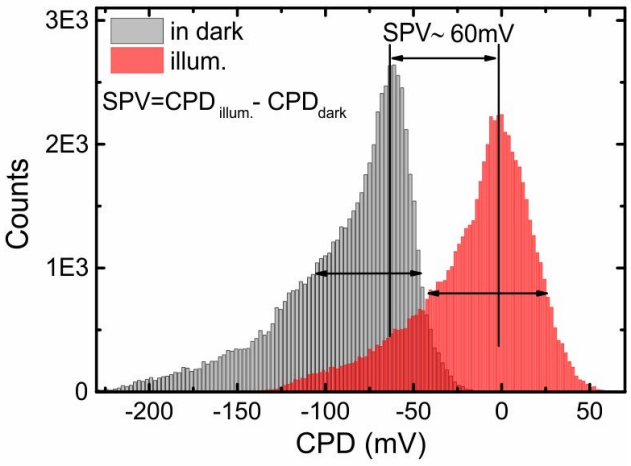

- Related to band bending
- Related to V_{OC} of device

- Simultaneous topography and CPD maps are taken at different locations
- A total of 25-30 images were analyzed per sample
- Measurements are done in dark and under illumination => SPV

N. Nicoara et al., ACS Appl. Mat. Interf. 9, 44173 (2017).

Surface morphology and electronic properties

RbF-CIGSe/CdS

CdS thickness →

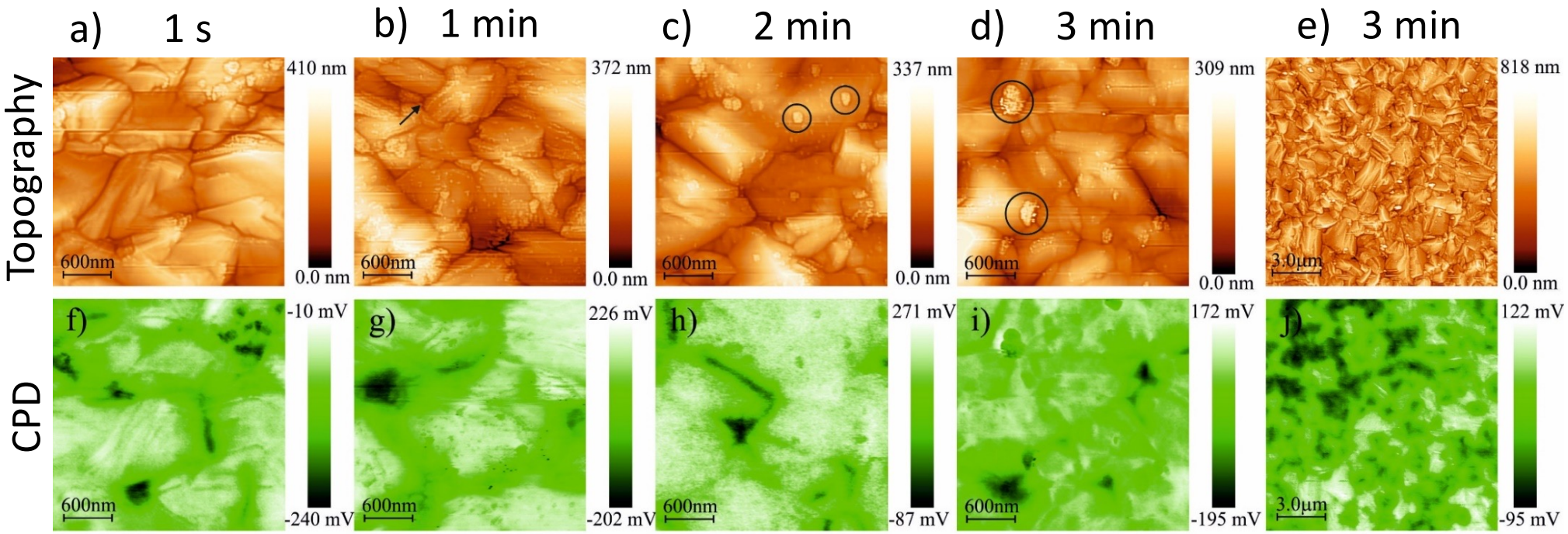

3 µm × 3 µm **15 µm × 15 µm**

- Facetted CIGSe surfaces
- Presence of clusters; increased density and size with increasing CBD time
- Lateral inhomogeneity in the surface potential (CPD maps) for 2 and 3 min CBD observed only at larger scale (> 3 μm^2)

N. Nicoara et al., ACS Appl. Mat. Interf. 9, 44173 (2017).

Surface potential dependence on CdS thickness

RbF-CIGSe/CdS

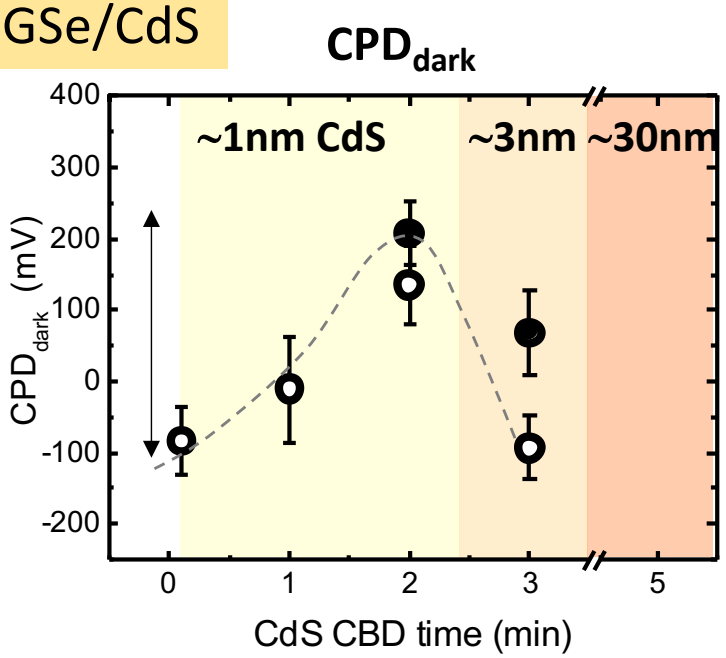

- Increase of CPD (+ 0.3 eV) up to 2 min, followed by a decrease for 3 min CBD
- Uniform CPD for 1 s and 1 min
- For CBD times ≥ 2 min, variation in CPD (solid, open symbols)

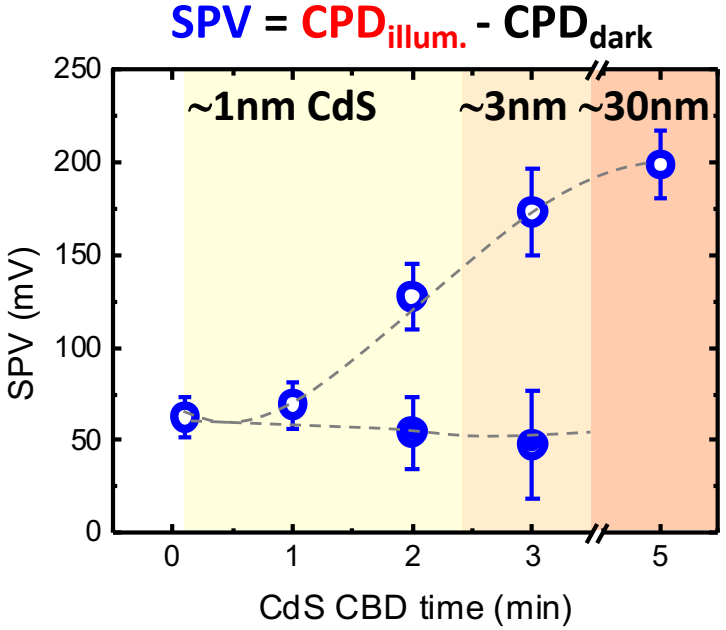

- Uniform, low SPV for 1 s and 1 min
- For longer CBD, two tendencies:
  - i) constant ~ 50 - 60 mV
  - ii) increasing with buffer coverage
- Lateral inhomogeneity: high CPD areas show low SPV and low CPD areas show high SPV

N. Nicoara et al., ACS Appl. Mat. Interf. 9, 44173 (2017).

Surface potential dependence on CdS thickness

RbF-CIGSe/CdS

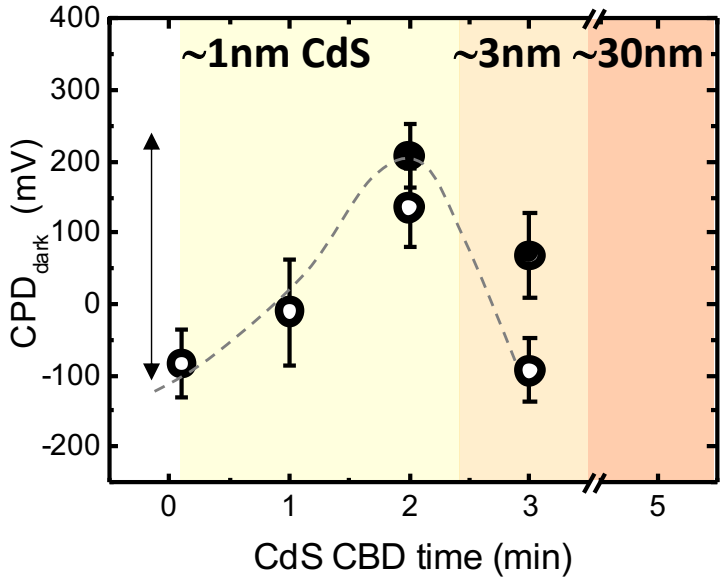

SPV = CPD$_{illum.}$ - CPD$_{dark}$

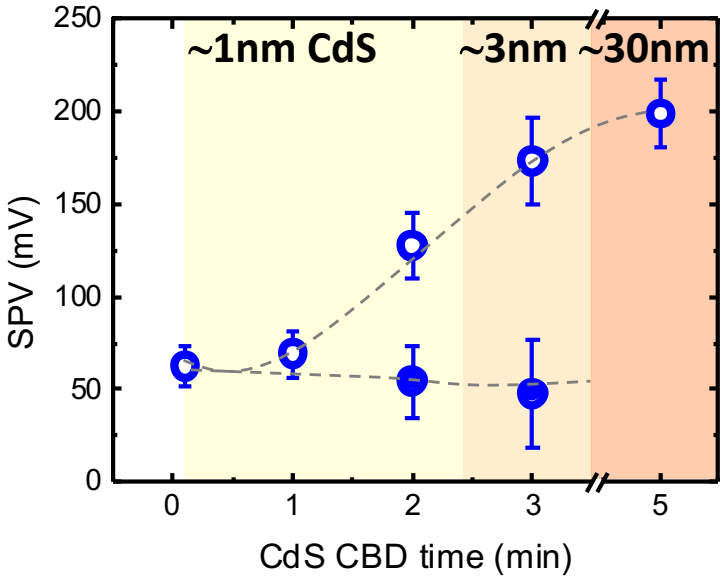

- For 1 s to 2 min CBD → CPD increases:
  - Complex interface with Rb, Cd, In, and Se observed in XPS
- The "thin" CdS layer does not provide sufficient charges to change the initial surface band bending

→ The SPV remains const. ~ 50 - 60 mV

N. Nicoara et al., ACS Appl. Mat. Interf. 9, 44173 (2017).

Surface potential dependence on CdS thickness

RbF-CIGSe/CdS

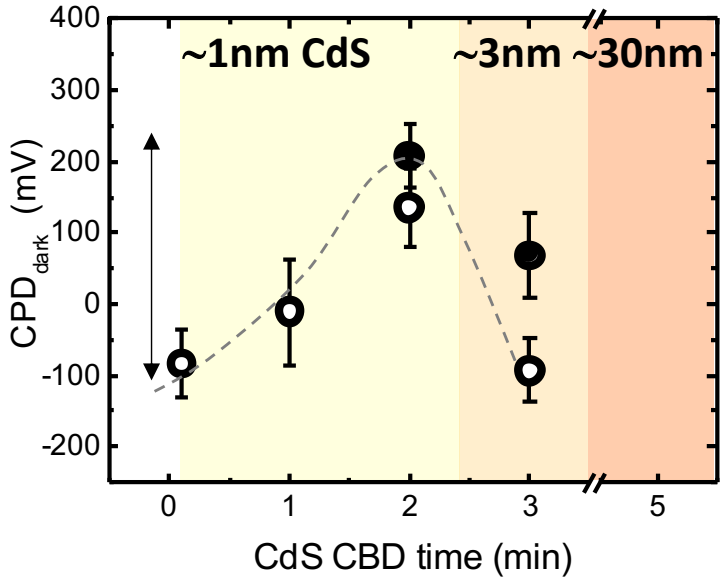

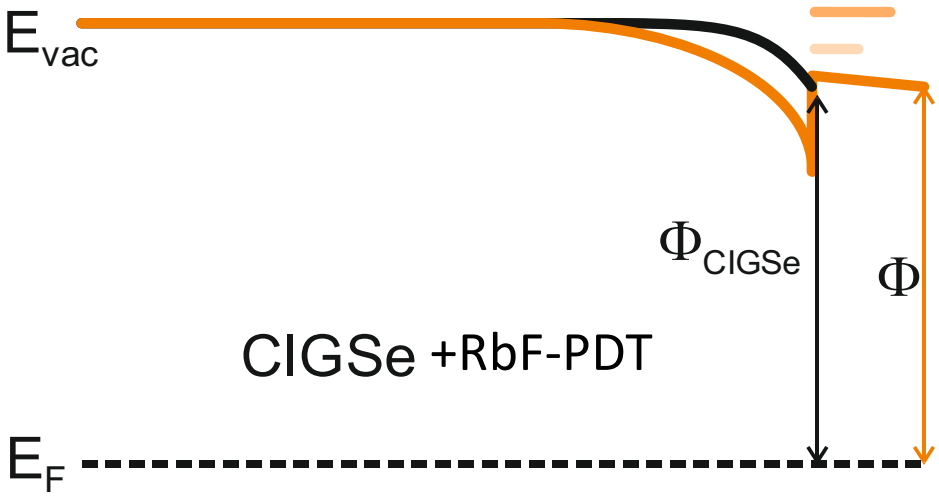

SPV = CPD$_{illum.}$ - CPD$_{dark}$

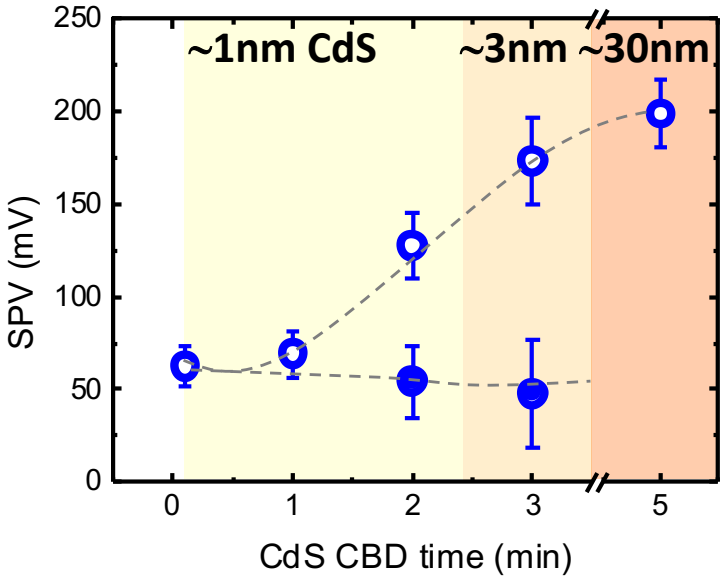

- For > 3 min, the CdS layer is thick enough and provide sufficient charges to modify the band bending, which now is stronger downwards

→ The CPD decreases due to downward band bending

→ The surface photovoltage increases

[N. Nicoara et al., ACS Appl. Mat. Interf. 9, 44173 (2017).

Surface morphology and electronic properties

RbF-CIGSe/Zn(O,S)

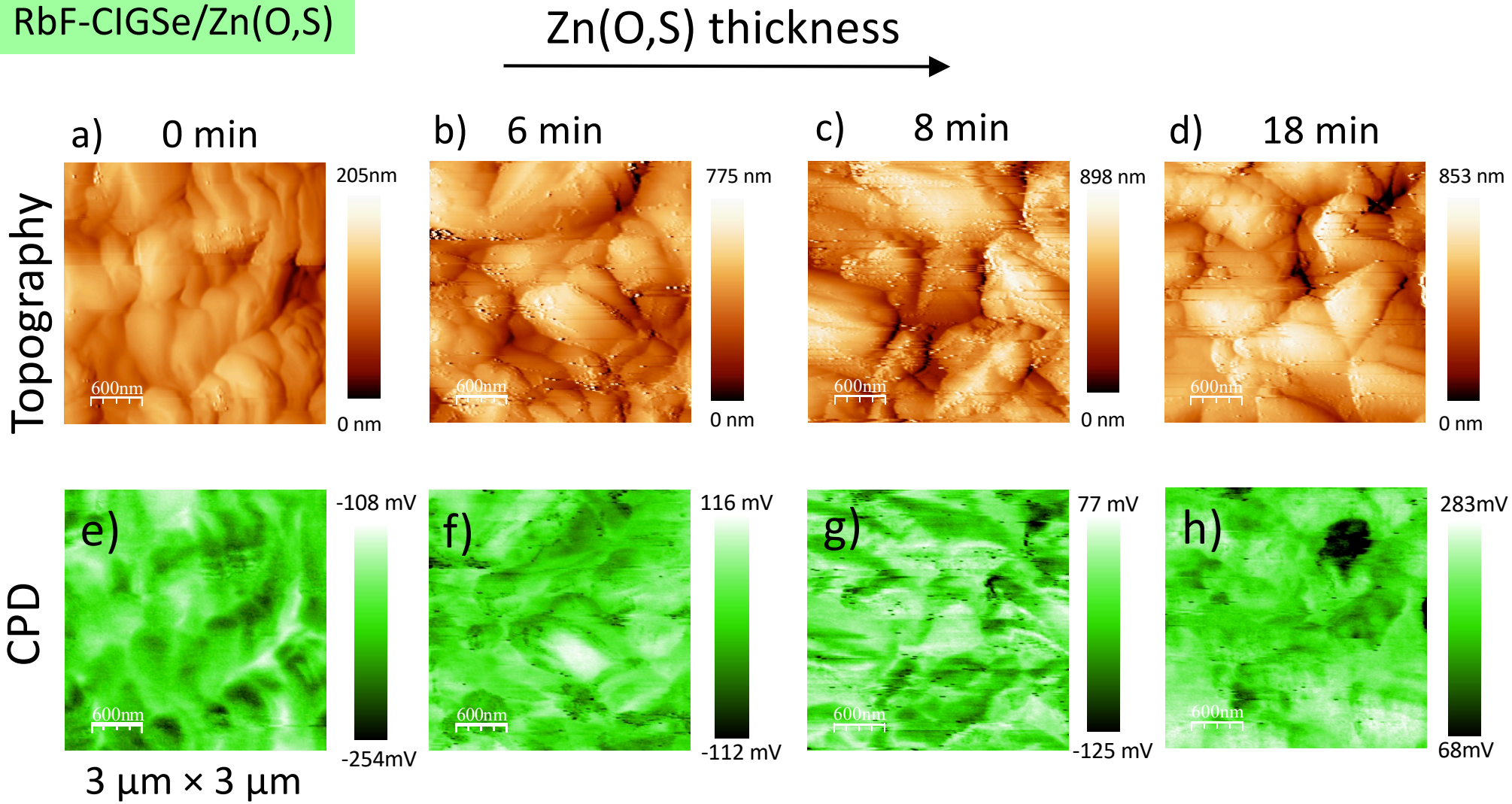

- Zn(O,S) deposition induced changes at the CIGS surface; tip instability due to presence of small features on the surface
- For 20 nm (18 min) Zn(O,S) clusters formation is observed

Surface potential dependence on Zn(O,S) thickness

RbF-CIGSe/Zn(O,S)

CPD_{dark}

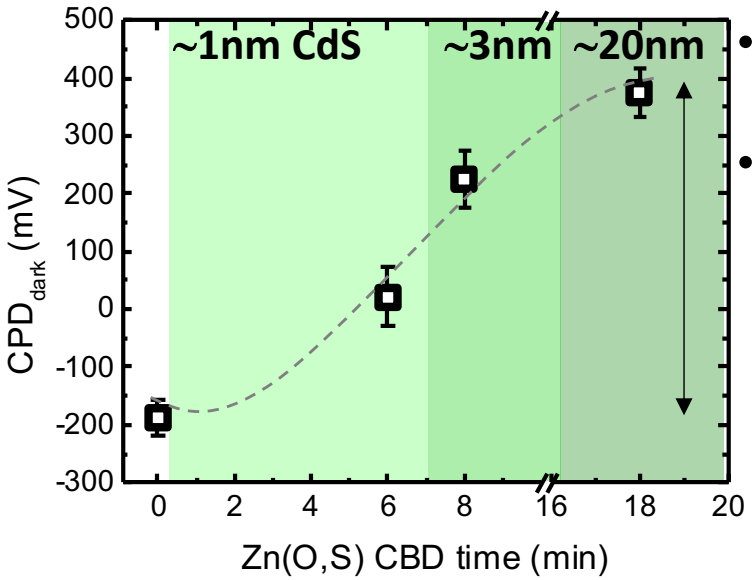

- Uniform CPD for all thicknesses
- CPD increase with increasing deposition time

SPV = CPD_{light} - CPD_{dark}

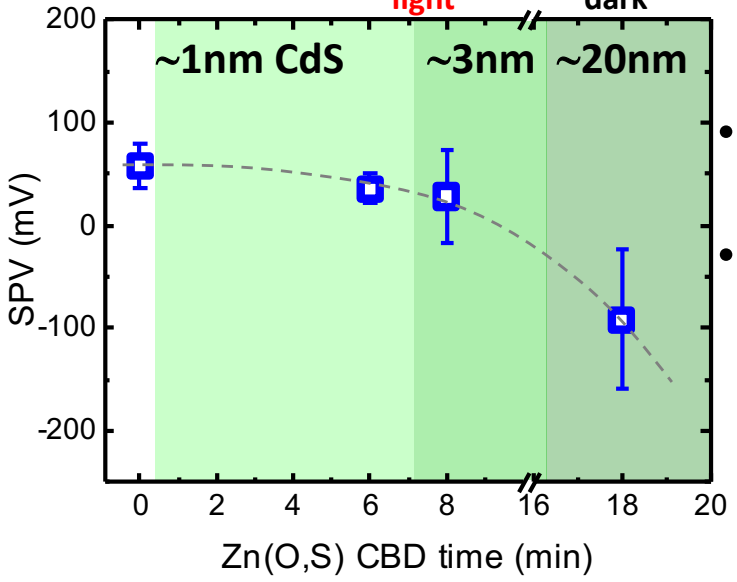

- Homogeneous, positive (35-55 mV) SPV up to 8 min
- Larger and negative SPV (up to ~ 170 mV) for 18 min CBD Zn(O,S)

Surface potential dependence on Zn(O,S) thickness

RbF-CIGSe/Zn(O,S)

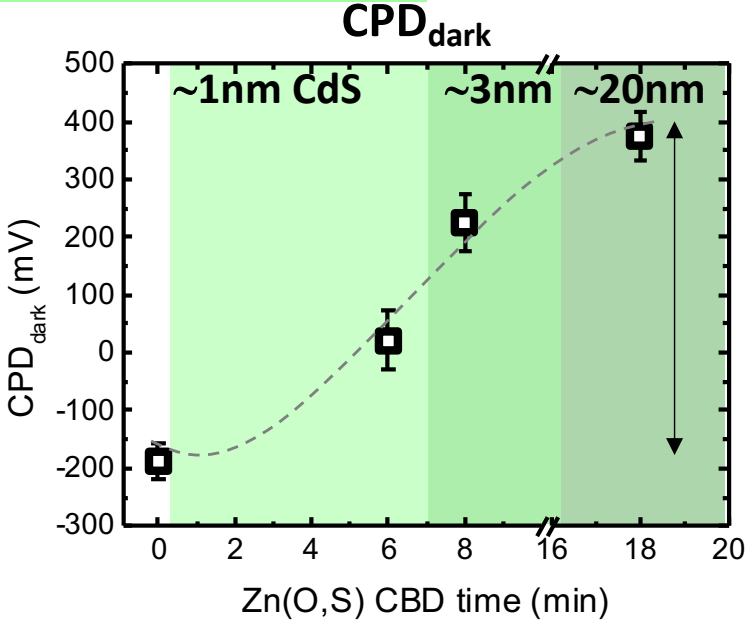

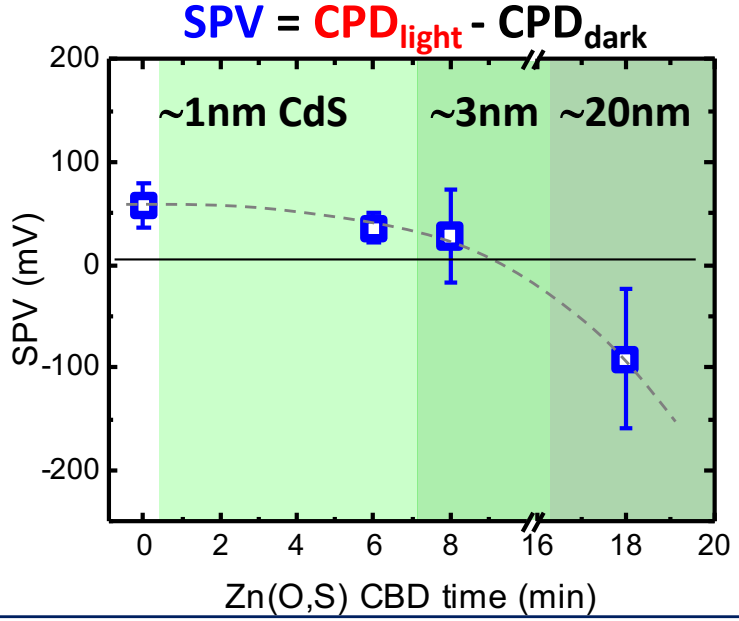

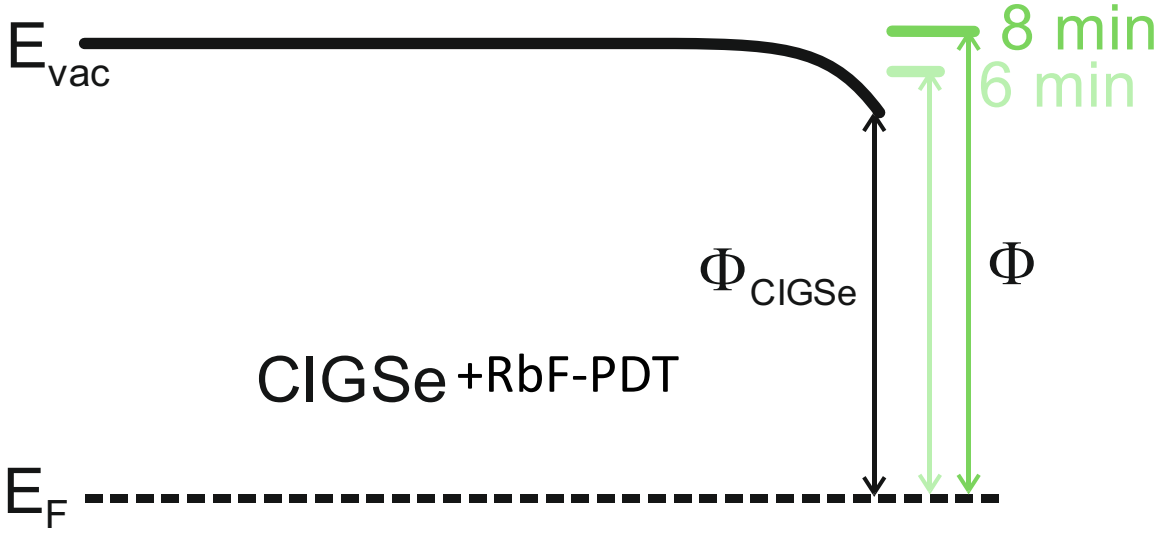

- Up to 8 min Zn(O,S) deposition, the CPD increases:
  - Complex interface formation ?
- The “thin” Zn(O,S) layer does not provide sufficient charges to change the initial surface band bending.

→ The SPV remains const. at ~ 50 mV

Surface potential dependence on Zn(O,S) thickness

RbF-CIGSe/Zn(O,S)

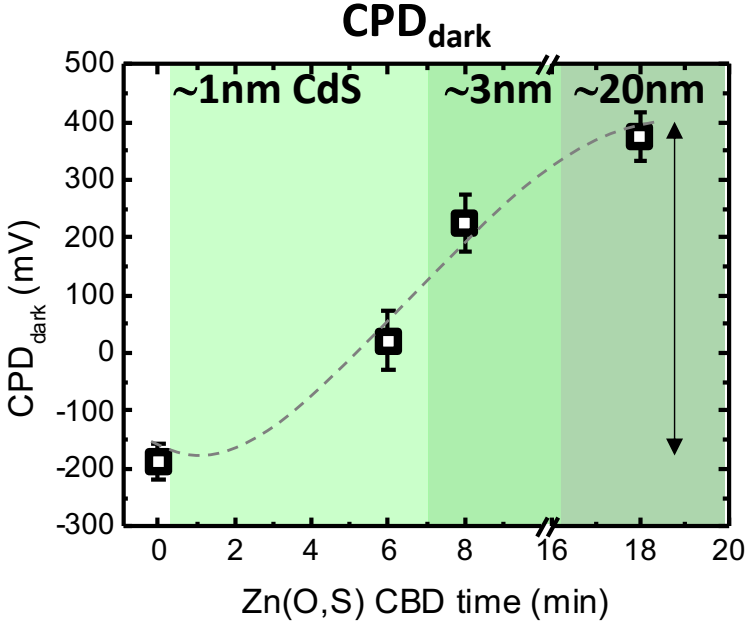

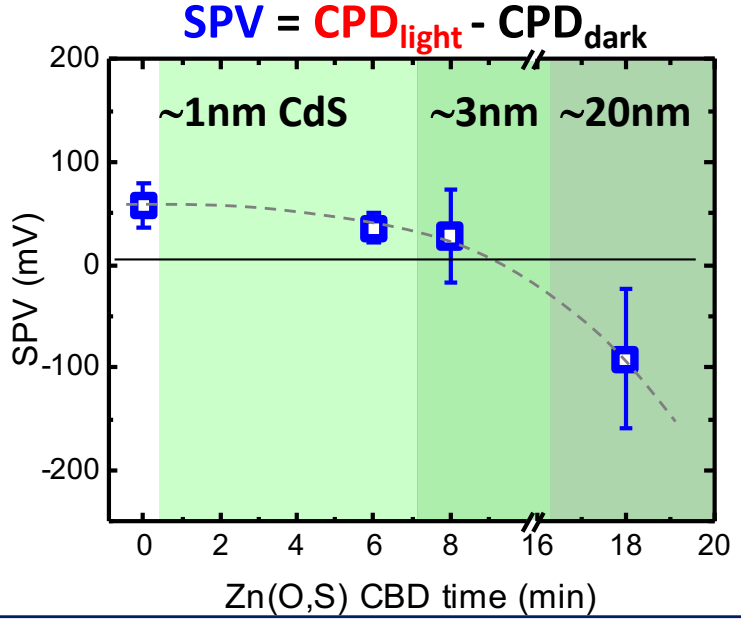

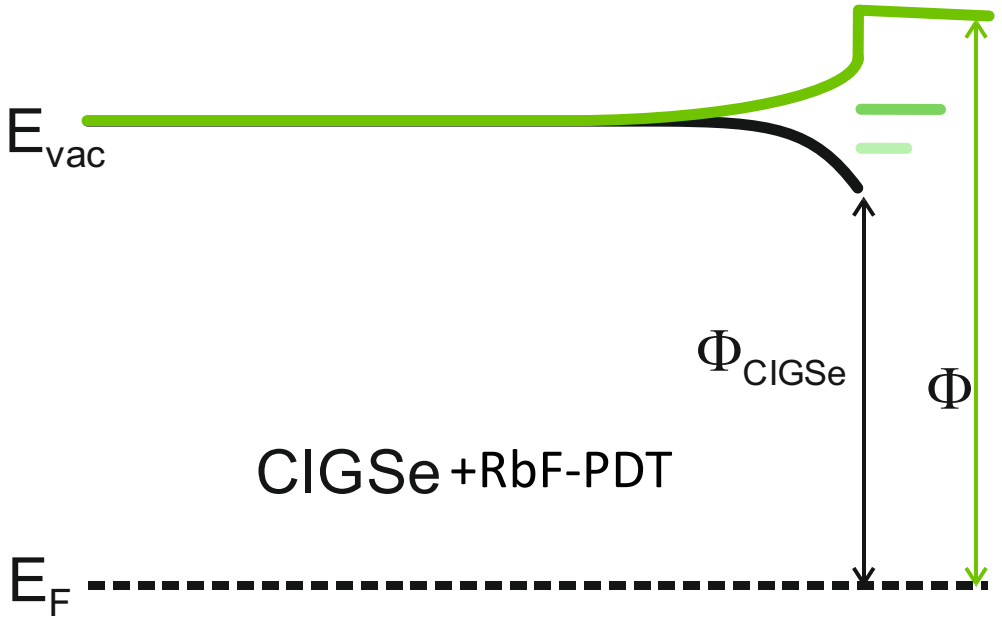

- For 18 min, the "thick" Zn(O,S) layer does not result in downward band bending (with a positive SPV) as expected
- Possible explanation:
  - Fixed charges (traps) at the surface of Zn(O,S)

→ The surface photovoltage is negative !

Part IV:
Time-resolved
Kelvin probe force microscopy

Quick Introduction to Time-Resolved KPFM

- Macroscopic tr-SPV measures directly the SPV decay after a short light pulse
- In KPFM the CPD is measured by a controller with *time constant ~1-10 ms*

$\Rightarrow$ Direct measurement of SPV decay not possible

$\rightarrow$ **Use a fast pulsed light sequence** and measure the averaged CPD to obtain SPV(t)

Effect of light on the surface potential

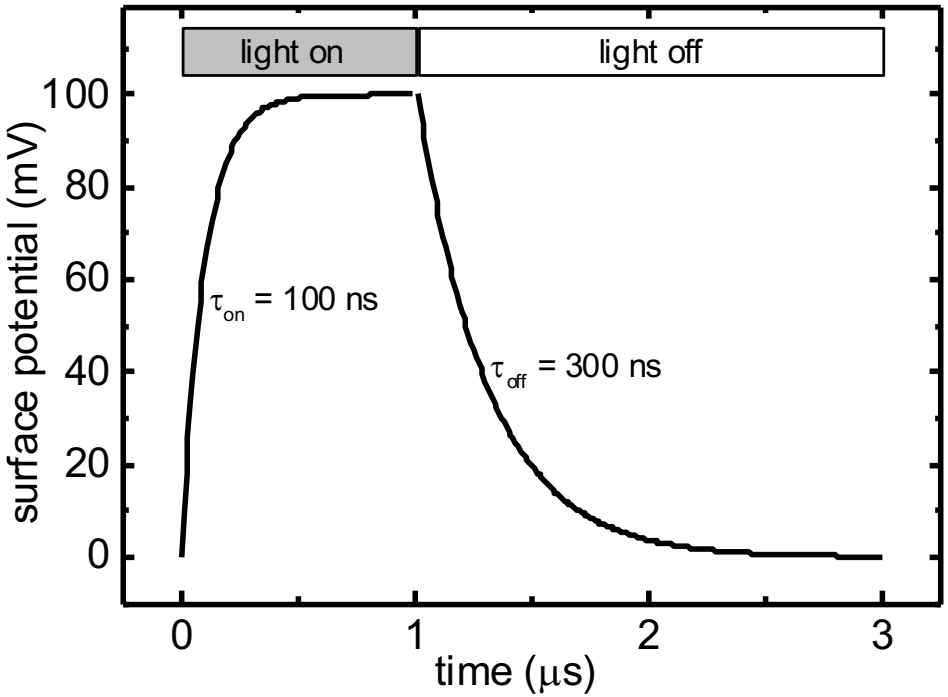

Repeated light pulses and measured CPD

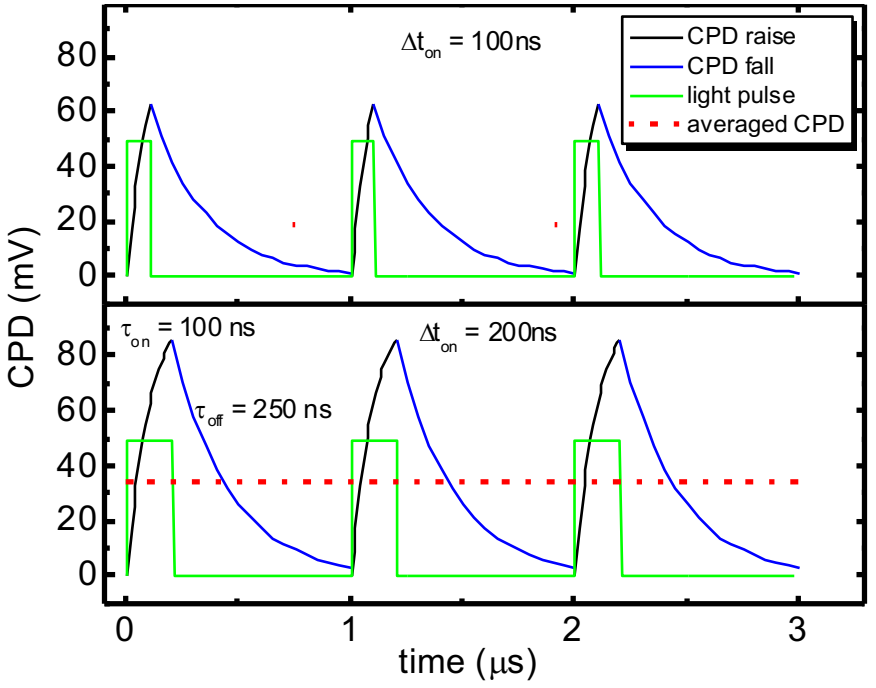

Quick Introduction to Time-Resolved KPFM

- Assume simple exponential CPD increase and decay:
- During light on: $SPV_{on}(t) = \Delta SPV \cdot e^{-t/\tau_{on}}$
- During light off: $SPV_{off}(t) = \Delta SPV \cdot \left(1 - e^{-t/\tau_{off}}\right)$
- Measured CPD = Integral of the increase and decay curves during the on- and off-time of the illumination:

$$\overline{CPD} = \frac{1}{\Delta t_{on} + \Delta t_{off}} \left[\int_0^{\Delta t_{on}} SPV_{on}(t)dt + \int_{\Delta t_{on}}^{\Delta t_{on}+\Delta t_{off}} SPV_{off}(t)dt \right]$$

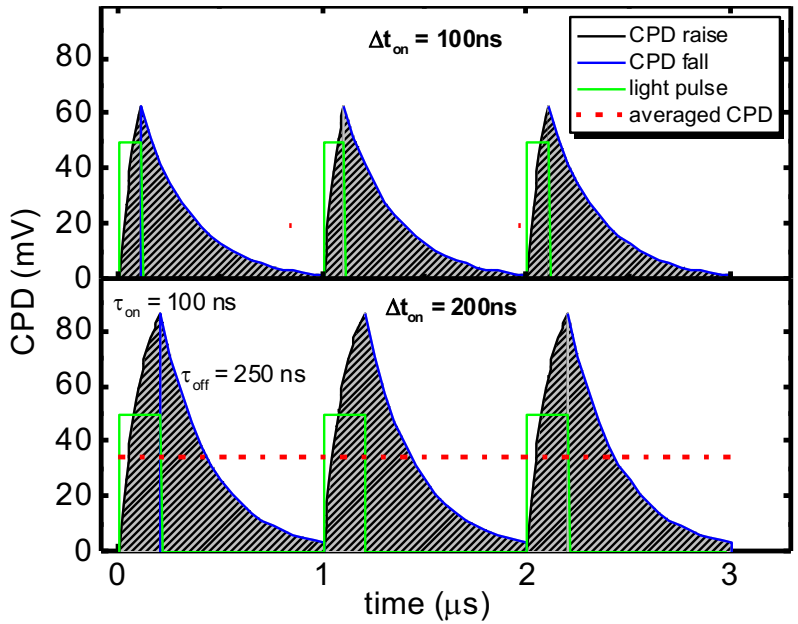

Chemical instability at chalcogenide surfaces impacts chalcopyrite devices well beyond the surface

D. Colombara, H. Elanzeery, **N. Nicoara, D. Sharma**, M. Claro, T. Schwarz, A. Koprek, M.H. Wolter, M. Melchiorre, M. Sood, N. Valle, O. Bondarchuk, F. Babbe, C. Spindler, O. Cojocaru-Miredin, D. Raabe, P.J. Dale, **S. Sadewasser**, and S. Siebentritt

INL – International Iberian Nanotechnology Laboratory, 4715-330 Braga, Portugal
… and 7 other institutions

Nature Communications 11, 3634 *(2020).*

$Cu(In,Ga)Se_2$ solar cells

- best optoelectronic properties for Cu-poor stoichiometry
- best structural properties for Cu-rich stoichiometry
- Cu-rich CIGSe leads to segregation of $Cu_{2-x}Se$ which can be etched by KCN solution
- KCN etch can lead to formation of different point defects below the surface

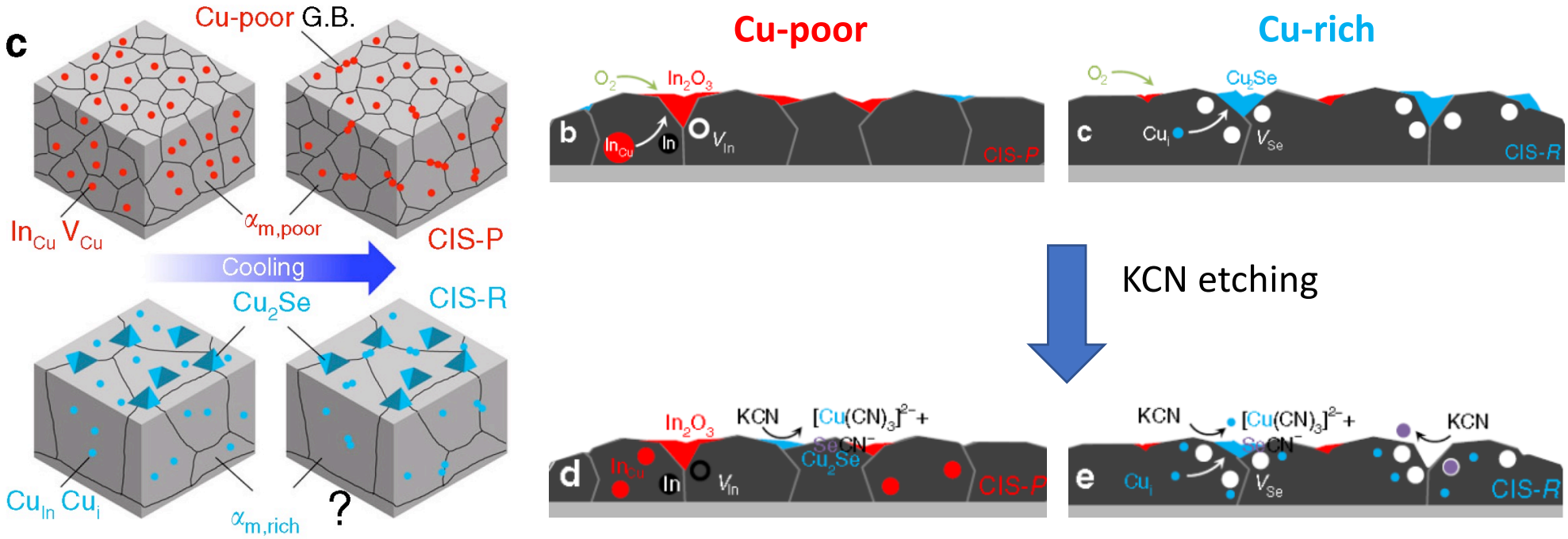

D. Colombara et al., Nature Communications 11, 3634 *(2020).*

$Cu(In,Ga)Se_2$ solar cells

- TR-SPV on Cu-rich and Cu-poor CIGSe after KCN etching

Cu-poor CIGSe

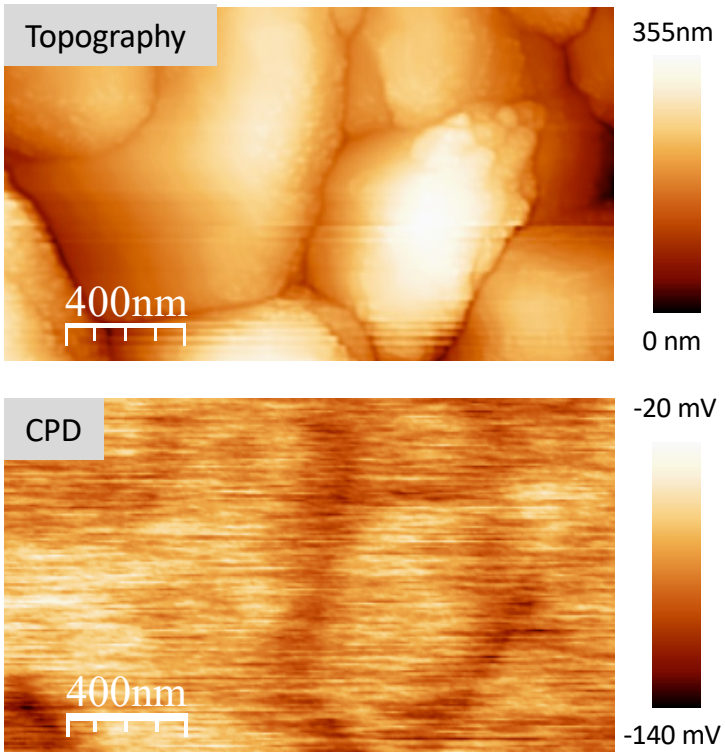

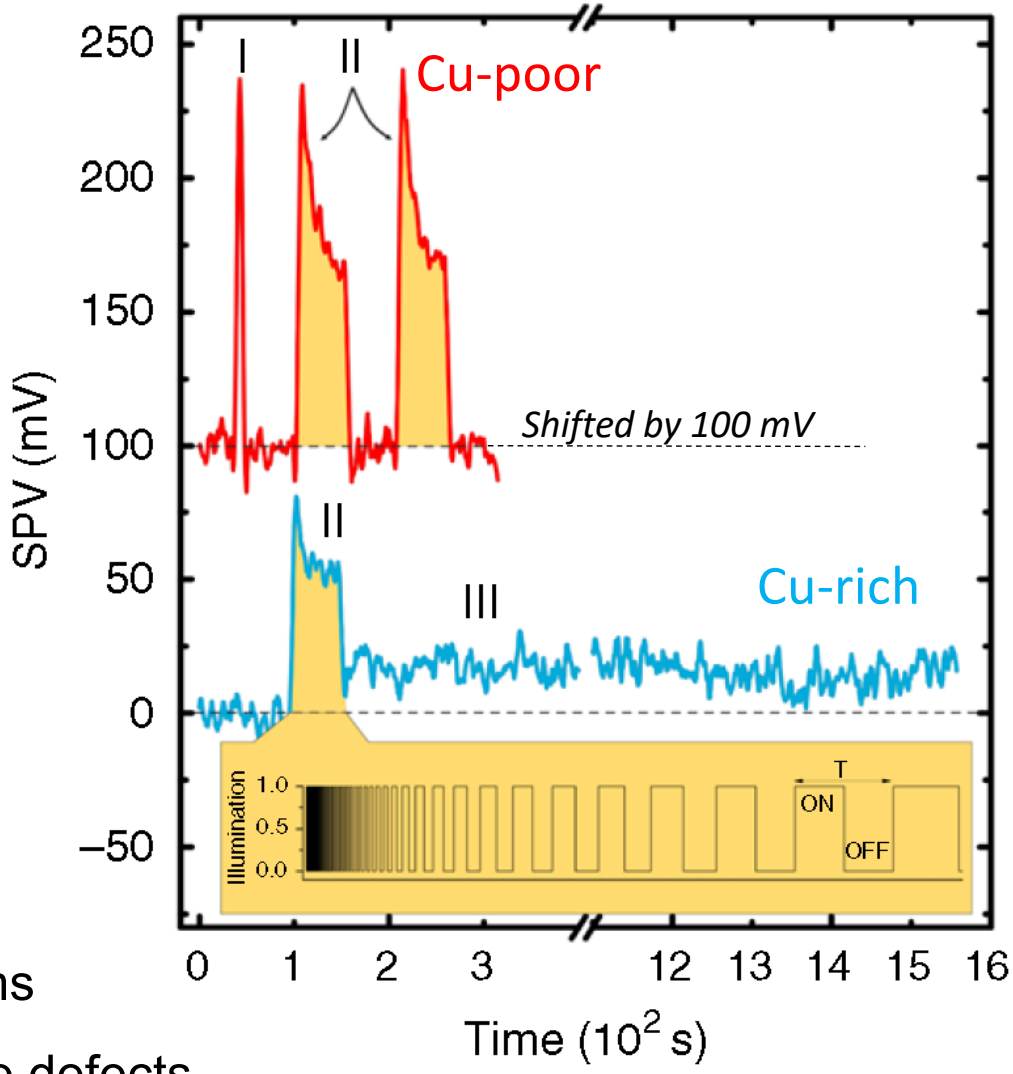

- Region I: 1 s light pulse → fast decay
- Region II: Pulse sequence 100 ns – 10 ms
- Region III: very slow decay → metastable defects

D. Colombara et al., Nature Communications 11, 3634 *(2020).*

$Cu(In,Ga)Se_2$ solar cells

- TR-SPV during pulse sequence (region II)

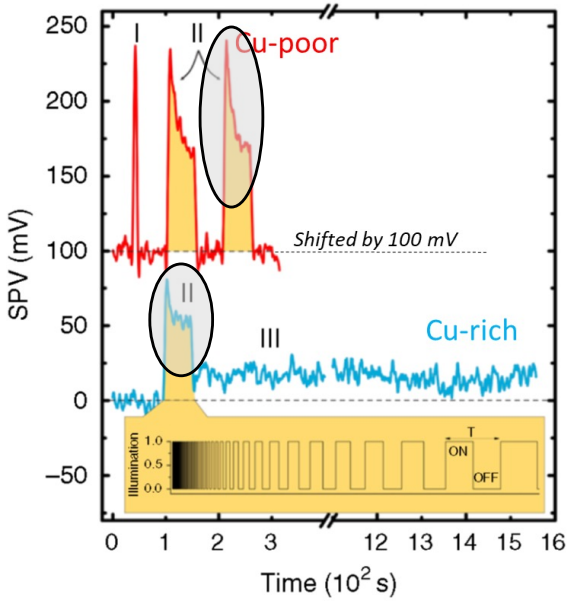

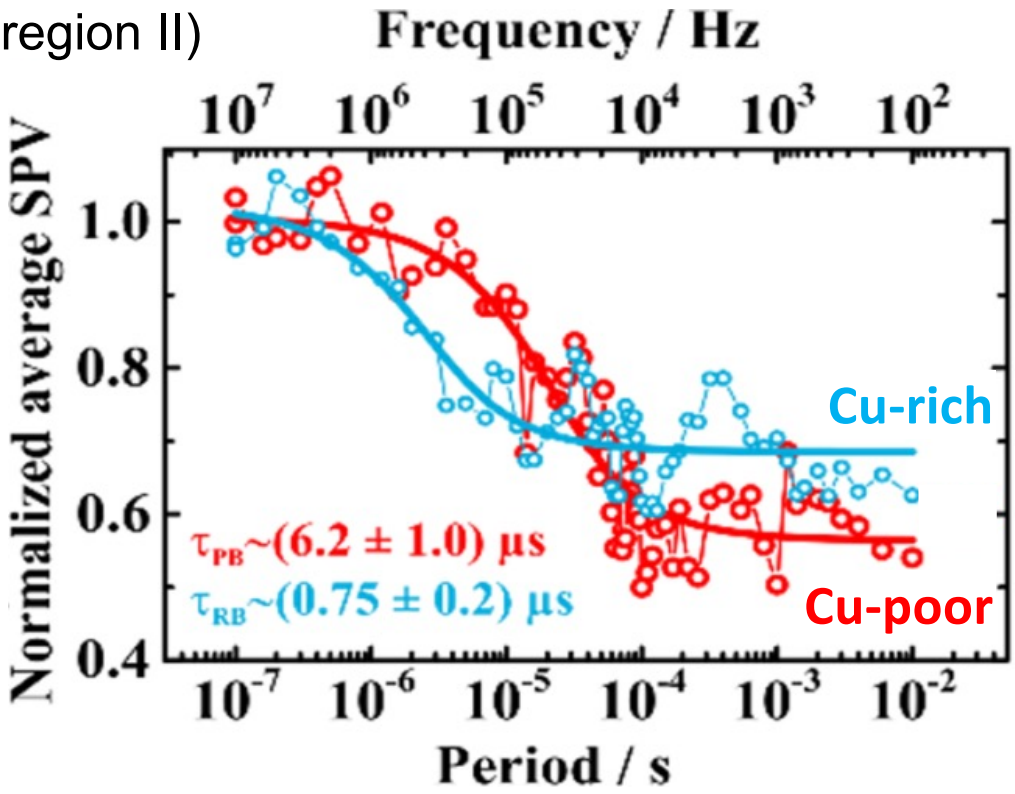

- Fit curves with exponential dependence [1] to evaluate decay time constants:
- $\tau_{Cu\text{-}poor}$ ~ (6.2 ± 1.0) µs
- $\tau_{Cu\text{-}rich}$ ~ (0.75 ± 0.2) µs

$$V_{avg}(f) = V_{dark} + SPV \cdot D + \tau \cdot SPV \cdot \left(1 - e\frac{-(1-D)}{\tau \cdot f}\right)$$

→ TR-SPV results corroborated by admittance spectroscopy and photo-electrochemical transients

→ Data consistent with metastable amphoteric di-vacancy ($V_{Cu}\,V_{Se}$)

[1] M. Takihara et al., Appl. Phys. Lett. 93, 021902 (2008).

D. Colombara et al., Nature Communications 11, 3634 *(2020).*

Fast photodetectors from 2D β-In_2Se_3 grown by molecular beam epitaxy

Marcel S. Claro, Justyna Grzonka, Nicoleta Nicoara, Paulo J. Ferreira, and Sascha Sadewasser

INL – International Iberian Nanotechnology Laboratory, 4715-330 Braga, Portugal

Adv. Optical Mat. 9, 2001034 (2021).

Motivation

- 2D materials have numerous interesting properties
- Fundamental science & applications
- Most devices fabricated from flakes and by manual transfer and stacking
- One device at a time

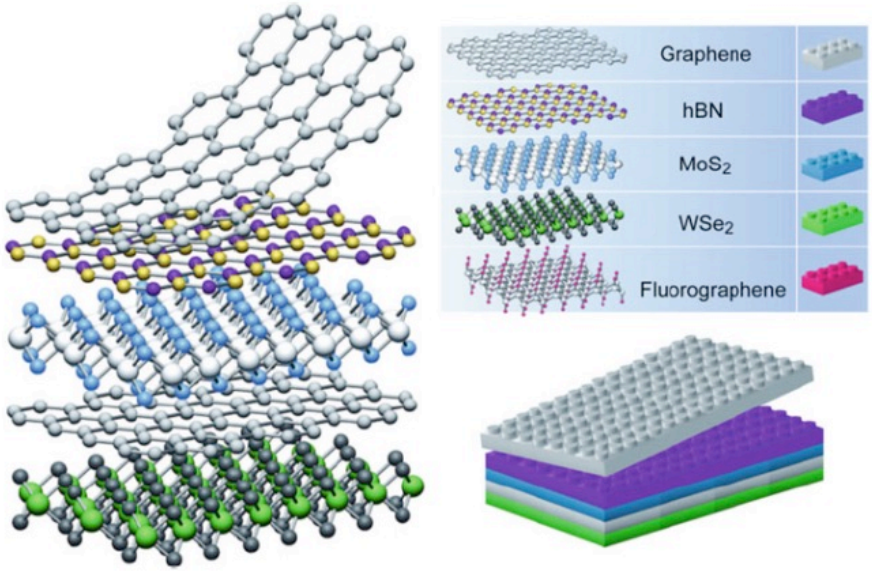

Geim & Grigorieva, Nature 499, 419 (2013).

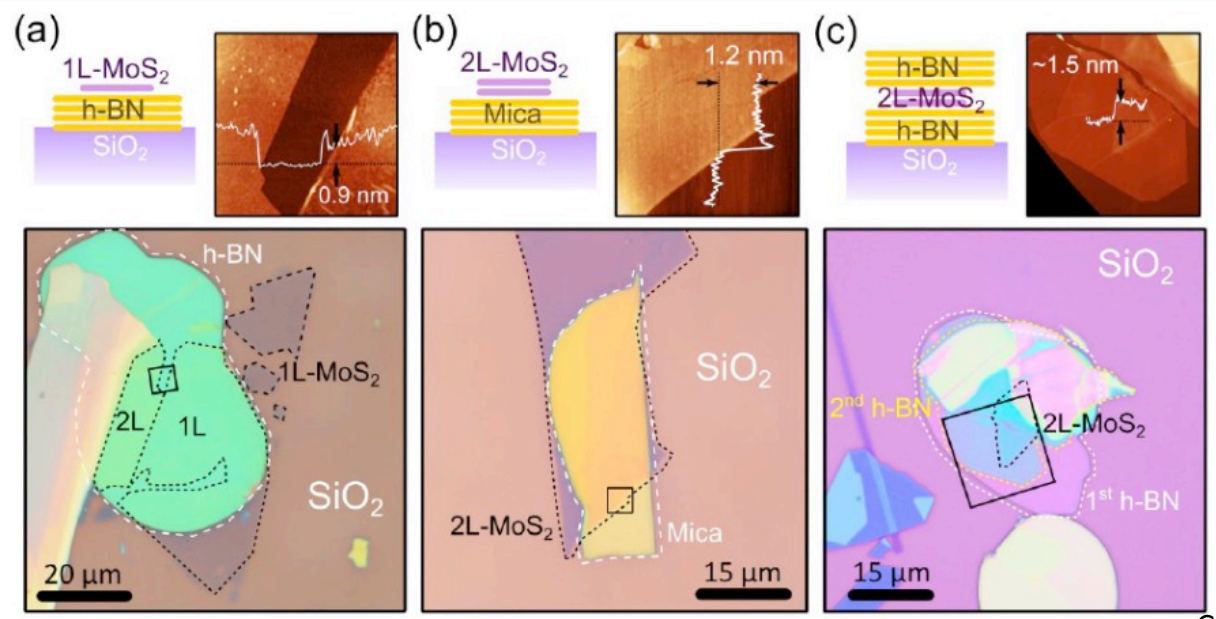

→ **Need to develop industry-compatible fabrication techniques**

Castellanos-Gomez *et al., 2D Mater.* 1, 011002 (2014).

Indium-Selenide Properties

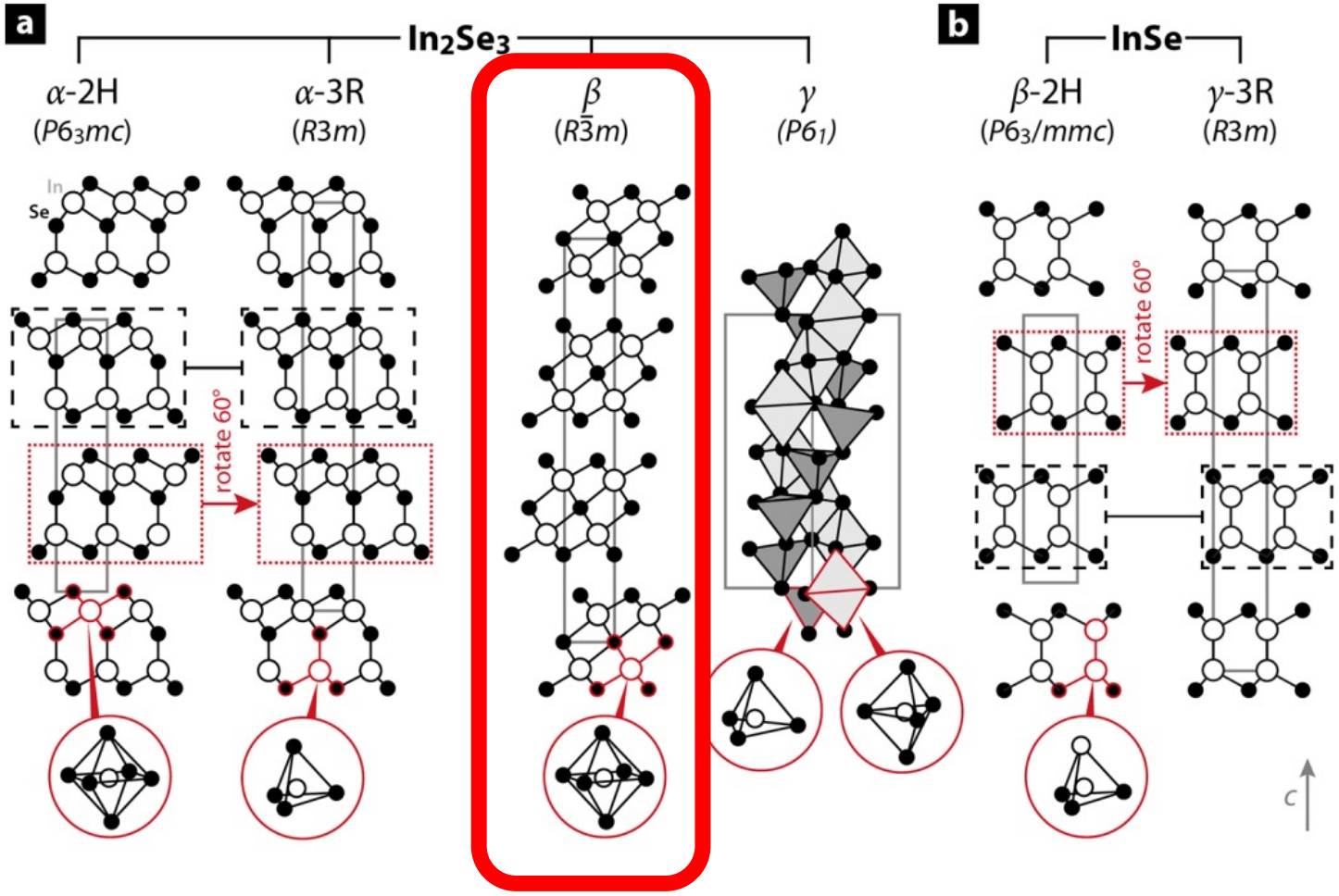

In_2Se_3:

α and β phases
- Layerd 2D material
- Quintuple layers

γ phase
- 3D material
- Wurtzite structure

InSe and GaSe:

β and γ phases
- Layered 2D material
- Quadruple layers

Inorg. Chem. 2018, 57, 11775−11781

Molecular Beam Epitaxy at INL

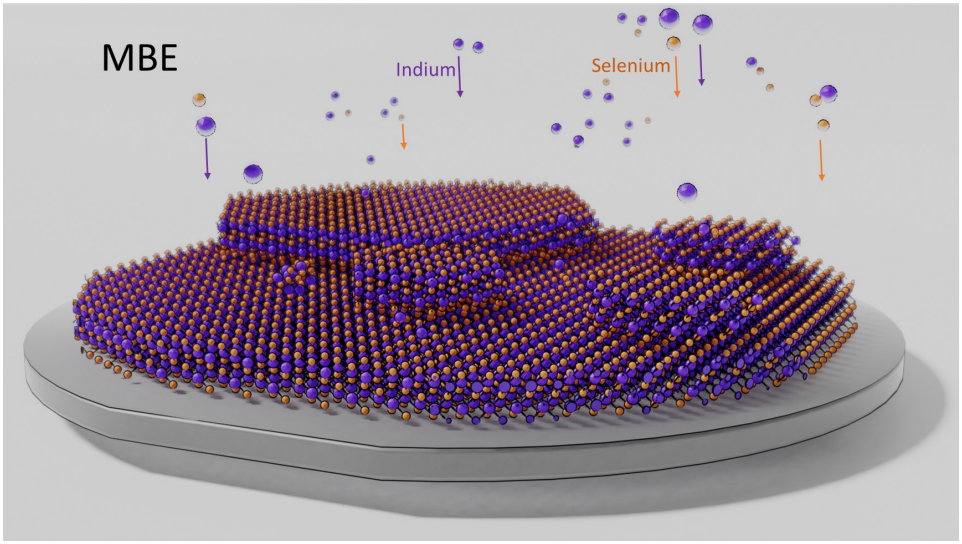

- Molecular beam epitaxy

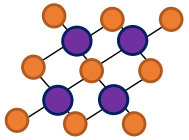

β-In_2Se_3

- 2 inch c-sapphire wafers

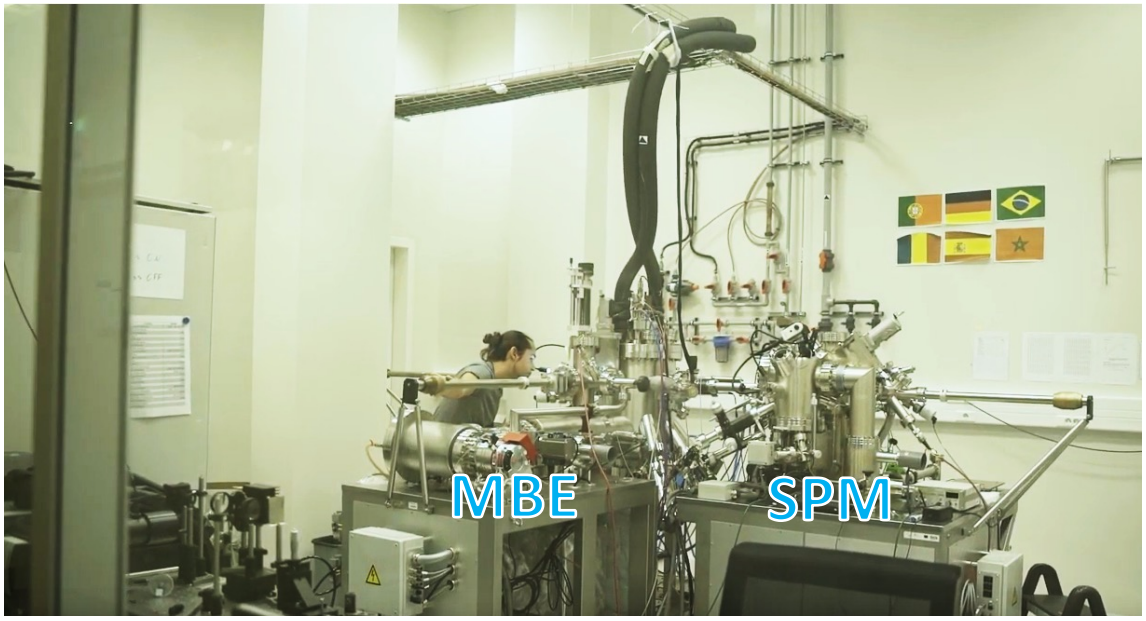

Omicron Nanotechnology, EVO 50

2-inch wafers

Substrates: sapphire, Si (111)

Materials:
- Indium
- Gallium
- Copper
- Bismuth
- Selenium

In-situ control by RHEED

Controlling the phase of Indium-Selenide

- Substrate temperature
- Se flux (Se valve opening)

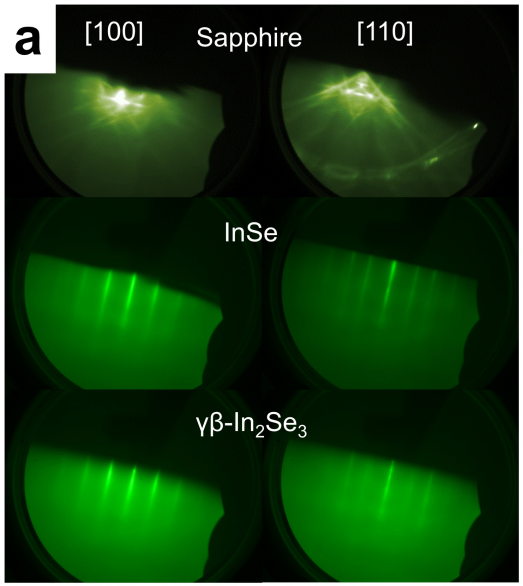

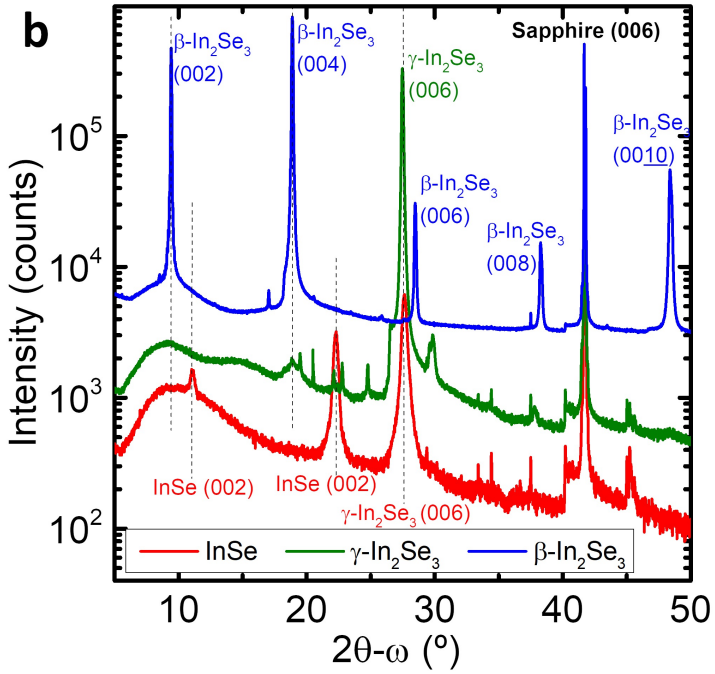

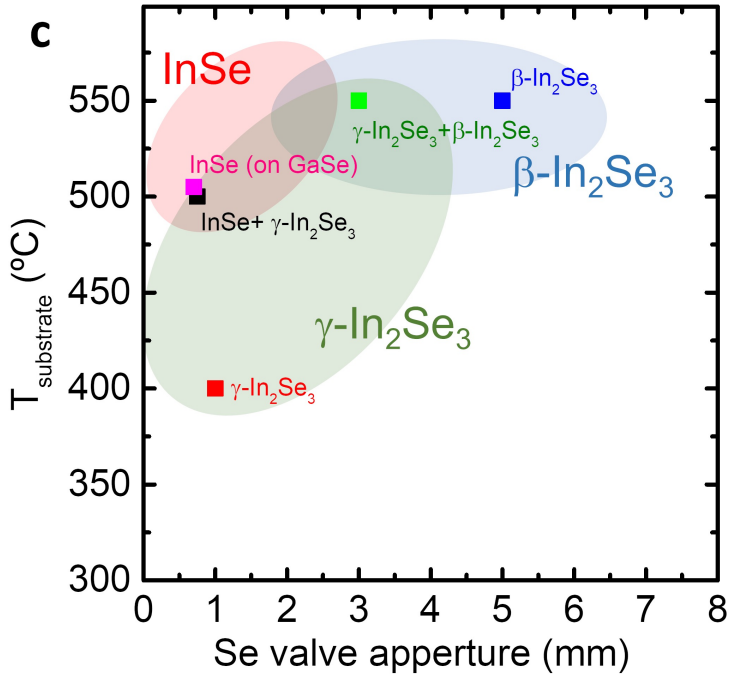

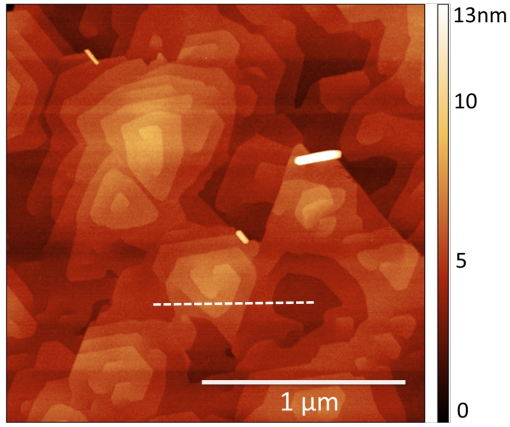

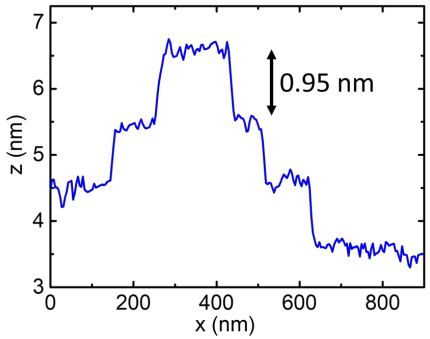

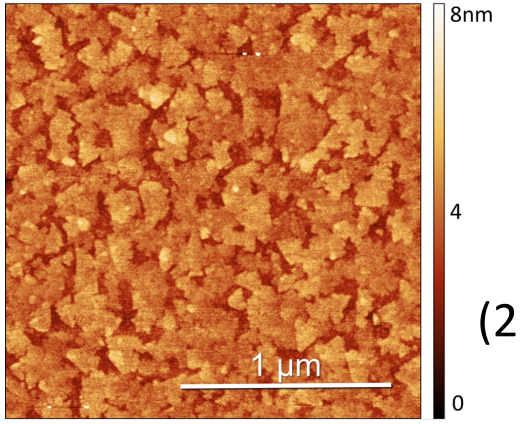

(2 ± 1) QL thickness

M.S. Claro et al., Adv. Optical Mat. 9, 2001034 (2021).

β-In_2Se_3 Materials Quality

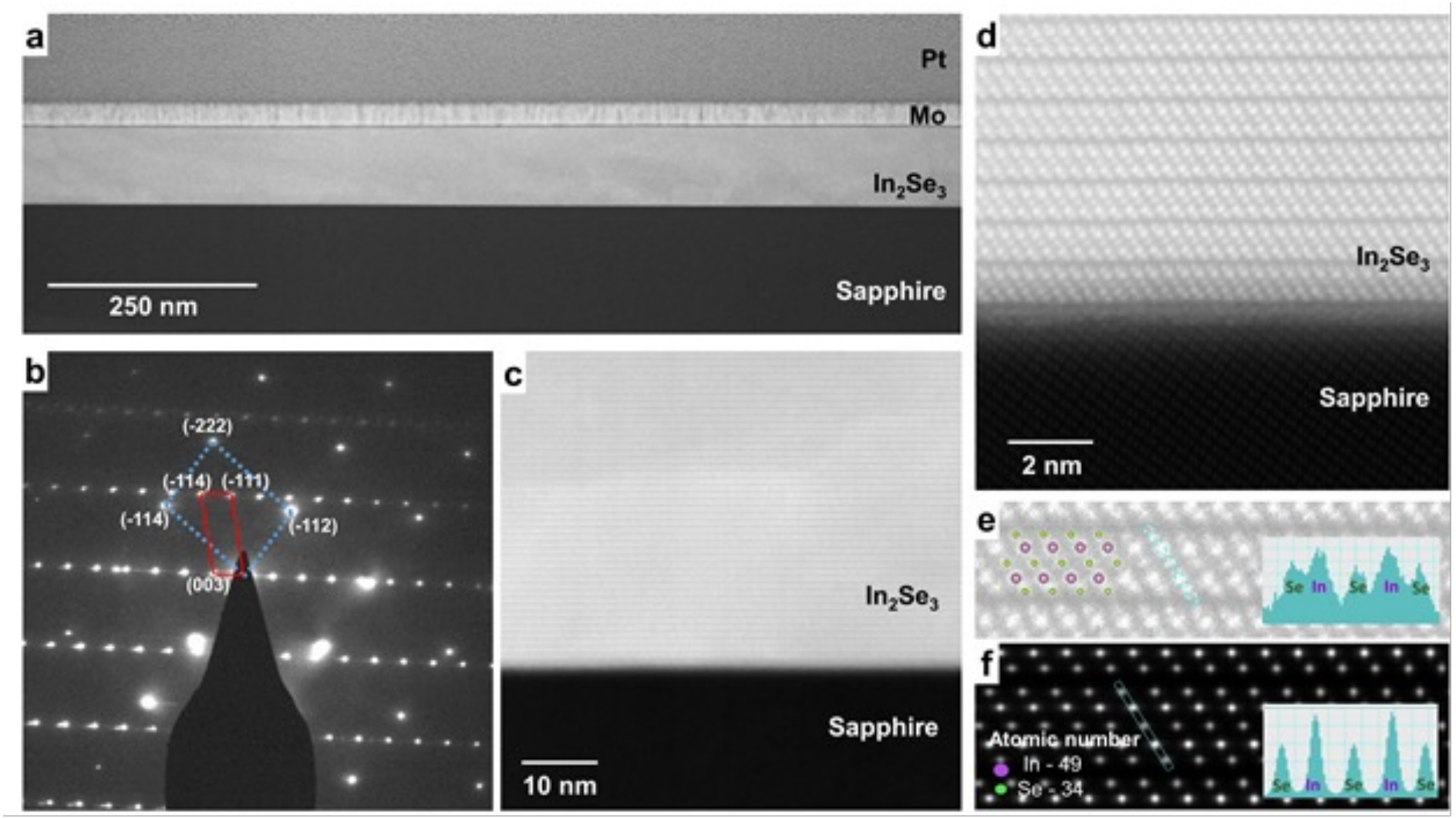

Transmission electron microscopy

- Homogeneous over wide area
- Very few defects
- Atomic structure confirmed through HR-TEM and SAED

Device Fabrication

- Fabrication of devices in INL's cleanroom
- Full 2-inch wafers
- "Standard" processing

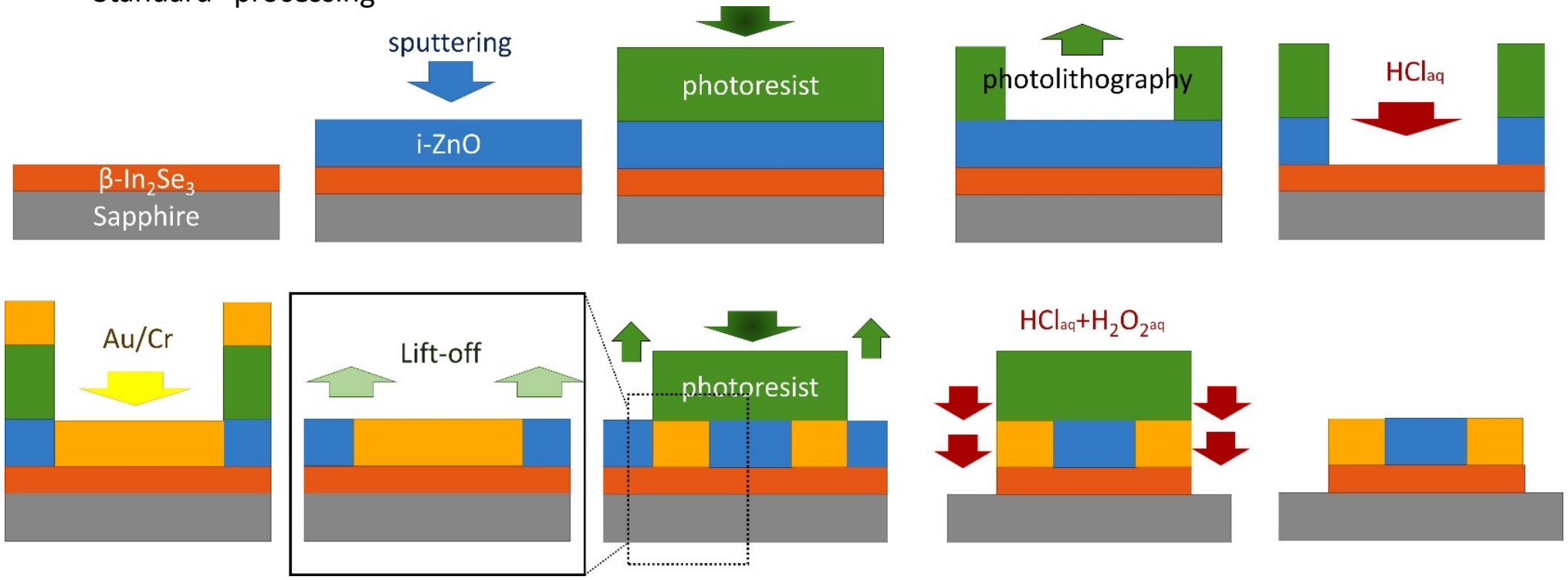

Wafer-scale fabrication of 2D photodetectors

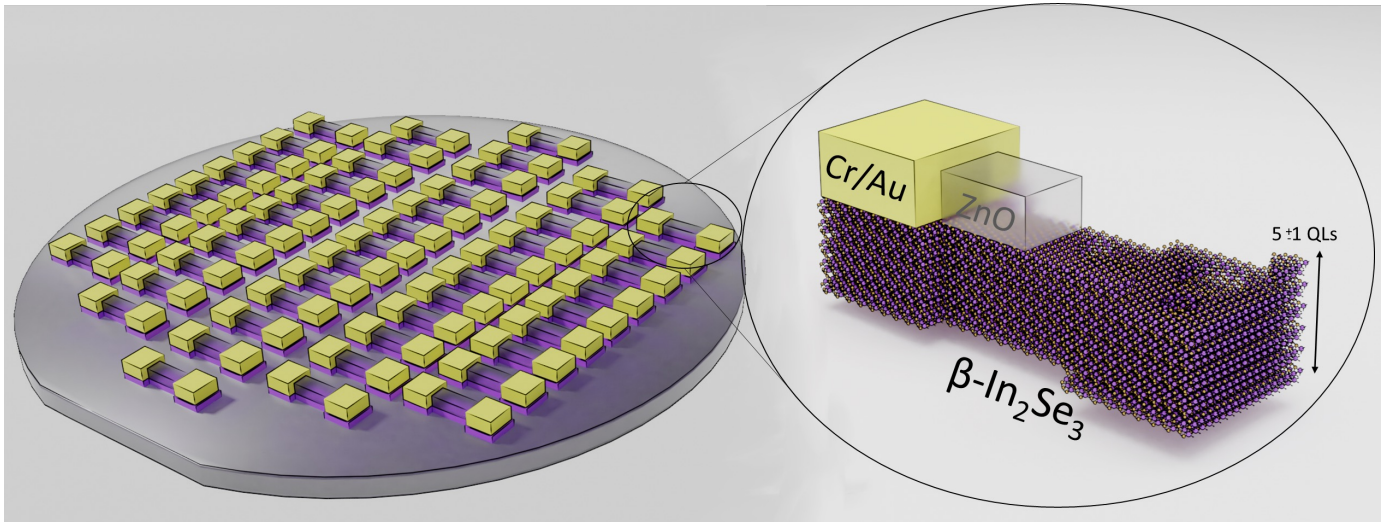

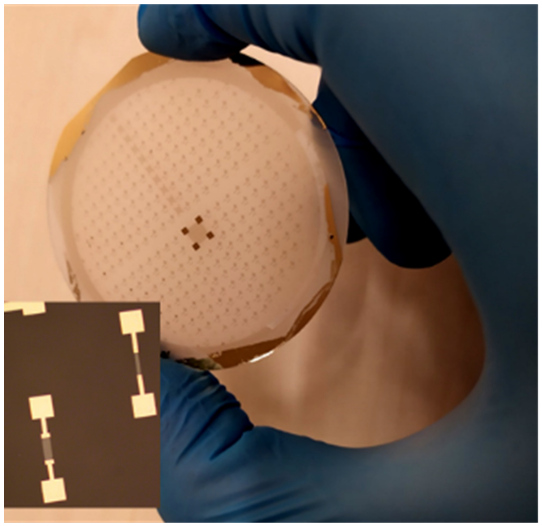

- Wavelength dependence

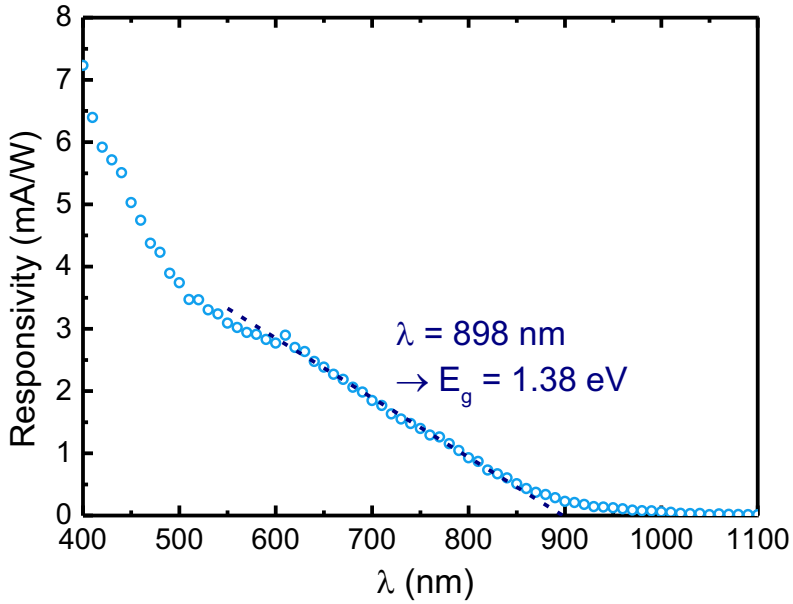

- Time dependent response

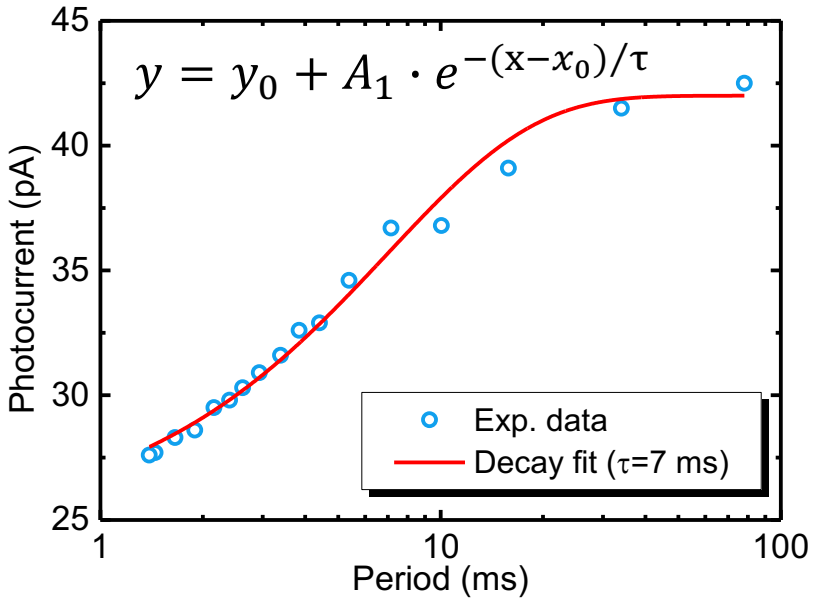

M.S. Claro et al., Adv. Optical Mat. 9, 2001034 (2021).

TR-SPV on β-In_2Se_3

- Is the time constant of photodetector controlled by interfaces in the device (contact/transparent dielectric), or is it a materials property of the β-In_2Se_3 ?

→ TR-SPV on bare material !

- 20 nm thick β-In_2Se_3 on GaN/sapphire substrate

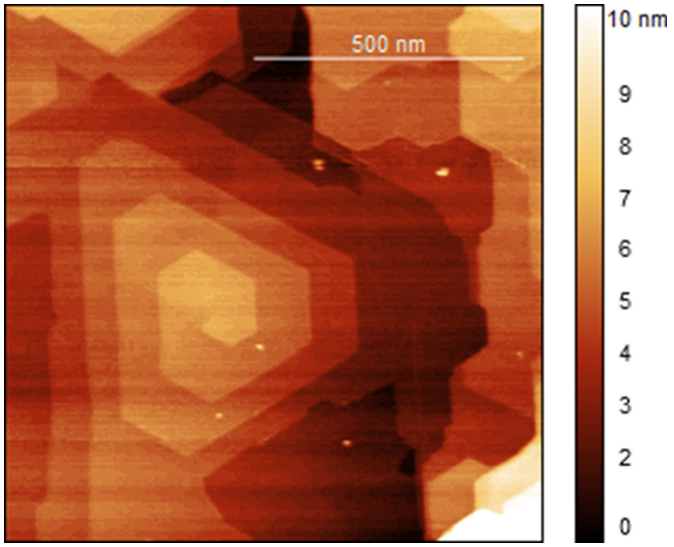

- 635 nm laser pulses (10 Hz – 10 MHz , 100 ns - 100 ms)

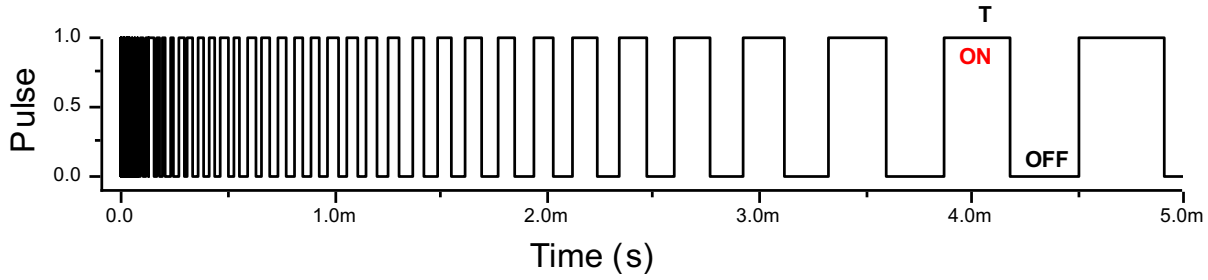

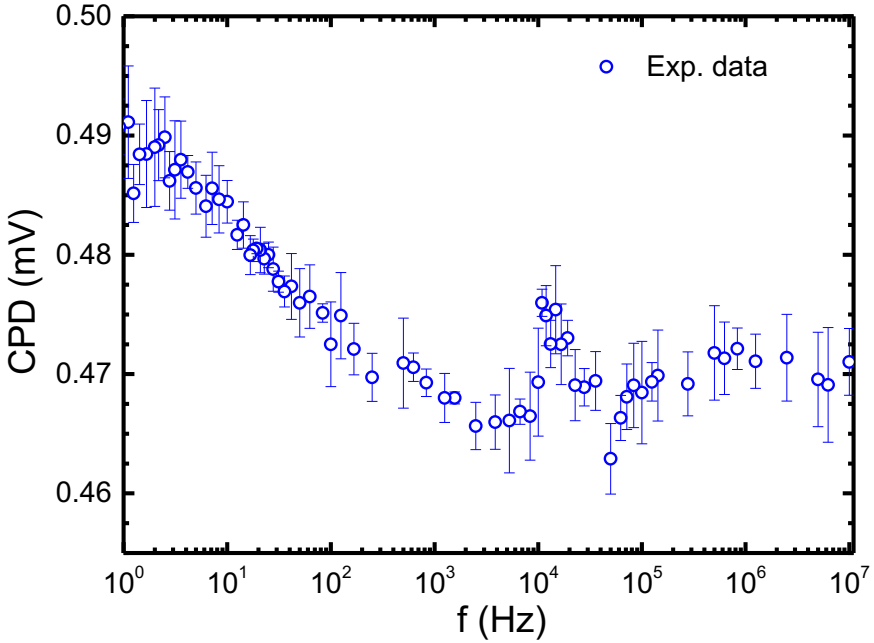

M.S. Claro et al., Adv. Optical Mat. 9, 2001034 (2021).

TR-SPV on β-In_2Se_3

- Fit frequency-dependent CPD curve [1,2]
- one build-up process: τ_b,
- two decay processes: τ_{d1} and τ_{d2}.

$$CPD(f) = CPD_{dark} + SPV_1 D \left(1 - e^{\frac{-(1-D)}{\tau_{d1} \cdot f}} e^{\frac{-D}{\tau_{b1} \cdot f}}\right) + SPV_1(\tau_{d1} \cdot f - \tau_{b1} \cdot f)\left(1 - e^{\frac{-(1-D)}{\tau_{d1} \cdot f}}\right)\left(1 - e^{\frac{-D}{\tau_{b1} \cdot f}}\right) + SPV_2 D + SPV_2(\tau_{d2} \cdot f)\left(1 - e^{\frac{-(1-D)}{\tau_{d2} \cdot f}}\right)$$

D – duty cycle, f – frequency

[1] P.A. Fernandez Garrillo et al., ACS Appl. Mater. Interfaces 8, 31460 (2016).
[2] P.A. Fernandez Garrillo et al., Beilstein J. Nanotechnol. 9, 1834 (2018).

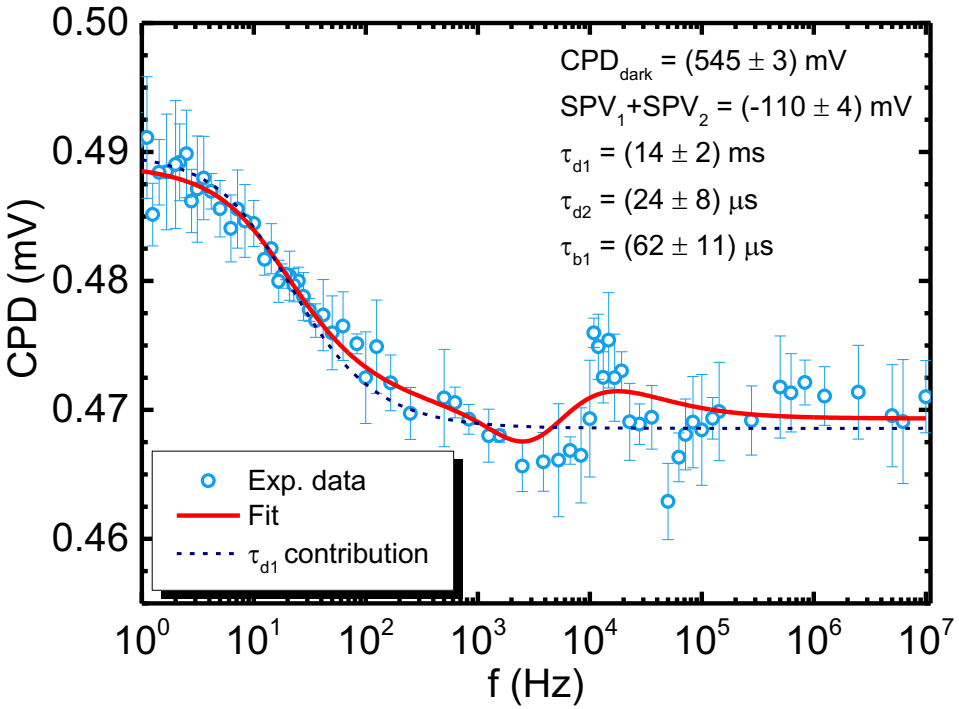

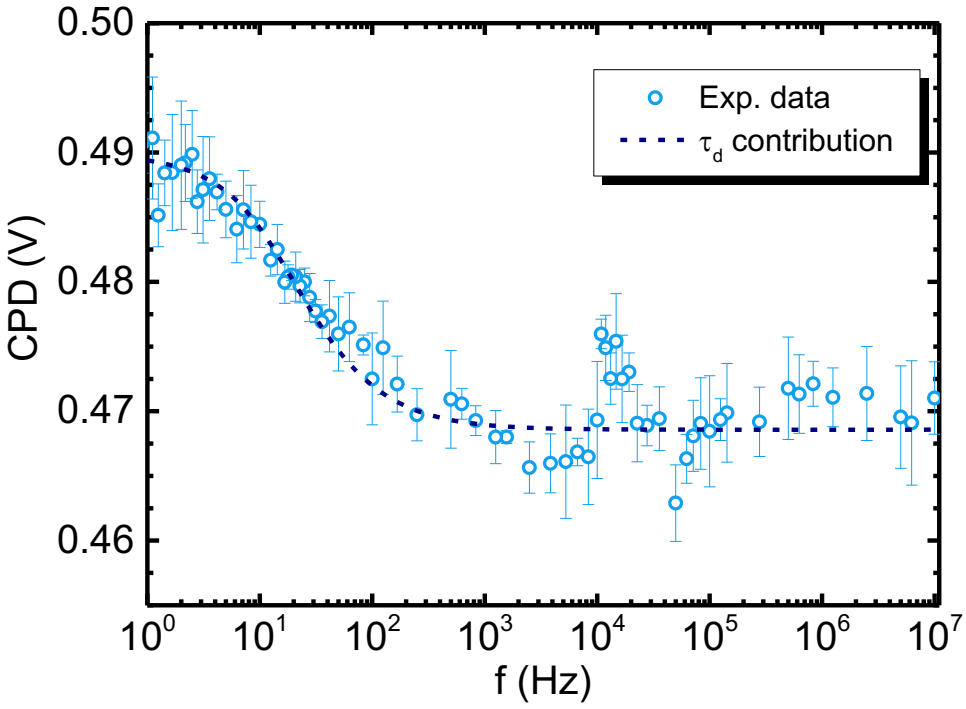

- Time constant of main decay process: τ_{d1} = 14 ms agrees with photodetector τ = 7 ms

→ Likely inherent materials process

M.S. Claro et al., Adv. Optical Mat. 9, 2001034 (2021).

Conclusions

- Introduction to Atomic force microscopy and Kelvin probe force microscopy
- Grain boundaries in Cu(In,Ga)Se_2 solar cell materials
- Epitaxial model samples with individual grain boundaries
- Surface photovoltage gives insights about electronic activity of interfaces
- TR-KPFM and TR-SPV measure dynamics of charge separation and relaxation

Further Reading

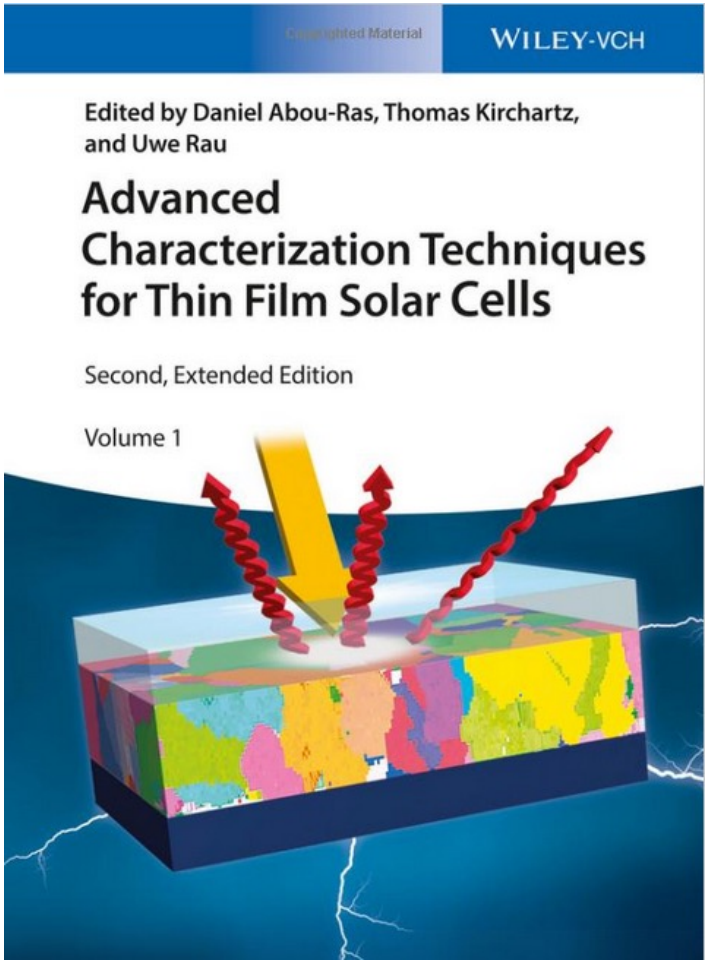

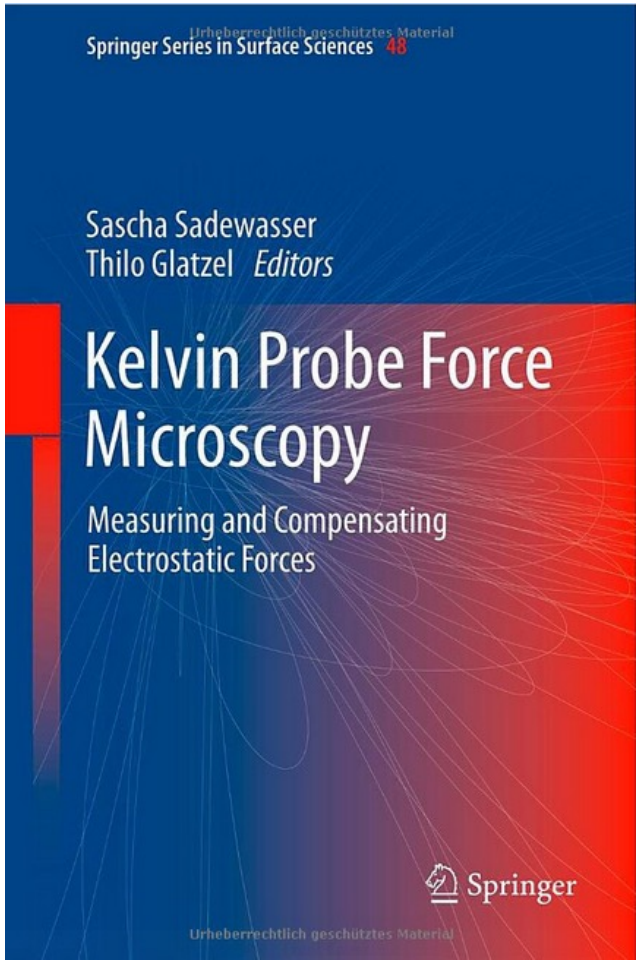

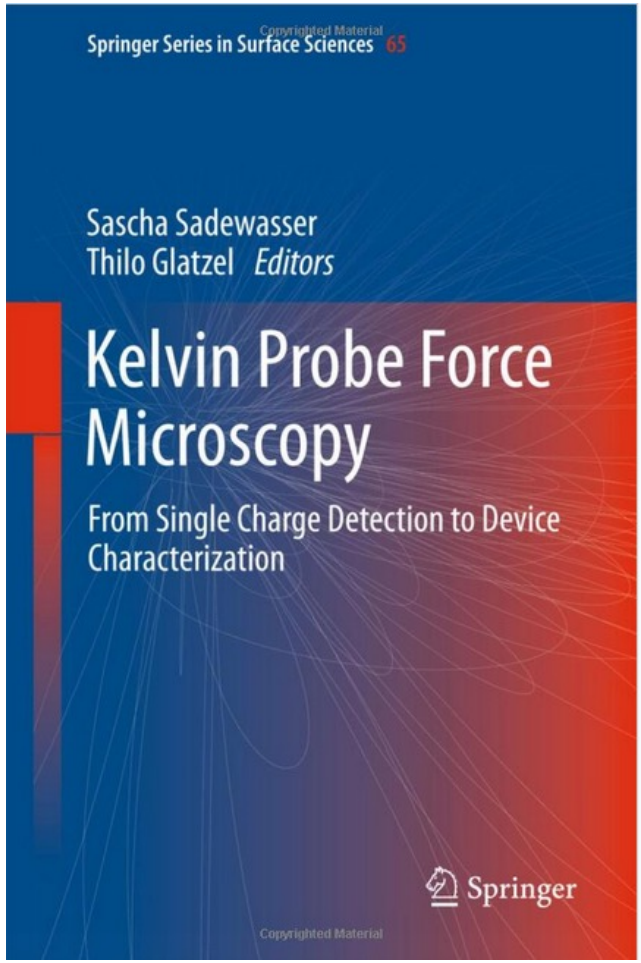

Acknowledgements

Group and collaborators at INL:

- N. Nicoara, R. Manaligod, M.S. Claro, P.F. Ferreira, J. Grzonka

Previous group and collaborators at Helmholtz-Zentrum Berlin:

D. Fuertes Marrón, Th. Glatzel, M. Hafemeister, C. Leendertz, J. Lehmann, H. Mönig, M. Ch. Lux-Steiner, D. Abou-Ras, S. Schmidt, S. Schuler, S. Nishiwaki, S. Siebentritt, R. Kaigawa, R. Klenk, Th. Schedel-Niedrig, T. Eisenbarth, Th. Rissom, M. Wimmer, P. Schubert-Bischoff, R. Caballero

Other collaborators:

- ZSW: W. Witte, D. Hariskos, P. Jackson
- Uni Parma: G. Sozzi, R. Menozzi

Funding:

H2020 project Sharc25, DFG project CORSO, BMU project DTSCM, FCT project NBFS, Cofund project NanoTrain4Growth,

INTERNATIONAL IBERIAN
NANOTECHNOLOGY
LABORATORY

Thank you for your attention !